NTNU – Trondheim
Norwegian University of
Science and Technology

Health monitoring of Composites using Optical Fibres

Magnus Lund Håheim

Mechanical Engineering
Submission date: June 2012
Supervisor: Andreas Echtermeyer, IPM

Norwegian University of Science and Technology
Department of Engineering Design and Materials

Problem text

THE NORWEGIAN UNIVERSITY
OF SCIENCE AND TECHNOLOGY
DEPARTMENT OF ENGINEERING DESIGN
AND MATERIALS

MASTER THESIS SPRING 2012
FOR
STUD.TECHN.
MAGNUS LUND HÅHEIM

HEALTH MONITORING OF COMPOSITES USING OPTICAL FIBRES
Tilstands overvåkning av kompositt med optiske fiberen

New optical fibres can measure strain with high accuracy along their entire length. This thesis shall explore how these fibres can be used as health monitoring systems for composites. The fibres shall be first calibrated against conventional strain measurement methods. Further the accuracy of measuring strain concentrations caused by defects shall be established. Finally the method shall be applied as a health monitoring system in simple composite structures. Methods for reliable transfer of the optical strain signal out of the specimens shall be developed.

The thesis should include the signed problem text, and be written as a research report with summary both in English and Norwegian, conclusion, literature references, table of contents, etc. During preparation of the text, the candidate should make efforts to create a well arranged and well written report. To ease the evaluation of the thesis, it is important to cross-reference text, tables and figures. For evaluation of the work a thorough discussion of results is appreciated.

Three weeks after start of the thesis work, an A3 sheet illustrating the work is to be handed in. A template for this presentation is available on the IPM's web site under the menu "Undervisning". This sheet should be updated when the Master's thesis is submitted.

The thesis shall be submitted electronically via DAIM, NTNU's system for Digital Archiving and Submission of Master's thesis.

Torgeir Welo
Head of Division

Andreas Echtermeyer
Professor/Supervisor

NTNU
Norges teknisk-
naturvitenskapelige universitet
Institutt for produktutvikling
og materialer

Acknowledgments

I would here like to express my gratitude to people who have supported me and whom I have collaborated with during my MSc and master thesis.

I would like to express my sincere gratitude to my supervisor professor Andreas Echtermeyer for valuable discussions, support and interesting work at the composite group through several years.

I would also like to thank all co-students and employees at Department of Engineering Design and Materials involved in my thesis. Especially should PhD candidates Jon Harald Lambert Grave and Stanislav Schebetov be mentioned: Grave for the teamwork in the Co-Patch project and Schebetov for all the previous laboratory work.

Preface

The following report is the master thesis of Magnus Lund Håheim written in the spring of 2012. It is the final work, finishing the degree of MSc in mechanical engineering. The work is a continuation of the project work conducted in the autumn of 2010. The candidate has been a part of the composite group at the Department of Engineering Design and Materials at Norwegian University of Science and Technology (NTNU).

Experimental work during the thesis has been performed as a part of the European Commission funded project Co-Patch. Experiments presented in chapter 7, except 6.9 and some in 6.3 and 6.8, were performed in the time between the project work and the thesis by the candidate, but are included due to the relevance and importance to the results presented here.

Stud. Techn. Magnus Lund Håheim, Trondheim, June 2012

Summary English

The work performed by the candidate in this thesis have successfully lead to knowledge and credibility in using the Optical Backscatter Reflectometer (OBR) 4600 as a sensor technology in health monitoring of composites. Fibre optical sensors have proven through the last decades that they are able to successfully being embedded in composites and where other sensor technologies does point measurements the OBR 4600 used in this thesis have demonstrated high quality distributed sensing.

The experimental work in this thesis has been a part of the European Co-Patch project. This project aims to develop methods for composite patch repairs and reinforcements on marine vessels and civil engineering infrastructures. The project has conducted many tests during the last years from the first small scale tests until now when the full scale test is prepared. In addition to the different surface treatment-, patch application methods and damage scenarios there has been attention to possible monitoring systems to be used. The supervisor of this thesis, professor Andreas Echtermeyer, is responsible for this work package and through that this thesis was formed.

The beginning of this thesis introduces the Co-Patch project, the fibre optical measurements methods and the health monitoring that is the fundament of this thesis. The theory presented in this thesis includes a short introduction to adhesion principles with focus on joints. Fibre optical theory with special attention to strain transfer, possible degradation of composite with embedded sensors in addition to the necessary fibre optical strain measurement theory. Structural Health Monitoring are an established engineering field and introduction to the classifications within SHM and research published on SHM with fibre optics, finishing with the future of health monitoring; namely damage prognosis.

Some of the extensive work put into the process of reaching the level of knowledge the candidate has today in fibre optical strain measurements are presented: methods for embedment, processing parameters and fibre coating proofing to mention a few. Following the establishment of measurement procedures are the experimental work performed in this thesis with specimens and manufacturing presented before test procedures and results with discussion.

Comparison has been done to confirm the accuracy of the measurements, and measurement characteristics at stress concentrations have been discussed.

Summary Norwegian

Kandidaten har i arbeidet med denne oppgaven oppnådd både kunnskap og forutsigbarhet i bruken av Optical Backscatter Reflectometer (OBR) 4600 som en måleteknologi i tilstandsovervåkning av kompositter. En har gjennom de siste tiårene bevist at en med stort hell kan støpe inn fiberoptiske sensorer i kompositter. De fleste kommersialiserte sensorene tar kun punktmålinger, mens OBR 4600 som er brukt i denne oppgaven kan ta høyoppløselige fordelte tøyningsmålinger.

Forsøkene i denne oppgaven har vært en del av EU-prosjektet Co-Patch. Dette prosjektet ønsker å utvikle metoder for å reparere og forsterke båter og konstruksjoner med kompositter. Gjennom prosjektet har det blitt gjennomført mange forskjellige tester, fra småskala frem til det i dag forberedes en fullskalatest. I tillegg til undersøkelser i egnede overflatebehandlinger, måter å påføre komposittreparasjonene og skadescenarioer har det blitt gjort undersøkelser i egnet overvåkningssystem for reparasjonene. Veilederen for denne oppgaven, professor Andreas Echtermeyer, er leder for arbeidspakken vedrørende overvåkning og ut fra dette ble denne oppgaven formet.

Oppgaven begynner med å introdusere Co-Patch prosjektet, fiberoptiske tøyningsmålinger og tilstandsovervåkning som legger grunnlaget for denne oppgaven. Videre blir teorien presentert med en kort innføring i prinsipper ved limforbindelser med spesielt fokus på skjøter. Fiberoptisk teori med spesielt fokus på overføring av tøyninger fra materialet til sensoren, mulige svekkelser av kompositten med innstøpte fiber i tillegg til nødvendig innføring i fiberoptisk strekkmålingsteori. Tilstandsovervåkning av strukturer er et etablert fagområde hvor det her blir introdusert noe av klassifiseringen av dette, publisert litteratur om fiberoptisk tilstandsovervåkning og til slutt fremtiden for tilstandsovervåkning, nemlig forutse kommende skader.

Noe av det omfattende arbeidet som er utført for å oppnå kunnskapen som kandidaten har om fiberoptiske strekkmålinger er presentert i oppgaven: innstøpingsmetoder, beregningsparametere og valg av egnet materiale på overflaten til fiber kabelen for å nevne noe. Etter at målemetoder er presentert følger forsøkene som er gjort i oppgaven med presentasjon av prøvene og fabrikasjonen av dem samt testmetoder og resultater med diskusjon.

I oppgaven er det sammenligning og diskusjon av måleresultater som er blitt gjort med andre målemetoder for å bekrefte nøyaktigheten og oppførselen ved spenningskonsentrasjoner.

Table of contents

PROBLEM TEXT ..... **I**

ACKNOWLEDGMENTS ..... **II**

PREFACE ..... **III**

SUMMARY ENGLISH ..... **IV**

SUMMARY NORWEGIAN ..... **V**

TABLE OF CONTENTS ..... **VI**

1 LIST OF FIGURES ..... **VIII**

2 LIST OF TABLES ..... **XI**

3 ABBREVATIONS ..... **XII**

4 INTRODUCTION **1**

4.1 FIBRE OPTIC STRAIN MEASUREMENTS 1

4.2 CO-PATCH 2

4.3 HEALTH MONITORING 3

5 THEORY **4**

5.1 ADHESION 4

5.1.1 Adhesion theories *4*

5.1.2 Adhesive joints *6*

5.2 FIBRE OPTIC STRAIN MEASUREMENT 9

5.2.1 Fibre optic cables *9*

5.2.2 Shear transfer *10*

5.2.3 Degradation of laminate strength and stress concentrations caused by fibre optic sensors *14*

5.2.4 Temperature and strain sensitivity *15*

5.2.5 Measurement technologies *16*

5.2.6 OBR 4600 – Distributed fibre optical strain measurement system *17*

5.3 STRUCTURAL HEALTH MONITORING 18

5.3.1 Classification of SHM *18*

5.3.2 SHM with fibre optics *20*

5.3.3 Damage prognosis *21*

6 ESTABLISHMENT OF MEASUREMENT PROCEDURES **23**

6.1 MICROSCOPIC IMAGES FROM EMBEDMENT 23

6.2 EMBEDMENT TECHNIQUES 23

6.2.1 Embedment *24*

6.2.2 Test results *25*

6.3 PARAMETER INFLUENCE 26

6.4 COATING TEST 29

6.4.1 Specimens *29*

6.4.2 Results *30*

6.5 SINGLE LAP SPECIMENS - CO-PATCH 31

6.5.1 Specimens *31*

6.5.2 Results *32*

6.6 FIBRE PROOFING 33

6.6.1 Specimens *33*

6.6.2 Results *33*

6.7 TEMPERATURE MEASUREMENTS 34

6.7.1 Experiment *34*
6.7.2 Results *35*
6.8 ENTERING AND EXITING OF FIBRE IN A LAMINATE 36
6.9 FILAMENT WINDING WITH OPTICAL FIBRE 39

7 CALIBRATION 41
7.1 CALIBRATION OF FIBRE IN AIR 41

8 EXPERIMENTAL WORK 45
8.1 WP3 – TASK 3.2 - P3 45
8.1.1 Specimens *45*
8.1.2 Testing *48*
8.2 WP3 – TASK 3.2 - IPE 100 BEAMS 49
8.2.1 Specimens *49*
8.2.2 Testing *50*
8.3 WP3 - RELAXATION TEST 52
8.3.1 Specimens *52*
8.3.2 Testing *52*
8.4 WP6 - FULL SCALE TEST 53
8.4.1 Test description *53*
8.4.2 Monitoring *54*

9 RESULTS 58
9.1 WP3 – P3 60
9.1.1 P3_4 ..... *60*
9.2 WP3 – TASK 3.2 64
9.2.1 GB #2 ..... *64*
9.3 RELAXATION TEST RESULTS 67

10 DISCUSSION 68

11 CONCLUSIONS 71

12 REFERENCES 72

13 APPENDIX A 75
13.1 PARAMETER INFLUENCE 75
13.2 CONFERENCE PAPER 78
13.3 OBR 4600 DATASHEET 86

14 APPENDIX B 89
14.1 TECHNICAL NOTE P3 SPECIMENS 89
14.2 CO-PATCH P3 TEST RESULTS 97
14.2.1 P3_1 ..... *97*
14.2.2 P3_2 ..... *101*
14.2.3 P3_3 ..... *105*
14.2.4 P3_4 ..... *108*
14.3 CO-PATCH TASK 3.2 TEST RESULTS 108
14.3.1 GB #1 ..... *109*
14.3.2 GB #2 ..... *110*
14.3.3 VI C/V #1 ..... *110*
14.3.4 VI C/V #4 ..... *113*
14.4 OPTICAL FIBRE SPECIFICATION 114
14.5 ADDITIONAL RESULTS AND INFORMATION 116
14.5.1 Calibration 1 ..... *116*
14.5.2 Tools developed *118*

1 List of figures

FIGURE 1 EXAMPLES OF COHESIVE AND ADHESIVE FAILURES. 6
FIGURE 2: EFFECT OF ADHESIVE MODULUS ON THE ADHESIVE 7
FIGURE 3: EFFECT OF THE ADHESIVE DUCTILITY ON THE STRESS 7
FIGURE 4: ADHESIVE SHEAR STRESSES IN A METAL/COMPOSITE DOUBLE-LAP JOINT. FROM [3] 8
FIGURE 5: LOAD TRANSFER AND SHEAR STRESS DISTRIBUTION IN 9
FIGURE 6: ADHEREND SHAPING IN JOINT DESIGN. FROM [3] 9
FIGURE 7: ILLUSTRATION FROM [4] SHOWING THE CORE AND CLADDING OF A FIBRE AND THE NOTATION FOR (4). 10
FIGURE 8: STRAIN TRANSFER FROM A HOST MATERIAL TO A FIBRE OPTIC SENSOR. 11
FIGURE 9: TRANSFER OF A SINGLE PERIOD OF A HARMONIC . FROM [8]. 12
FIGURE 10: STRAIN DISTRIBUTION CALCULATED BY OKABE'S MODIFIED 13
FIGURE 11: STRAIN DISTRIBUTION CALCULATED FOR A 0 DEGREE LAYER, COATED- AND UNCOATED FIBRE IN LONGITUDINAL DIRECTION. (A) WITH AN AVERAGE TENSILE STRESS OF 359MPA. (B, RIGHT) AVERAGE TENSILE STRESS OF 815MPA. [11] 13
FIGURE 12: INCREASE IN NOMINAL STRESS FOR A CF LAMINATE WITH AN EMBEDDED FIBRE LOADED IN TRANSVERSE DIRECTION. FROM [15] 14
FIGURE 13: WAVELENGTHS OF BACKSCATTERED RADIATION FROM [18]. 17
FIGURE 14: EXAMPLE OF AN OFDR-BASED DISTRIBUTED STRAIN SENSING SYSTEM. FROM PATENT PUBLICATION NUMBER: US 2011/0317148 A1. 17
FIGURE 15: THE GENERAL COMPONENTS OF A DP PROCESS FROM [36]. 21
FIGURE 16: FIBRE OPTIC CABLE EMBEDDED IN UNIDIRECTIONAL GLASS FIBRE LAMINATE. 23
FIGURE 17: EMBEDDED FIBRE OPTICAL SENSOR EXITING THROUGH SURFACE. 24
FIGURE 18: FIBRE OPTICAL CABLE PLACEMENT DURING MANUFACTURING. 25
FIGURE 19: STRAIGHT GLASS FIBRE SPECIMEN 26
FIGURE 20: DOG BONE SHAPED GLASS FIBRE SPECIMEN WITH EMBEDDED ACRYLATE COATED FIBRE. 27
FIGURE 21: DEVIATIONS IN MEASUREMENT DATA DURING COMPRESSION. 28
FIGURE 22: GLASS FIBRE SPECIMEN WITH 4,5MM HOLE BEFORE AND AFTER TEST. 30
FIGURE 23: COMPARISON OF MEASUREMENTS WITH ACRYLATE AND POLYIMIDE COATED FIBRE. 30
FIGURE 24: POLYIMIDE FIBRE BONDED PARALLEL ON SPECIMEN 31
FIGURE 25: 12MM SINGLE LAP SPECIMENS DURING MANUFACTURING. 31
FIGURE 26: 200MM SINGLE LAP SPECIMEN WITH GLASS FIBRE PATCH. 32
FIGURE 27: FIBRE OPTICAL MEASUREMENT RESULTS FROM 200MM OVERLAP SPECIMEN 32
FIGURE 28: CLOSE UP OF FIBRE IN 200MM SINGLE LAP SPECIMEN. 33
FIGURE 29: FIBRE OPTICAL STRAIN MEASUREMENT COMPARED TO STRAIN GAUGE 34
FIGURE 30: TEMPERATURE MEASUREMENTS IN A TEMPERATURE BATH USING FIBRE OPTICAL SENSOR. 35
FIGURE 31: TEMPERATURE MEASURMENTS AT 70 °C 35
FIGURE 32: UNPROTECTED MEASURING FIBRE BROKEN DURING MANUFACTURING. 36
FIGURE 33: FIRST ATTEMPT IN PROTECTING THE MEASURING FIBRE DURING MANUFACTURING. 36
FIGURE 34: OPTICAL FIBRE PROTECTION 37
FIGURE 35: DETAIL PICTURE OF FIBRE EXITING THE RELAXATION TEST SPECIMEN. 37
FIGURE 36: LEFT (A): THE EMPIRE CONNECTOR AND RIGHT (B): EMBEDDED CONNECTOR. PICTURES FROM DEUTSCH "FIBRE OPTICS" CATALOGUE. LITERATURE CODE: FO-D08005-2008. 38
FIGURE 37: PICTURES OF TENSILE FAILURE FOR SPECIMENS WITH EMBEDDED MT-FERRULES. (A) WITH CUTOUTS, AND (B) NO CUTOUTS. FROM [40] 39
FIGURE 38: CLOSE UP OF FILAMENT WINDING WITH FIBRE OPTICAL CABLE BARELY VISIBLE AT THE TIP OF THE ARROWS. 40
FIGURE 39: EXPERIMENTAL SETUP CALIBRATION IN AIR 42
FIGURE 40: TOTAL STRAIN MEASURED 42
FIGURE 41: STANDARD DEVIATION OF INCREMENTAL VALUES 43
FIGURE 42: MEASURED VALUES AT THE DIFFERENT INCREMENTS 43
FIGURE 43: MEASUREMENTS FROM ONE SIDE IN TEST 2. 44
FIGURE 44: P3 SPECIMEN DIMENSIONS. BY J.H. GRAVE 46
FIGURE 45: P3 SPECIMEN FIBRE SENSOR PLACEMENT. 46
FIGURE 46: P3 SPECIMENS DURING LAYUP. PHOTO BY: AIMEN 47

Figure 47: Finished P3 specimens. Photo by: AIMEN 47
Figure 48: Test setup P3 fatigue test. 48
Figure 49: IPE-100 beams with fibre placement illustrated. 50
Figure 50: IPE-100 beams with strain gauge placement illustrated. By J.H. Grave 50
Figure 51: Test setup IPE-100 beams 51
Figure 52: CMOD and strain gauges next to the crack 51
Figure 53: Relaxation test specimen. 52
Figure 54: Overview picture of catamaran. 53
Figure 55: Sketch of fibre placement crack 1 56
Figure 56: Patch of crack 1 with fibre sensors. 57
Figure 57: Sketch of fibre placement, crack 2. 58
Figure 58: Patch of crack 2 with fibre sensors. 58
Figure 59: Sensor parameters to be chosen for strain calculations with the OBR 4600 59
Figure 60: Illustration of influence of gage length on P3_4. 59
Figure 61: P3_4 cycle maxima 61
Figure 62: P3_4 Cycle minima 61
Figure 63: P3_4 Normalized plots 62
Figure 64: Crack in P3 before (left, steel side) and after (right, patch side) patch failure. 63
Figure 65: P3_4 - Comparison of FBG and OBR at cycle maxima. 63
Figure 66: P3_4 - Comparison of FBG and OBR at cycle minima 64
Figure 67: Specimen VI-C/V #4 after failure. 65
Figure 68: GB #2 Measurement results 65
Figure 69: GB #2 Normalized plots 66
Figure 70: Strain measured in relaxation tests 67
Figure 71: Parameter influence, 0,05cm gage length 75
Figure 72: Parameter influence, 0,06cm gage length 75
Figure 73: Parameter influence, 1cm gage length 76
Figure 74: Parameter influence, equal gage length and sensor spacing 76
Figure 75: Parameter influence, 1cm sensor spacing 77
Figure 76: P3_1 Cycle maxima. 97
Figure 77: P3_1 Cycle minima 98
Figure 78: P3_1 Normalized plots 98
Figure 79: P3_1 - Comparison at cycle maxima. 99
Figure 80: P3_1 - Comparison at cycle minima. 99
Figure 81: P3_2 Cycle maxima 101
Figure 82: P3_2 Cycle minima 101
Figure 83: P3_2 Normalized plots 102
Figure 84: P3_2 - Comparison at cycle maxima 102
Figure 85: P3_2 - Comparison at cycle minima 103
Figure 86: P3_3 Cycle maxima 105
Figure 87: P3_3 Cycle minima 105
Figure 88: P3_3 Normalized plots 106
Figure 89: P3_3 - Comparison at cycle maxima 106
Figure 90: P3_3 - Comparison at cycle minima 107
Figure 91: GB #1 109
Figure 92: GB #1 Normalized plots 109
Figure 93: GB #2 Parameter control 110
Figure 94: VI C/V #1 Elastic load/unload, embedded fibre 111
Figure 95: VI C/V #1 Elastic load/unload, surface fibre 111
Figure 96: VI C/V #1 Loading to failure, embedded fibre 112
Figure 97: VI C/V #1 Loading to failure, surface fibre 112
Figure 98: VI C/V #4 Loading to failure, embedded fibre 113
Figure 99: VI C/V #4 Loading to failure, surface fibre 113
Figure 100: Calibration 1 116
Figure 101: Calibration 2 116
Figure 102: Calibration 3 117
Figure 103: Calibration 4 117
Figure 104: Calibration 5 118
Figure 105: Fixtures used in the "Calibration in air" test. 118

FIGURE 106: SKETCH OF TOOL TO APPLY PRESSURE WHEN BONDING FIBRE.....119
FIGURE 107: SIMPLE CABLE HOLDER RIG. HERE WITHOUT CONNECTORS. 119
FIGURE 108: FRONT PANEL OF LABVIEW PROGRAM FOR REMOTE CONTROL OF THE OBR 4600. 121
FIGURE 109: BLOCK DIAGRAM OF LABVIEW PROGRAM. 121

2 List of tables

TABLE 1: APPROXIMATED CONSTANT VALUES FOR STRAIN AND TEMPERATURE CALCULATIONS. 15
TABLE 2: STATISTICAL DATA FOR DEVIATIONS IN MEASUREMENTS DURING COMPRESSION. 28
TABLE 3: STATISTICAL DATA FOR DEVIATION IN MEASUREMENTS DURING TENSION 29
TABLE 4: P3 SPECIMEN PROPERTIES 45
TABLE 5: IPE-100 BEAM TEST SCHEME WITH PROGRESS REPORT. 49
TABLE 6: MONITORING PLAN, FULL SCALE TEST. 54
TABLE 7: LOAD AND STRAIN DATA P3_1 100
TABLE 8: LOAD AND STRAIN DATA P3_2 104
TABLE 9: LOAD AND STRAIN DATA P3_3 107
TABLE 10: LOAD AND STRAIN DATA P3_4 108

3 Abbrevations

Co-Patch	-	Composite Patch Repair for Marine and Civil Engineering Infrastructure Applications
OBR	-	Optical backscatter reflectometer
FBG	-	Fibre Bragg grating
NDT	-	Non-destructive testing
NTUA	-	National Technical Univeristy of Athens
WP	-	Work package
SHM	-	Structural health monitoring
AICP	-	Adhesives implemented via a chemical process
PSA	-	Pressure-sensitive adhesive
CRFP	-	Carbon Reinforced Polymer
OFDR	-	Optical frequency domain reflectometer
SWI	-	Swept wavelength interometry
FE	-	Finite Element
IVHM	-	Integrated vehicle health management
UD	-	Unidirectional
CN	-	Cyanoacrylate
UAC	-	Umoe Advanced Composites
ENP	-	Estaleiros Navais de Peniche SA
AIMEN	-	*Asociación de Investigación Metalúrgica del Noroeste*
IPE	-	I-Profile European
LVDT	-	Linear Variable Displacement Transducor
CMOD	-	Crack mouth opening displacement
FPB	-	Four point pending
GB	-	Grit blasted
VI C/V	-	Vacum infused, Carbon/vinyl ester
ECCM	-	European conference on composite materials

4 Introduction

As stated in the problem text, this thesis will investigate how a fibre optic measurement system may be used for health monitoring in composites. The advantages of using fibre optic measurements instead of other traditional Non-destructive testing (NDT) methods or e.g. strain gauges are many, but for us the main advantage is the ability to embed the optical fibre in the composite without affecting the mechanical properties of the structure.

This thesis will both investigate the practical use of fibre optics and its accuracy as well as the applied use in different tests in the Co-Patch project.

4.1 Fibre optic strain measurements

The system that will be used and discussed in this thesis was procured as a part of the project work in the autumn of 2010. It is the Optical Backscatter Reflectometer (OBR) 4600 from Luna Technologies. This system is capable of measuring the wavelength and amplitude of the light reflected back, after emitting light through a fibre optic cable. With its software it is then capable of measuring any strain or temperature change along the length of the fibre. This will be further explained in chapter 5.2.6.

Fibre optic strain measurements have been developed through many years, and from the introduction at the end of the 90's Fibre Bragg Grating (FBG) have been the most widely used system. It is often used as the reference and/or example for fibre optic measurements and will also be used for that in this thesis. Its advantages are its user-friendly systems with well developed software, fairly high sample rate and well documented performance. Compared to the system used in this thesis the main difference is that it is a point sensor with normally up to 10 sensors per channel with e.g. 3-5mm length, where the OBR have distributed sensing with up to 10 "sensors"/data points per cm. The details will be further discussed in chapter 5.2. Despite the OBR system is more labour intensive due to some fabrication of the sensor and post processing, the price difference of the sensors is still huge. The price per FBG sensor, independent of how many on the fibre, is approximately 900NOK ex. VAT, where as the price of the measurement fibre used in this thesis is approximately 40NOK ex. VAT per meter. With connectors it is a "sensor"/data point price, included connectors (that may be reused), of 0,8NOK

Features listed by Kreuzer in [1] about advantages for FBG sensors are valid for other fibre optical systems as well:

- FBG match fairly well with composite materials and may be either embedded or bonded to the surface as normal strain gauges.
- When embedded strain could be measured at any desired layer of the composite.
- FBG can measure very high strain (>10 000 με)
- FBG are small sized (<250 με) and lightweight.
- FBG are immune to electromagnetic interference.

- FBG are intrinsically passive.
- FBG signals are not distance-dependant.
- The long-term stability is very high for fibre optic cables.
- Special versions of fibres may be used at very high temperatures (>300°C)
- Very low magnetic field interactions.

Weaknesses are of course existing:

- FBG is temperature dependant, hence temperature compensation is necessary.
- The gage factor is only approximately k=0,8.
- FBG is sensitive to non-axial forces, which may lead to disturbance of the signal.
- The bending radius of the fibre must be >10mm, hence a rosette will be quite large.
- The sensing fibre core is distanced to the host by coating.
- Interrogators are still expensive.

4.2 Co-Patch

Co-Patch, or Composite Patch Repair for Marine and Civil Engineering Infrastructure Applications is a project co-ordinated by National Technical University of Athens (NTUA) with 15 partner organizations, funded by the European Commission under the seventh framework (FP7).

With inspiration from composite patch repair in aerospace industry, the project aims to develop a novel, effective repair/reinforcement method for defects in large steel structures. With several industrial stakeholders the project ultimately seeks to develop an internationally recognised training programme for personnel to examine, certificate and repair defects with composite patches. An abbreviated list of project aims and advantages of composite patch repair is made by NTUA [2]:

Project aims

- To demonstrate that composite patch repairs or reinforcements can be environmentally stable and can be used as permanent repair measures on large steel structures.
- To show that composite patch repair technology is an innovative and highly competitive product that caters to the needs of marine vessels and civil engineering infrastructures, the latter in the form of steel bridges.
- To demonstrate the reduction in maintenance costs and extension of design life of many large steel structures.
- The give the project partners the capability of providing high technology and high added value services worldwide, thus improving Europe's competitiveness in specialized and advanced repair work.

Advantages of composite patch repair

- Composite patch repairs and/or reinforcements overcome many disadvantages of the traditional repair methods.
- They do not involve hot works in any way and, therefore, existing deadweight loading and proximity to explosive environments have no particular consequences.
- Patches can be applied directly on corroded steel members by performing a simple surface preparation.
- They can be completed faster.
- They exhibit good fatigue resistance.
- They do not cause stress concentrations.
- They result in low added weight.

The project is divided in seven work packages, where NTNU is responsible for work package 2 – Monitoring (WP2). Different partners are using different measurement systems for the monitoring of tests where for two of the tests presented here three different systems are used. The OBR 4600 is NTNU's chosen monitoring system where all procedures and tools are developed as a part of the project work and this thesis. Different systems for NDT and Structural Health Monitoring (SHM) have pros and cons, and will at the end of the Co-Patch project be evaluated for future use in monitoring of patch repairs.

4.3 Health monitoring

Health monitoring of structures is a technology that is developed in parallel to the constant evolution of even more optimized products. The industry develops new materials and designs that is pushing the limit of structures and it is therefor important to monitor the health of the structure before a potential catastrophic failure. Earlier most of this monitoring was either not performed, visually or by inspectors with NDT equipment at time intervals. Today new sensor technology is able to be a part of the structure just like the nervous system in the human body. Still considerable work has to be done during design of each system to analyse the structure and damage response in order to interpret the sensor output. The goal is to develop systems that will tell the user if the structure is damaged, where and how severe.

Different structures and applications will of course need different sensors and setups. In this thesis it is presented some information about the SHM theories and components as well as how fibre optic strain measurements may be used for SHM in composites. The different lessons learned about utilizing fibre optics in composites, precautions to take, possibilities and extensive experimental work with the OBR 4600 to investigate behaviour of composites using fibre optical strain sensors is presented in this thesis.

5 Theory

5.1 Adhesion

A complete theory about adhesive theory is outside the scope of this thesis, but the fundamental elements and physics of bonding will be necessary for the understanding of the experimental work of the thesis. For the Co-Patch project the different elements of composite patching of steel is treated by the different partners and their analyses. The following is written as a summary of relevant theory from the book "Handbook of Adhesion Technology" by da Silva et al. [3]

An adhesive may be defined as a material which when applied to surfaces of materials (adherend) can join them together and resist separation. The ability of the adhesive to resist separation or failure is dependent of several elements: Surface preparation (Roughness, cleaning, chemical primer, etc.), wetting and spreading of solids, adhesive composition, environmental effects, and geometry of adhesive/adherend. The adhesives used during manufacturing of the specimens in this thesis are in the group of step-growth polymerization AICP (Adhesives Implemented via a Chemical Process), namely epoxy and vinyl ester. A pressure-sensitive adhesive (PSA) have successfully been used for the bonding of fibre to the surface of specimens.

5.1.1 Adhesion theories

To describe the theory of adhesion several theories have been developed through the last century and it is necessary to describe the different processes and parameters of adhesion. It is argued in the handbook that these classical theories are best regarded as emphasizing a different aspect of a more comprehensive model developed in the later years. For a thorough investigation instruments available today like electron microscope and atomic force microscope are able to measure the surface-free energy of a material. Surface-specific information may be provided with X-ray photoelectron spectroscopy, Auger electron spectroscopy and time-of-flight secondary ion mass spectrometry. It is argued in the handbook that this is essential for adhesion investigation due to the forces responsible for adhesion to operate over very short length scales. Neither of these instruments have been utilized in this project, hence only the classical theories will be discussed here.

To make an adhesive joint fail, energy must be supplied to break the bonds to make the joint fail and create two new surfaces. These bonds are considered to be either primary or secondary bonds. Accordingly, either: covalent bonds, with dissociation energies in the order of hundreds of kilojoules per mole or van der Waals bonds with dissociation energies in the order of tens of kilojoules per mole. This does necessary imply that an adhesive bond with primary bonds are the strongest. The energy required to form new surfaces in an adhesive joint is surface energy. This is defined as the work of adhesion and for a failure between material 1 and 2 given by equation (1), where γ_1 and γ_2 are the respective surface energies of the materials, and γ_{12} is the interfacial energy between 1 and 2.

$$W_A = \gamma_1 + \gamma_2 - \gamma_{12} \tag{1}$$

In practice, the magnitude of the fracture energy, G, is bigger than the surface energy term W_A, now written as G_0, due to other energy-absorbing processes during the fracture process. This gives equation (2) for fracture energy per unit area, where ψ is the other energy-absorbing processes, such as plastic- and viscoelastic deformation. The loss term, ψ, is much larger than G_0, but are coupled such that an increase in G_0 will increase the ψ. For some mechanically simple adhesive bonds, this is stated to be directly proportional.

$$G = G_0 + \psi \tag{2}$$

The fracture stress of an adhesive bond is dependant of the fracture energy. It is given by equation (3), where k is a constant, l is the length of the critical crack, which leads to fracture and E, is the effective modulus:

$$\sigma_f = k(EG/l)^{1/2} \tag{3}$$

Four theoretical models are reviewed in the Handbook of Adhesion Technology, and they will here be presented in short. The *adsorption theory* have the essential idea that when a liquid adhesive comes into molecular contact with a solid substrate there will be forces of attraction between them. The forces will be depending on the chemical nature of the surface of the materials. Several studies discuss what type of bonds that is formed, but it is agreement that there will be physical- or chemical adsorption and at least London dispersion forces.

The *mechanical theory* emphasises and explains how surface roughness is an important factor in adhesion. The texture of the surface may be natural, or a result of pre-bonding treatment. A rough surface will have a larger surface area for the adhesive to bond to, and according to equation (1) the free surface energy will increase accordingly. Surface preparations have for the Co-Patch project two purposes: Removing old paint, corrosion and grease and to give a suitable surface roughness for optimal adhesion. Despite increase in roughness have proven to give increased strength, this will not be achieved without proper wetting and spreading. A good wetting is observed when the liquid adhesive will have a low contact angle when applied on a surface, e.g. water on a steel surface. A 0° degree angle will indicate spreading, where as more than 90° degrees, e.g. mercury on glass, is considered as “poor wetting”. Good wetting, or spreading of the adhesive is crucial in forming a good bond and gives the molecules the opportunity to form adhesive interactions. Good wetting will also help ensuring filling of interstices and decrease stress concentrations at the adhesive border.

For the record, the handbook also presents the *Electrostatic theory, Diffusion theory* and *Weak-Boundary-Layer theory*, but because they are not given much interest in todays research or have any relevance to this thesis no further presentation will be given.

5.1.2 Adhesive joints

The adhesive joints in the Co-Patch project have, in addition to the load carrying and durability, a requirement and aim to arrest the crack growth of the host material. This implies that a high stiffness of the patch and adhesive might be important. This contradicts somewhat the preferred adhesive joint design rules. The factors that affect a joint strength are presented in the Handbook of Adhesion Technology, and will be shortly summarized here as a basis for discussion of the results from the experimental work. When discussing failures, the different failure modes and locations are presented in Figure 1.

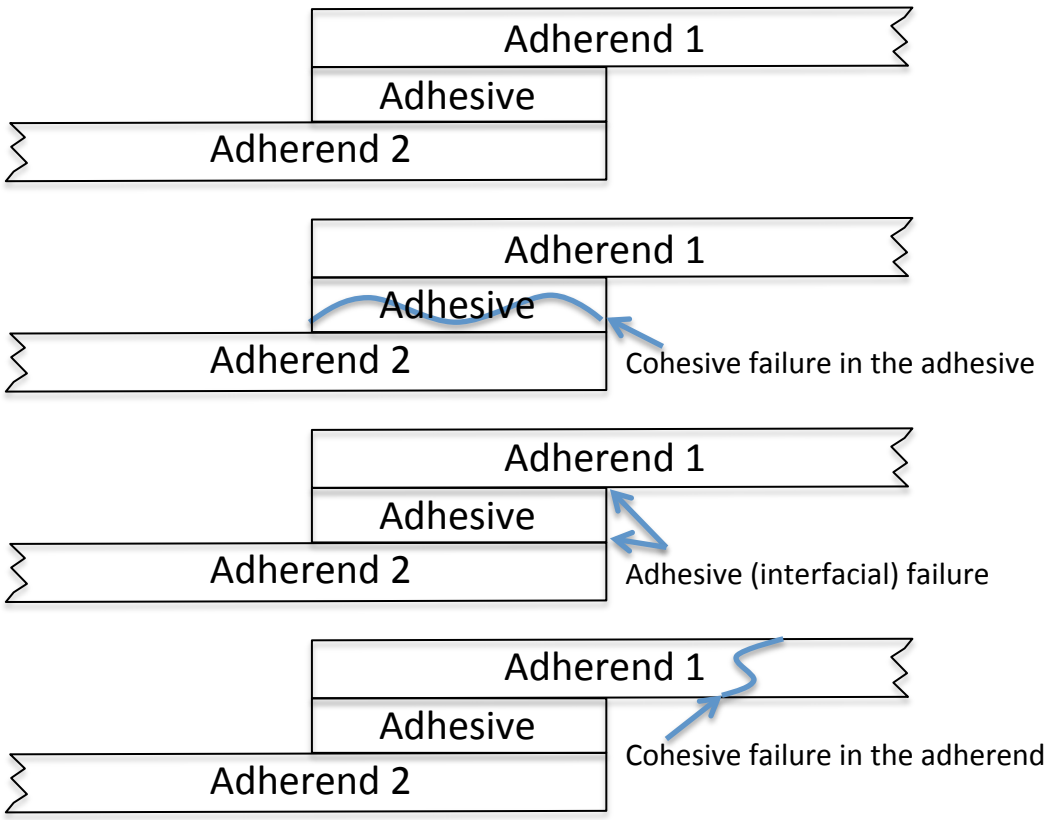

Figure 1 Examples of cohesive and adhesive failures.

The adhesive properties that are interesting for an adhesive joint are the strength, ductility and stiffness. A low strength, but high ductility will distribute the stress more uniform along the overlap and deform plastically during loading. The load is distributed over the length of the joint, which makes it more resistant to crack propagation and increases the fatigue strength. A brittle adhesive will have higher stress concentrations at the ends of the overlap as well as a concentrated shear transfer. Figure 2 illustrates the difference in stress distribution with a stiff or flexible adhesive, and Figure 3 illustrates how the ductility of the adhesive will affect the stress distribution along the overlap during loading.

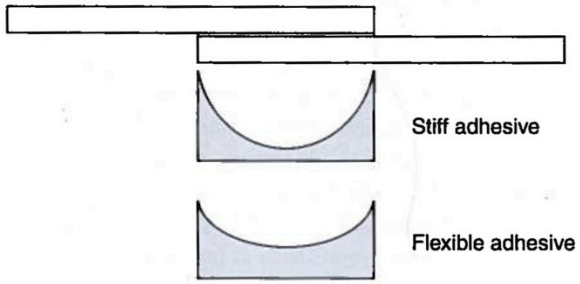

Figure 2: Effect of adhesive modulus on the adhesive stress distribution. From [3].

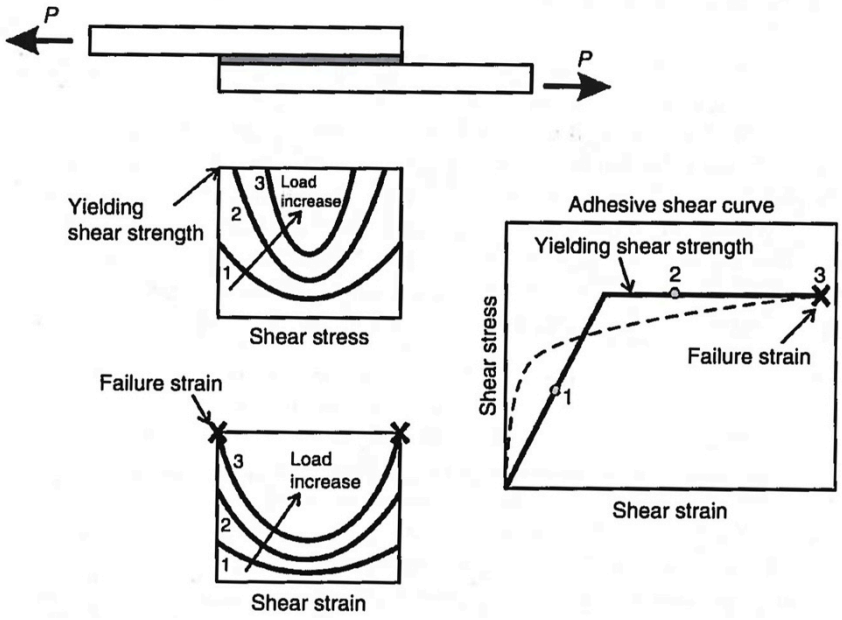

Figure 3: Effect of the adhesive ductility on the stress distribution in an adhesive joint. From [3].

The adhesive thickness will also be determining the stress distribution. A thicker bondline will have a more uniform stress distribution, where the thin will reach yielding stress at a lower load. However, when yielding does occur in a thicker joint, there is a less "elastic reserve" to sustain further loading, thus yielding spreads more quickly. Most research agrees that a thick bondline reduces the joint strength.

The modulus and the strength of the adherend have a big influence on the joint strength. As for the adhesive, a more ductile adherend will allow deformation in the load-transferring zone without cracking. For a metallic adherend, yielding can cause premature failure; hence it is the adherend yielding that controls the failure. For composite laminate adherends, the through-thickness strength is very low, and an interlaminar fail will make the joint fail. High peel stresses at the joint end must therefor be reduced with e.g. tapering of the adherend. Similar longitudinal stiffness of the adherends is recommended to reduce nonuniform stress distribution.

The effect of increasing the overlap length depends on the type of adhesive and the adherend yielding strength as well as the combination of them. For elastic adherends and ductile adhesives, the joint strength is approximately proportional to the overlap, due to effective redistribution of the stress during loading. For that case the failure criterion is the global yielding of the adhesive. For adhesives with intermediate ductility, the adhesive fails due to high adhesive shear strain at the ends. For elastic adherends and brittle adhesives, the joint strength reaches a plateau due to stress concentrations at the joint ends. Increase of the overlap length will then not alter the stress distribution. For adherends that yield, a maximum load plateau will be reached and the failure is dictated by the adherend yielding.

Residual stresses in the joint will be created if the adherends have different coefficients of thermal expansion. The thermal mismatch will lead to a decreased joint strength. The residual bond stresses are especially concentrated at the ends of the joint. This would lead to one end having positive and the other negative shear stresses, as illustrated in Figure 4.

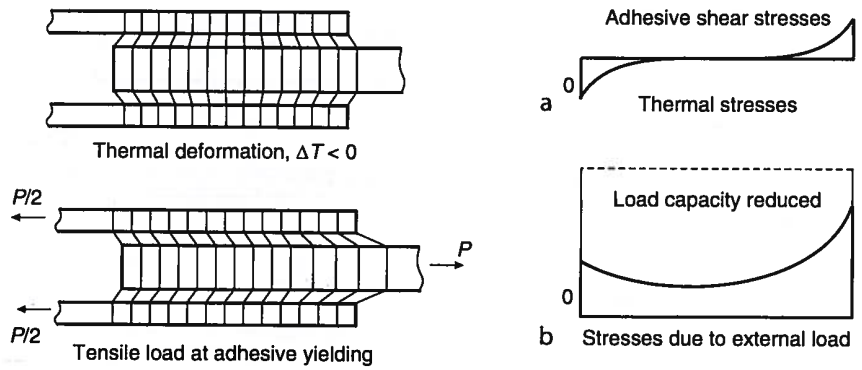

Figure 4: Adhesive shear stresses in a metal/composite double-lap joint. From [3].

According to the knowledge about the factors affecting the joint strength, it is the ends of the joint that will need improvement to increase a joint strength. The load transfer will need to be spread as much as possible to reduce the shear stress as illustrated in Figure 5. For a joint with two solid adherends it is suggested several different techniques to change the geometry of the adherend and adhesive at the ends. Tapering of the adherend is suggested as excellent methods to reduce the peel stresses at the ends of the overlap. For the Co-Patch project with metal/composite joints, the composite is built up on the steel prior to curing. Hence the choices of tapering geometry are limited, but an outside taper, as suggested in the handbook, are used. Three different tapering designs are proposed in the handbook, as seen in Figure 6.

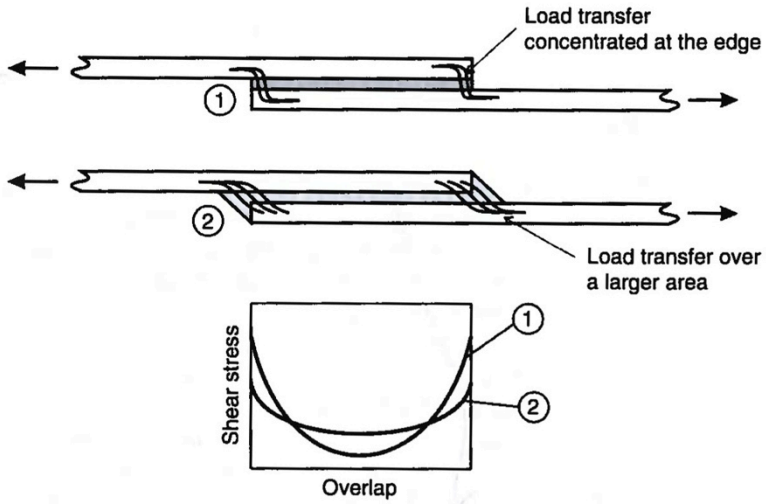

Figure 5: Load transfer and shear stress distribution in single-lap joint. From [3].

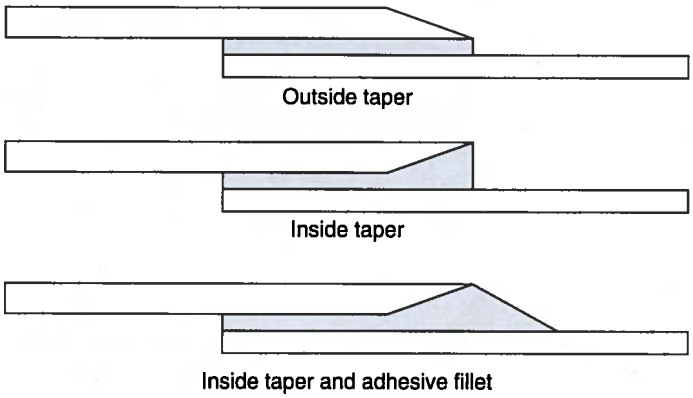

Figure 6: Adherend shaping in joint design. From [3]

5.2 Fibre optic strain measurement

Regardless of the fibre optic strain measurement system used, there are several physical effects influencing the measurements as well as the structure. For any measurement systems it is critical to know the boundary conditions and possible interference to the system. Here is outlined some research in the area of strain transfer from the host to the measurement fibre and possible degradation of the composite. First some theory about the fibre optic cable:

5.2.1 Fibre optic cables

Fibre optic measurement is using a single mode fibre optic cable for both transmitting the signal as well as being the sensor. Hence it is the physical properties of the fibre and the transmitted light that is utilized in these systems. Fibre optic cables are able to transmit light in a curved cable by utilizing the phenomenon of total reflection. It is simply that when light hits the interface between two mediums it will be totally reflected if the angle of incidence is greater than the critical angle. This is determined by the refractive index (n) of a medium, and given by [4]:

$$\phi_c = \sin^{-1}\left(\frac{n_2}{n_1}\right) \tag{4}$$

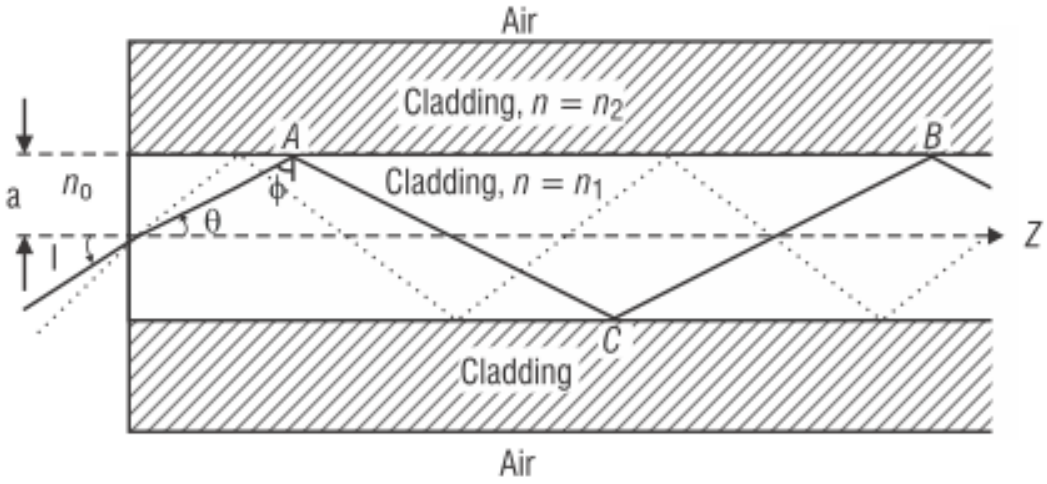

Figure 7: Illustration from [4] showing the core and cladding of a fibre and the notation for (4).

It follows from (4) that, depending of the composition of the fibre, bending the fibre decreases the angle of incidence and hence a too small radius will result in signal losses. Manufacturers therefor produce fibres with high bending tolerances for special applications. The long-term minimum bending radius of the measuring fibre used in this thesis is 17mm to ensure no signal loss. With lower radius there will be a signal loss, but for sensing applications that is normally not a problem.

Small radius bending of the fibre is not only occurring in macro scale by handling and placement, but also in micro scale. Different scenarios during embedding in composites and adhering to a structure, micro-bends could be introduced. This is in many cases a source of noise and a problem, but is also utilized in sensor technology. Knowles et al. describes a fuel quantity sensor for aircrafts in [5] where they create micro bends with two serrated plates. It has also been done research on a damage detection sensor by simply embedding the fibre in a composite laminate and investigating the signal loss in [6].

For the fibre optic cable the mediums are silica core and silica with a different composition and slightly lower reflective index around it. The fibre is built up as illustrated in Figure 7. Most fibre is in addition to the cladding, coated with a coating suited for the application for which the cable is going to be used. The coating will for example give it colour, protect it against chemicals, enhance bonding, etc. The coating may even be built up of several layers of different polymers and fibre reinforcements when the fibre is used for e.g. telecommunication to give it mechanical strength, but that will not be discussed here.

5.2.2 Shear transfer

The adhesion and shear transfer between the fibre and the host material or adhesive are vital to obtain correct measurements. The theory concerning this is

similar to standard adhesion theory, except that the boundary conditions are slightly different than normal. When embedded the fibre is surrounded by the adhesive, and when glued to a surface the circular shape of the fibre is not giving an ideal contact surface. Different research have been done in this field, both for FBG sensors with special coating developed for civil structures [7] as well as a generalized case with fibre embedded in an host material. Zhou develops models for their multi layer coated sensors in [7], where thin (less than 10mm) CFRP coated sensors is found to have an error rate of less than 2,5%.

Duck and LeBlanc [8] have outlined a method to predict in-fibre-strain for a two layer system as illustrated in Figure 8. The model is for a continuous sensor with a radius r, and for a surrounding coating material with a radius R. The surrounding coating has a strain field with an axial variation $\varepsilon_z^m(R,z)$ experienced at the surface and hence $\varepsilon_z^f(r_f,z)$ is the measured strain field.

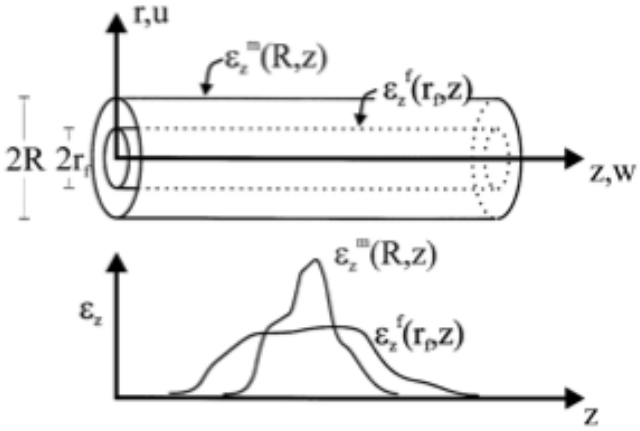

Figure 8: Strain transfer from a host material to a fibre optic sensor.

From Duck and LeBlanc [8].

The expression presented by Duck and LeBlanc is given with respect to $k = 1/\lambda_s$ and R, where k is the wavenumber and λ_s the spatial wavelength. The wavenumber is the number of wavelengths per unit distance (here: meter), hence the width/length of a strain peak in z-direction.

$$\hat{\varepsilon}_z^m(R,k) = \int_{-\infty}^{\infty} \varepsilon_z^m(R,z)\exp(-2\pi ikz)dz \tag{5}$$

$$\overline{\varepsilon}_z^f(z) = \int_{-\infty}^{\infty} H(k)\hat{\varepsilon}_z^m \exp(2\pi ikz)dz \tag{6}$$

From equation (5) and (6) it is presented in [8] different scenarios illustrating how k affects the shear transfer and hence the accuracy of measured strain in the fibre. These curves are presented in Figure 9.

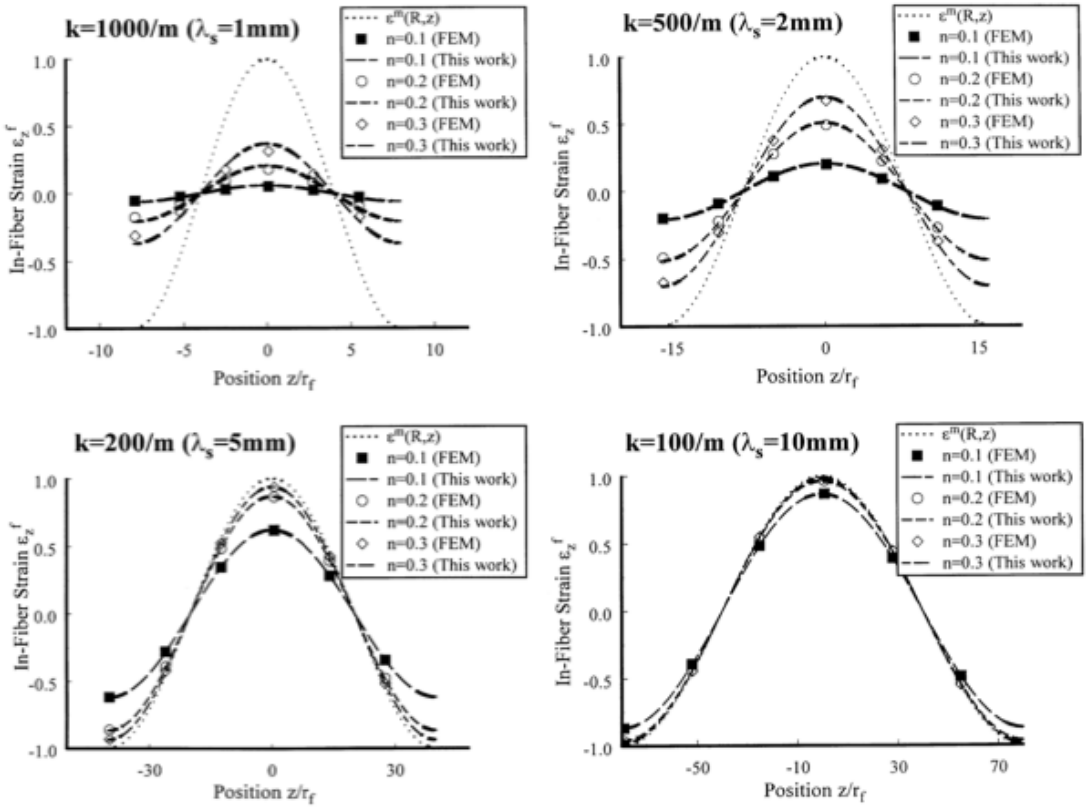

Figure 9: Transfer of a single period of a harmonic $\varepsilon_z^m(R,z)$. From [8].

It is easily seen from Figure 9 that too short wavelengths lead to a mismatch between the fibre- and host strain field. It is also visible that it is a tendency of improved strain transfer from higher n. The shear-lag parameter, n, is defined for single-fibre model composites by Galiotis in [9] with models from Cox [10] as well as experimental work. The shear-lag parameter is most commonly used in a method for prediction of stress transfer characteristics in composites. The shear-lag method was originally presented by Cox [10] and n is derived by him as β in equation (7).

$$\beta = \left(\frac{2G_m^R}{r^2 E_f \ln(R_{Cox}/r)} \right)^{1/2} \tag{7}$$

In (7) G_m^R is the shear modulus of the matrix cylinder of radius, $R_{Cox,}$ which is defined as beyond the influence of the fibre upon the deformation of the matrix. The radius and modulus of the fibre is respectively r and E_r. The shear modulus is affected by interface chemistry of the fibre and the matrix, e.g. surface treatment, materials, fibre sizing, presence of matrix oligomers, etc. [9].

Okabe further developed Ducks' model in his work to detect cracks in CFRP using FBG [11]. A multiple-cylinder model was proposed to increase the accuracy of the strain transfer. Duck's model is simplified to omit axial stresses in the soft polyimide coating, where Okabe's model is useful if the stiffness of the coating is similar to that of the fibre. For polyimide coating, he shows that Duck's model and his agrees well, as seen in Figure 10.

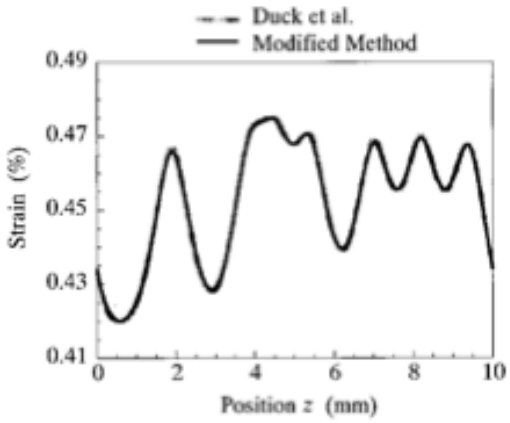

Figure 10: Strain distribution calculated by Okabe's modified method and Duck's method for polyimide coated FBG sensor. [11]

For the detection of transverse cracks in composites in [11], Okabe also investigates the difference between coated and uncoated fibre by calculations and experiments. His calculations confirm what is intuitive, that coated fibre will give a smoothened and sometimes attenuated strain distribution. This is seen in his example in Figure 11a, but Okabe concludes what is seen in the scenario presented in Figure 11b, that the coating does not prevent crack detection in composites even with high saturation of cracks. The calculations were also confirmed experimentally. In the experiments the difference between the coated and uncoated was higher, and was suggested to be non-axisymmetric stresses that is relieved by the coated fibre. These stresses are suggested to be from thermally induced internal residual stresses in the laminate by post curing or in cured prepreg. This is not considered in the uniaxial calculations of Okabe. This is further discussed by Martin and Guemes in [12] and is indicated to be interesting in future SHM application. Then the distortions of the signals are interesting for damage detection and not simple strain measurements.

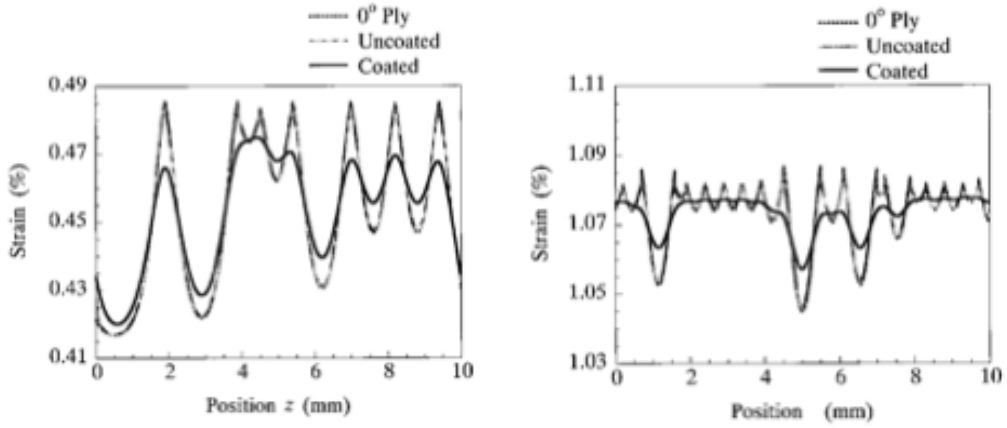

Figure 11: Strain distribution calculated for a 0 degree layer, coated- and uncoated fibre in longitudinal direction. (a) With an average tensile stress of 359MPa. (b, right) Average tensile stress of 815MPa. [11]

5.2.3 Degradation of laminate strength and stress concentrations caused by fibre optic sensors

Studies have been performed by Levin [13] in his doctoral thesis on "Durability of embedded fibre optic sensors in composites" to investigate possible degradation of composites with embedded fibre optical sensors. He did not discover any degradation in strength of fatigue life of the composite and did not find any premature failures caused by the optical sensors. His work shows that embedding fibres along the fibre direction of a laminate is recommended, as seen in Figure 16, chapter 6.1. Embedding transverse to the fibre direction will induce a resin rich layer if fibre sensors are embedded by less than approximately 1mm spacing. When more than 1mm there will only be a resin "eye" around the fibre.

The effects on the stress-/strain field in the laminate caused by the introduction of the fibre sensor are discussed by several authors. According to Levin [13] the local geometry of the embedded sensor will induce local stress concentrations. When mechanically loaded or as a result of temperature or moisture this could ultimately lead to debonding at the interface due to a complex stress field. This would of course lead to wrong sensor output.

In the doctoral thesis of Etches [14], several publications about possible degradation of the composite are presented. The conclusion indicates that neither research has proven a significant reduction of strength in a tensile test, but several authors agree that fatigue life may be reduced. As in static, it is when the fibre is embedded non-parallel to reinforcement fibres or in an interface between two layers of different orientation that degradation is most noticeable.

For a transverse loading situation, it is seen in the numerical example from the model developed by Balać et al. [15] that for a 125 µm fibre in a 1mm CF laminate the nominal stress increases by 40% next to the fibre in the plane direction (x-direction). The stress level is reduced to a 10% increase, 200 µm from the fibre. In the out of plane direction (y-direction), there is a 20% compression due to Poisson effect. As seen in Figure 12, the peak values are not experienced on the boundary surface, and his conclusion is that the fibres will not compromise the strength of the composite laminate.

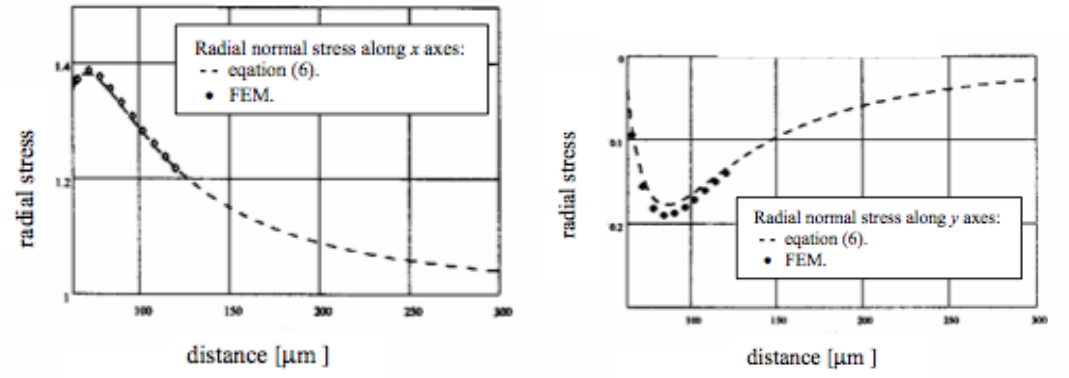

Figure 12: Increase in nominal stress for a CF laminate with an embedded fibre loaded in transverse direction. From [15]

5.2.4 Temperature and strain sensitivity

All types of fibre optic sensors are affected by strain and temperature simultaneously, according to equation (8). How they are affected is fibre dependant. This means that the sensor system is capable of both strain and temperature sensing, but unfortunately for us, either has to be isolated by us in the measurement setup. The following equations are from [1], but somewhat modified for our use.

$$\frac{\Delta\lambda}{\lambda_0} = k \cdot \varepsilon + \alpha_\delta \cdot \Delta T \tag{8}$$

In equation (8), $\Delta\lambda / \lambda_0$ is the output from the interrogator, where $\Delta\lambda$ is the wavelength shift and λ_0 is the initial wavelength. In (9) the following is given:

$$\varepsilon = \varepsilon_m + \varepsilon_T \tag{9}$$

The strain is caused by both mechanical force ε_m and temperature ε_T. Where ε_T is given by the thermal expansion of the measured system:

$$\varepsilon_T = \alpha \cdot \Delta T \tag{10}$$

This leads to the general equation:

$$\frac{\Delta\lambda}{\lambda_0} = k(\varepsilon_m + \alpha \cdot \Delta T) + \alpha_\delta \Delta T \tag{11}$$

For the measurement fibre used in this thesis the constants in (11) are given in Table 1. Also presented are approximated thermal expansion constants α for different materials. For the general case the notation α_{sp} is used for the expansion constant of the specimen material. For a measurement setup these will have to be defined for the specific materials used.

Table 1: Approximated constant values for strain and temperature calculations.

Constant	Description	Value
k	Gage factor	$6{,}67 \cdot 10^{-6}$
α_δ	Change of refractive index	$0{,}725 \cdot 10^{-6} / K$
α_{glass}	Expansion coefficient glass	$0{,}55 \cdot 10^{-6} / K$
α_{steel}	Expansion coefficient steel	$11 - 13 \cdot 10^{-6} / K$
α_{carbon}	Expansion coefficient carbon fibre	$-0{,}6 \cdot 10^{-6} / K$
α_{GF}	Expansion coefficient glass fibre	$6 \cdot 10^{-6} / K$

Depending on the setup different equations may be derived. For pure temperature sensing without straining the fibre the thermal expansion of the glass in the core of the fibre will be present in equation (12):

$$\frac{\Delta\lambda_{air}}{\lambda_{0air}} = (k \cdot \alpha_{glass} + \alpha_\delta)\Delta T \tag{12}$$

For a sensor bonded to a specimen, e.g. steel, and exposed for both strain and temperature equation (13) will be valid. Then the expansion of the steel will be governing, and the expansion of the glass will be neglectable.

$$\frac{\Delta\lambda_m}{\lambda_{0m}} = k \cdot \varepsilon_m + (k \cdot \alpha_{steel} + \alpha_\delta)\Delta T \tag{13}$$

To compensate for changes in temperature the most recommended method are to bond a sensor to a part of the structure that experience the same temperature changes, but not the mechanical strain. That will result in measurements according to equation (14).

$$\frac{\Delta\lambda_c}{\lambda_{0c}} = (k \cdot \alpha_{sp} + \alpha_\delta)\Delta T \tag{14}$$

The equation for mechanical strain in the specimen may then be derived from (13) and (14) as in equation (15):

$$\frac{\Delta\lambda_m}{\lambda_{0m}} - \frac{\Delta\lambda_c}{\lambda_{0c}} = k \cdot \varepsilon_m$$

$$\varepsilon_m = \frac{1}{k}\left(\frac{\Delta\lambda_m}{\lambda_{0m}} - \frac{\Delta\lambda_c}{\lambda_{0c}}\right) \tag{15}$$

For a situation where it is no position on the specimen without an area not strained, a similar specimen that is not strained may manufactured and be positioned to experience the same temperature changes with a sensor bonded or embedded. If this is not feasible or it is not desired to isolate the thermal strain one should at least subtract the influence from the change in refractive index of the fibre caused by the temperature by having a unstrained sensor attached close to the specimen. For the OBR 4600 system this could be accomplished by simply having some of the measurement fibre not bonded or embedded in the specimen.

5.2.5 Measurement technologies

Many different sensor technologies have been developed the last three decades based on fibre optic technology, which are utilizing the different physical properties of optical fibres. Examples are pressure sensors, liquid level sensors, hydrophones, vibration sensor, acceleration sensor, etc. [16]. In this thesis it is the strain and temperature sensing that will be presented, and even within this area several different technologies are developed. It is not within the scope of this thesis to review all the different strain measurement systems, but suggested reading would be e.g. [16]

The different measurement systems are normally divided into point measurement and distributed measurement systems. The point measurement systems as the FBG systems can be so-called quasi distributed by introducing several gratings into the fibre optic cable. This indicates that the location and number of grating must be specified and specially ordered for the measurement situation. The number of gratings is limited to the wavelength range of the interrogator. Normally this is limited to about 20 sensors, but research by e.g. Voisin [17] demonstrates systems capable of up to 35 sensors.

Distributed sensing systems was developed from the early beginning of fibre optical sensing, but despite that the sensor could be more than a kilometre long they could at that time only provide a spatial resolution from one to a few meters [16]. The different distributed sensing systems are based on measurement of backscattered light in the fibre caused by interactions between emitted light and the optical fibre. Different physical effects causes different backscatter, as illustrated in Figure 13 and further explained in [18] by Güemes et al. In this

thesis the distributed sensing system OBR 4600 is used, which is measuring the Rayleigh backscatter.

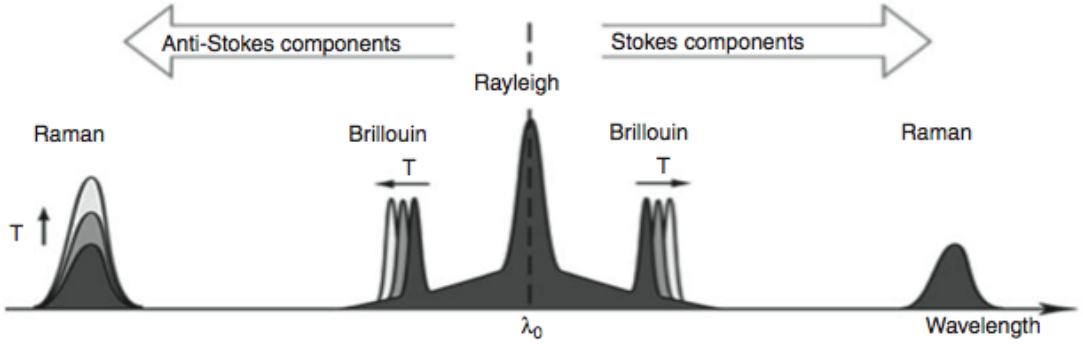

Figure 13: Wavelengths of backscattered radiation from [18].

5.2.6 OBR 4600 – Distributed fibre optical strain measurement system

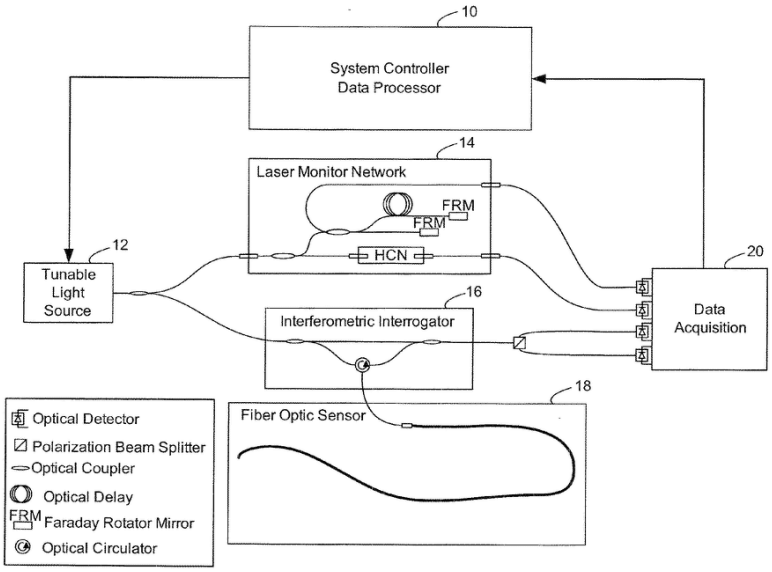

Figure 14: Example of an OFDR-based distributed strain sensing system. From patent publication number: US 2011/0317148 A1.

Out of the box, the OBR 4600 consists of an interrogator and a laptop with a system controller/user interface, but it consists of several components in a setup illustrated in Figure 14. The Optical Backscatter Reflectometry system (OBR) consists of a tuneable laser source (12) and an Optical Frequency Domain Reflectometer (OFDR) (20), used to measure the Rayleigh backscatter, in an interferometry setup (16), [19]. Interferometry enables the system to measure the amplitude and the phase of the Rayleigh backscatter and with the help of Fourier transform [20] they are able to get information about changes in the backscatter profile and the position along the length of the fibre [21]. The use of multiple wavelengths in swept wavelength interferometry (SWI) enables the system to achieve high spatial resolution of the measurements. The accuracy of the system is achieved with the laser monitor network (14) that serves as an absolute wavelength reference by using a gas cell, e.g. hydrogen cyanide (HCN) cell.

The Rayleigh backscatter profile of fibre optic cables is a result of a heterogeneous reflective index, randomly distributed along the length of the fibre. This is a result of the manufacturing of the fibre and is unaltered until any external stimulus (like strain) causes a temporal and spectral shift locally in the backscatter pattern [19]. These shifts are used to calculate the changes in strain along the length of the cable when compared to the unstrained reference state. The degree of changes in mechanical properties along the length could be observed in a calibration experiment in this thesis where it is causing variations in strain level when tensioned in air. The curves from this experiment are found in appendix 14.5.1.

The maximum length that is feasible to measure with the OBR is given by the physical properties of the system, and as discussed in [20], increasing the length it will eventually be higher noise level in the system than the Rayleigh backscatter. Today the interrogator has two modes, namely 30 and 70m sensing range.

5.3 Structural health monitoring

The basic concept of SHM is fairly easy to interpret and is analogous to the nerve system of humans. SHM are widely investigated in many disciplines of engineering. Bridges, dams, ships, defence, but especially aerospace have all high payoffs for SHM since damage may lead to catastrophic failures. According to [22] in 1999, about 27% of the life cycle cost of an aircraft was spent on inspection and repair. Hence it would be very lucrative to develop a system that could reduce this cost, and this is probably why numerous technologies are proposed in different publications.

Currently it is non-destructive testing by trained personnel that perform the inspection of structures during maintenance. The SHM philosophy is to have a system that is a part of the structure and is able to detect and interpret changes in the structure. The ultimate goal is according to Menendez et al. [23] to: a) Reduce weight by means of structural optimization, b) Reduce number and cost of non-scheduled inspections, and c) To eliminate current schedule-based inspections and replace it with condition-based maintenance.

5.3.1 Classification of SHM

It is normal to divide the systems into live measurements, either with local logging or with transmission of the results, or a system with an external measurement unit used during inspection, but with in-situ sensors. In both cases the SHM could be divided into different layers according to the depth of the diagnosis of the structure are proposed by Menendez et al. in [23], and are similar to the levels proposed by Rytter in [24]. Higher levels increase the complexity of the system where level 4 is a part of the ultimate goal c) listed above:

- **Level 1:** Determination of damage existence.
- **Level 2:** Determination of the geometry of damage.
- **Level 3:** Quantification of the severity of the damage.
- **Level 4:** Prediction of the remaining life of service.

To develop a SHM system several components must be prepared and defined. Kessler and Spearing [25] divides it into the following categories:

- **Architecture:** The physical layout of the components, the critical areas, choice of real time or not, sensor density, etc.
- **Damage characterization:** The foundation of the damage detection. Knowledge about what damages to be detected and what changes will be measured from these damages. Basis for choice of sensor.
- **Sensors:** Used to measure variables on a structure that is linked to damage development, such as strain, sound waves, pressure, temperature, etc. Depending on the situation, various sensors would be needed due to their different advantages and characteristics. A summary made by Kessler and Spearing could be seen in [25]. In addition to those listed, there are constantly new sensor technologies developed, such as Carbon Nano Tubes (CNT) based sensors[26], microwave sensors, "Smart coatings", Comparative Vacuum monitoring, etc. Different types of fibre optic sensors, that are relevant to this thesis, are discussed in chapter 6.2.5.
- **Computation:** Different levels of computation are needed in a SHM system. Locally the analog signal from the sensor must be converted to digital as well as data storage. Either locally or globally algorithms need to analyse the results and assess the severity of changes in measurements. Failure predictions, severity and location may be presented to an end-user.
- **Communication:** Important for an implemented SHM system will be communication between the components. Communication between sensor locations on a structure could be important for redundancy and verification. Communication from sensors to the processing unit, and to end-user should be designed.
- **Power:** Depending on the application the power needed for the sensor system should be considered. If the sensors need individual power supply, like piezo actuators, wiring would be needed.
- **Algorithms:** Essential for a working SHM system is well developed algorithms. They would interpret the signals and analyse the structure before presented to the user. Parts of the algorithms would be specially designed for the system after analyses and/or small-scale tests giving knowledge about expected damage progress.
- **Intervention:** A potential future of a SHM system would be to include some sort of intervention mechanism. Either by being able to control material properties, like for shape memory alloys, or if possible reducing the applied load of the structure.

Instead of listing what should be included in a SHM system, or adapting such a list to different structures, Worden et al. [27] have developed from literature from the last 20 years some accepted general principles. They have proposed a set of axioms to be used as fundamental truths in discussions and to give researchers a starting point in SHM. All the axioms are further derived in [27].

Axiom I: All materials have inherent flaws or defects.
Axiom II: The assessment of damage requires a comparison between two system states.
Axiom III: Identifying the existence and location of damage can be done in an unsupervised learning mode, but identifying the type of damage present and the damage severity can generally only be done in a supervised learning mode.
Axiom IVa: Sensors cannot measure damage. Feature extraction through signal processing and statistical classification is necessary to convert sensor data into damage information.
Axiom IVb: Without intelligent feature extraction, the more sensitive a measurement is to damage, the more sensitive it is to changing operational and environmental conditions.
Axiom V: The length- and time-scales associated with damage initiation and evolution dictate the required properties of the SHM sensing system.
Axiom VI: There is a trade-off between the sensitivity to damage of an algorithm and its noise rejection capability.
Axiom VII: The size of damage that can be detected from changes in system dynamics is inversely proportional to the frequency range of excitation.

5.3.2 SHM with fibre optics

Martin and Güemes establishes in [12] three principles for SHM analysis for FBG monitoring after experience from embedded sensors in composite laminates:

1. Global strain perturbation in a loaded structure.
2. Perturbations in local strain fields, that promotes spectral distortions in close FBGs.
3. Transverse stress release, that promotes birefringence effects in nearby FBGs.

Number one is well known and the intended use of a standard FBG system. The two other are presented because they have investigated the need to analyse the full spectrum and that a peak detection system is not sufficient. Martin and Güemes have successfully demonstrated such spectral distortions from FBG's embedded along the bond line of flanges of two hat stringers on a test panel from an AIRBUS fan cowl.

Several research projects have been conducted in damage detection using fibre optical sensors. For composite structures it is mostly in the aerospace industry, and some for windmill blades. Examples of such publication are [28-32]. Damage detection for composite patch repair, which are relevant for this thesis, are investigated in e.g. [33-35]. In [34, 35], Tsamasphyros et al. investigates the damage progression in a specimen similar to the P3 specimen investigated in this thesis with FBG. He successfully detects delamination and crack propagation and compares it with FE calculations. In [34] they also presents a neural network for the specimen with all four levels from chapter 6.3.1 implemented.

In [33] Baker presents work done in a fatigue test of a patched crack on a wing from a F-111C fighter jet. They used electric strain gauges during the test, and the results were confirmed with ultrasonic NDI methods. They successfully detected debonding and crack growth in the patch during the fatigue test. The strain-based SHM method evaluated the efficiency of the strain transfer from the structure to the patch by comparing strain measured on the patch and on the structure located in a similar stress field. Any change in the ratio between the two indicates a loss of load transfer of the patch. This could only be caused by a disbond of the patch. As presented by Baker, the strength of this approach is that it would work for any load without knowing the load.

The far field normalisation/comparison with the patch strain level is also suggested by professor Echtermeyer as a suited approach for the composite patch work in this thesis. Developed here is also a comparison within the patch by considering any nonlinear behaviour during loading. Such analysis may form the basis for algorithms used in a SHM system. The advantage is as presented by Baker that no knowledge about the load or the structure is needed for such a criteria for level 1 and 2. For level 3 and 4, analyses must be performed and knowledge acquired.

5.3.3 Damage prognosis

For a SHM system to reach level 4, damage prognosis must be performed. Different approaches will be developed, all trying to forecasting the future performance of the structure. It will need simulations, past experience probabilistic description of expected failure rates and several technologies combined. As Farrar and Lieven [36] concludes in their comprehensive review of damage prognosis (DP), all the necessary components of the system is realizable today. Several challenges, including nonlinearities and the need for a system more robust than the structure it self makes deployment and validation difficult.

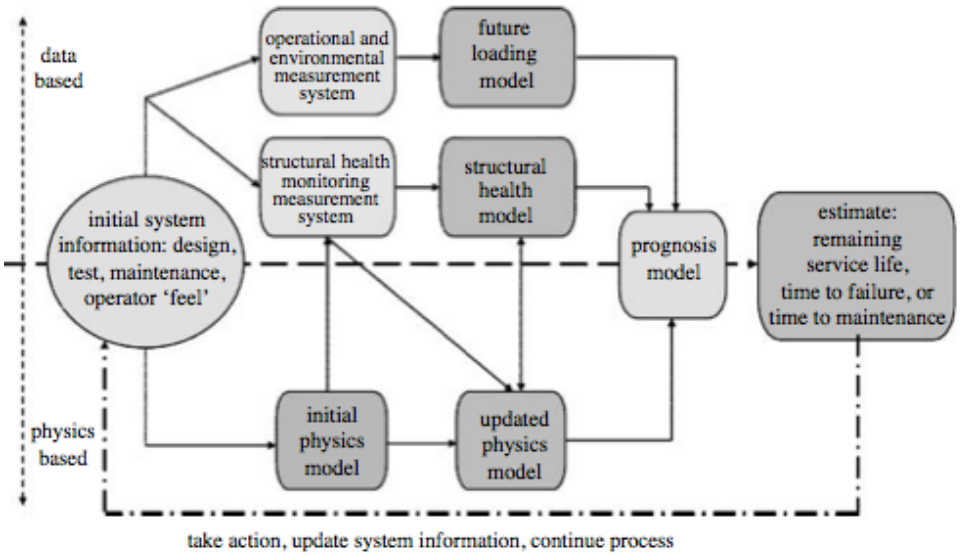

Figure 15: The general components of a DP process from [36].

Discussion and further development of a next generation health management system for aerospace is done by Mueller in [37]. It is combining different

technologies as impact monitoring, diagnosis of structural damage and prognostics of remaining useful lifetime. It is continuous updating structural models to improve the decision-making system. They call the complete SHM system Integrated Vehicle Health Management (IVHM) and have future air and space transportation systems in mind. This is probably the industry that will be in the front of this research in the future. Fully deployed systems will probably first be introduced in unmanned vehicles due to life-safety.

6 Establishment of measurement procedures

After the OBR 4600 was purchased there have been performed several small-scale experiments where some are worth mentioning. Working with, and embedding fibres call for experience in handling it as well as knowledge about boundary conditions for a successful infusion and/or curing. Some of the experiments that have given us valuable knowledge about the use and interpretation of results is presented below.

6.1 Microscopic images from embedment

In the project work in autumn 2010 a series of specimens were manufactured to investigate the behaviour of the fibre when embedded between layers in a laminate with different layup. As expected the fibre blends best with the laminate when embedded between two unidirectional layers along the fibre direction. Seen in Figure 16 the fibre blends with the glass fibre even in this laminate with low fibre content and voids. The fibre used here is a 250 micron cable, where the fibre used in this thesis is 165 micron which should give even better results. Published in [32] and [38] a better embedment may be seen.

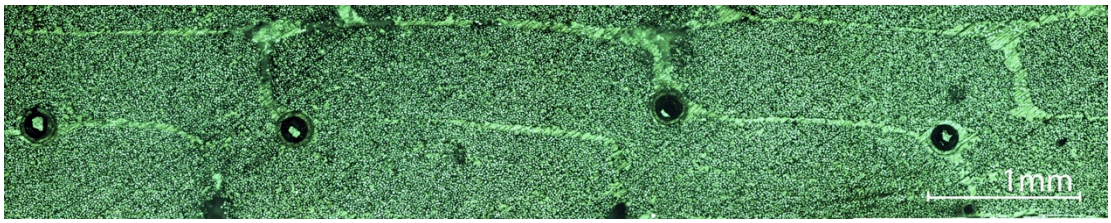

Figure 16: Fibre optic cable embedded in unidirectional glass fibre laminate.

Mechanical tests were also performed to investigate possible degradation of the strength due to the embedded fibres. Despite the fairly small sample size of the mechanical tests (less than 20), there was not discovered any reduction in strength.

6.2 Embedment techniques

Specimens for material testing here at the department are mostly made by resin infusing flat laminates before machining/cutting them to specific shapes and sizes. Together with PhD candidate Stanislav Shchebetov there was produced a set of specimens with different methods of embedding before they were water jet cut to different test specimen shapes.

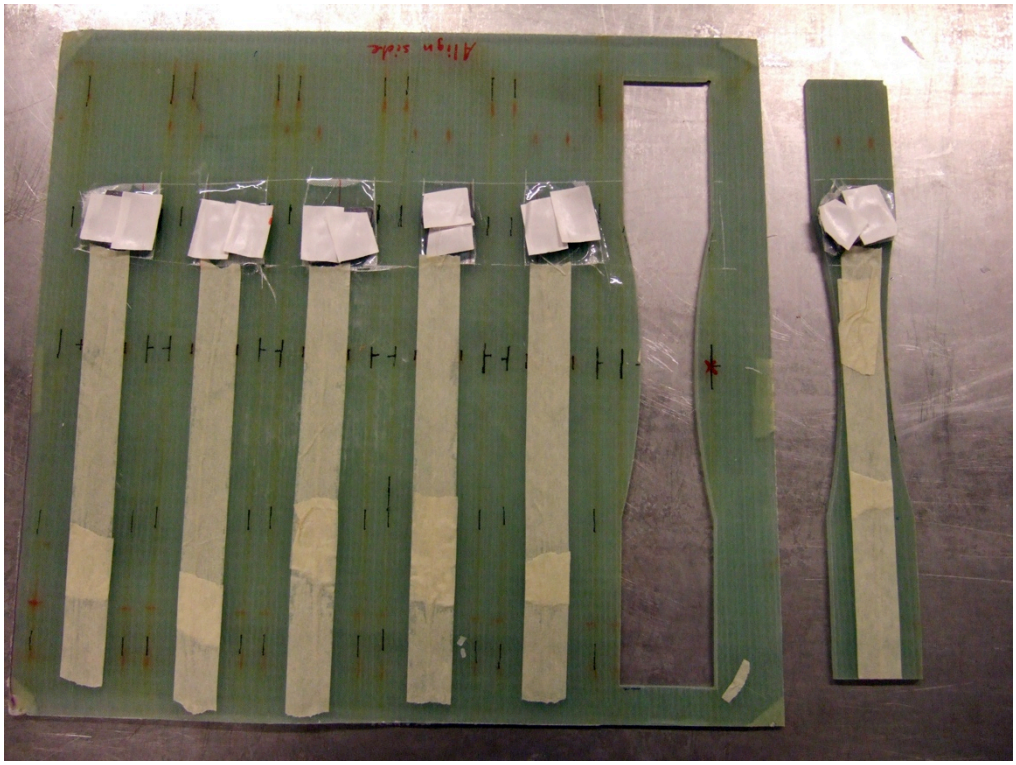

Figure 17: Embedded fibre optical sensor exiting through surface.

6.2.1 Embedment

Embedding a fibre optic cable in a composite laminate is challenging in several ways. A fibre optic cable is almost transparent, have springy characteristics and does not want to be placed curved, is easily broken and as discussed in chapter 5.2.3, the direction of the fibre should be evaluated. For these tests several techniques were tested. Figure 18 shows how a barbeque spit was used to "sew" the fibre under the supporting fibres or the stitching. This is a successful technique ensuring a good placement without adding anything to the laminate. This of course limits the choices of direction of the fibre. Because of that, also "epoxy film" was attempted to stick the fibre onto the glass fibre (As seen in green in Figure 18). This works well for straight fibre or large radius's, but smaller radius's will not stay in position for a longer period of more than about 30min. "Epoxy film" also requires a post curing after infusion and mixing of resin systems is not recommended.

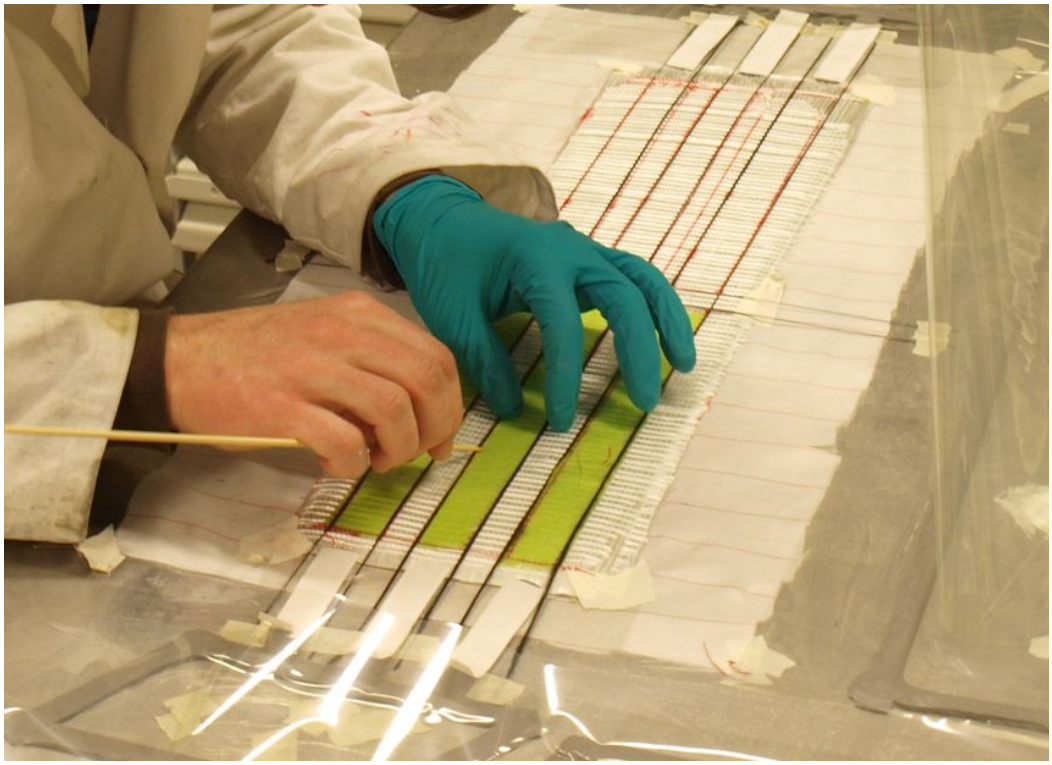

Figure 18: Fibre optical cable placement during manufacturing.

Two techniques of exiting the fibre were also attempted. Exiting the fibre out one end of a specimen, here protected by "sealing tape", only worked for some of the specimens due to braking during machining and handling. This method does not allow machining of that end, and need extra space inside the grips of a testing machine. Exiting through the surface was performed by stacking the top layers of the laminate, marking the exit point and thread the fibre optic cable through them. Additional holes were made in the bag at marked points for the fibre to exit. The holes were sealed with "sealing tape". This worked well during infusion, and when taking of the bag it was cut with knife around the exit holes and the fibre taped along the length of the specimen. The result is visible in Figure 17. At least one fibre broke due to handling, but the method worked OK and allowed for machining around the specimen as well as no extra space was needed in the grips.

6.2.2 Test results

Only four specimens were tested from this batch of specimens due to problems with data files for the water jet cutting and fibre optic cable braking. The testing was performed in an Instron 100kN test machine with displacement and load logging as well as an Instron extensometer. Before the test, additional fibre was glued to the surface of the specimen along the length with "epoxy film" and cured in oven.

Two important lessons were learned from the mechanical testing. An acrylate coated fibre is not suitable for strain measurements, and it is clearly visible in Figure 19 that at a strain level of about 4800 microstrain the fibre no longer adheres to the specimen and slips inside the epoxy. In addition to this, the coating is causing the fibre not to measure the actual strain. In both Figure 19

and Figure 20 a transition from zero to maximum strain is visible in addition to the not straight level of strain inside the glued area. Hence the comparison of the fibre optic versus the extensometer was not very good.

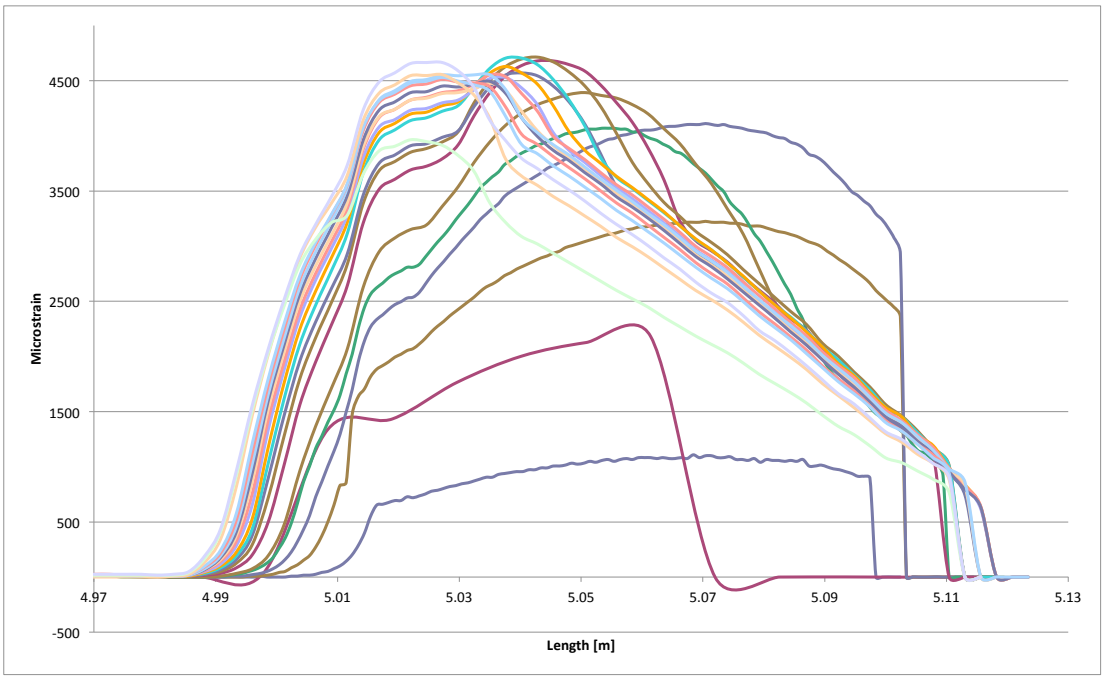

Figure 19: Straight glass fibre specimen

6.3 Parameter influence

After the series of tests in the embedment experiments there was raised questions about whether the parameters controlled in the software affect the measured value. The background for this was the experience from the specimens that was water jet cut with the fibre running only once along the length of the specimen. The end of the measured length of the fibre proved to be difficult to get results from.

Using the results from one of the specimens, many different combinations of the two parameters "Gage length" and "Sensor spacing" were tested (Further explained in chapter 9). An example is seen in Figure 20, and the rest is found in Appendix 13.1. It is clearly visible how the observed scatter is only a problem for the last 10cm of the fibre. None of the combinations give a perfect curve, but averaging several would give a good estimate of the actual strain level. Low gage length generally gives a scattered result.

The phenomenon causing this scatter is called Fresnel reflection and is caused by some of the light exiting the fibre and into another media with different reflective index and is reflected back. The reflections apparently disturb the Rayleigh backscatter signature, but only at the end of the fibre. From this it therefor recommended to embed at least 10cm extra fibre to ensure good measurement results. This also emphasises that it is important that the fibre is not broken at the insertion or inside a laminate during testing or operation. A broken fibre will hence not only lead to loss of signal after the fracture, but also scattered results 10cm before it.

The experiment proved that the parameters do not affect the strain value significantly in normal conditions. It does indeed show that changing parameters, and use a set of data with different parameters may give trustworthy results in difficult measurement situations such as stress concentrations, delamination, micro bending, etc.

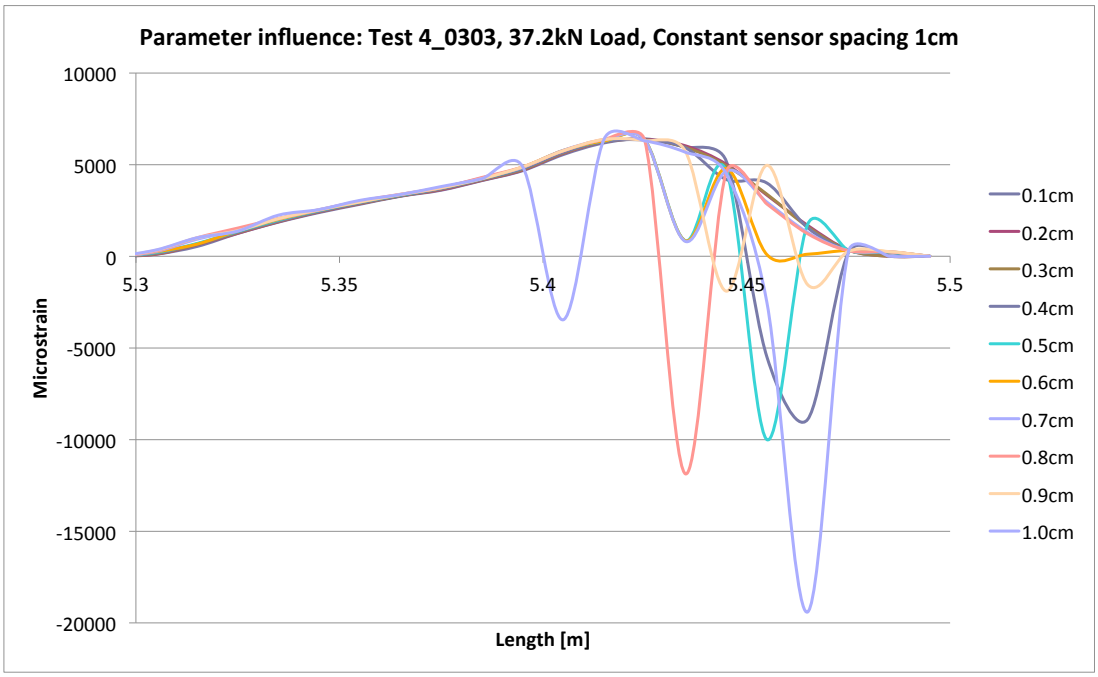

Figure 20: Dog bone shaped glass fibre specimen with embedded acrylate coated fibre.

Monitoring performed for an external customer by bonding measurement fibre to the surface of glass fibre specimen before subjected to bending produced results with a lot of scatter. Work was done after that to again analyse the influence of the calculation parameters on the results. In this specific case with compression, as seen in Figure 21, the noise was only data points with higher value than the average. For the tension case the noise was only lower than the average, where both cases is normal. Some analyses of the data are presented in Table 2 and Table 3. The tables present first the number of deviations for each data point with six different parameters. It was considered a deviation if the data point was more than half the absolute value different than the expected value. Secondly the table show the number of succeeding deviations along the length of the fibre, hence the percentage of single-, double or triple deviations.

As seen in Table 2 and Table 3 the measurement from the specimen subjected to tension gave the least scatter, with only 7% of the data points having more than three unwanted data points. Of the 40% of the data that was deviating from the average, 91% was single data points.

By presenting a dataset with different calculation parameters it is visually fairly simple to see what data points that are unwanted. For future work it should be developed a script that uses a set of Boolean rules to evaluate each data point against the surrounding data as well as the agreement with different parameters.

Weighted mean, standard deviation or confidence interval could also be helpful together with an increase of different calculations parameters evaluated. As seen in Figure 75 in appendix 13.1 smaller changes in the parameters give more consistent data.

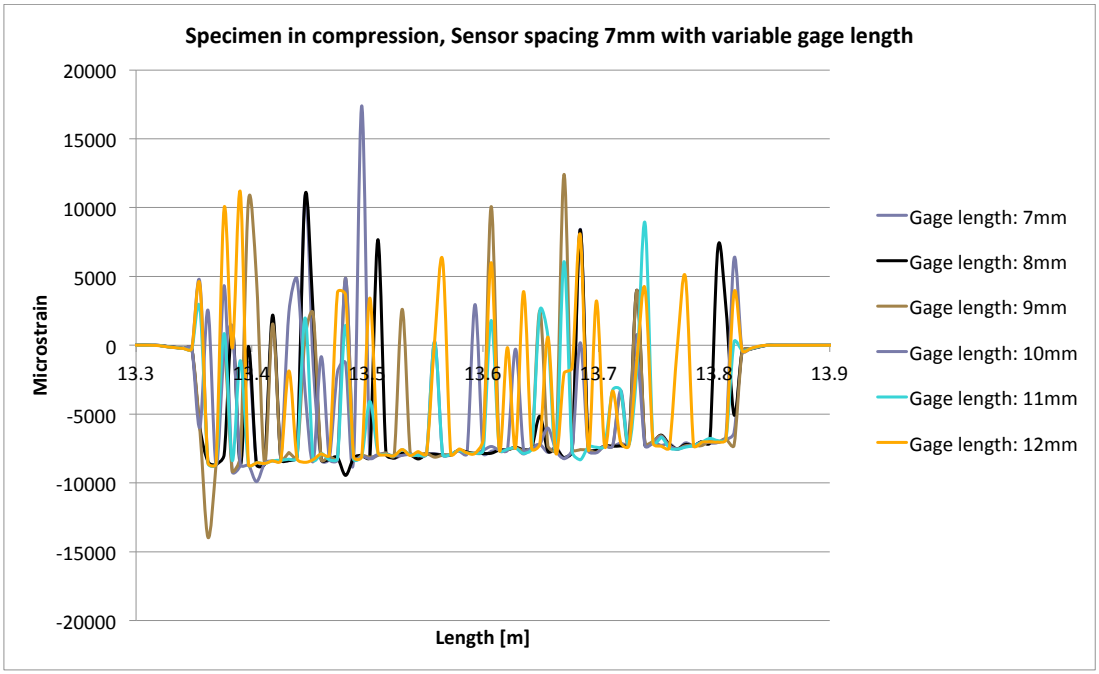

Figure 21: Deviations in measurement data during compression.

Table 2: Statistical data for deviations in measurements during compression.

Static compression:

Distance between data points:	7mm
Number of data points:	66
Sensing range:	455mm

Deviations	**0**	**1**	**2**	**3**	**4**	**5**	**6**
Number	28	18	6	10	2	1	1
Percentage distribution	42.4	27.3	9.1	15.2	3.0	1.5	1.5

Succeeding deviations	**1**	**2**	**3**	**4**
Number	49	14	3	0
Percentage distribution	74.2	21.2	4.5	0.0

Table 3: Statistical data for deviation in measurements during tension.

Static tension:

Distance between data points:	7mm
Number of data points:	72
Sensing range:	497mm

Deviations	**0**	**1**	**2**	**3**	**4**	**5**	**6**
Number	43	12	7	5	4	1	0
Percentage distribution	59.7	16.7	9.7	6.9	5.6	1.4	0.0

Succeeding deviations	**1**	**2**	**3**	**4**	**>4**
Number	41	4	0	0	3
Percentage distribution	91.1	8.9			

For specimens where a lot of noise has been a problem, it has been successful to use the previous measurement as reference for every measurement and thereby decreasing the strain difference between the measurements. The quality of the data is increased and the results are simply summarized in e.g. Excel to get the total strain.

6.4 Coating test

An important goal for the use of the OBR 4600 is the possibility of measuring the strain distribution around a stress concentration. Due to bad results from previous tests using the acrylate coated fibre from Draka, the polyimide fibre received as a part of the procurement of the OBR was compared to the acrylate coated.

6.4.1 Specimens

For this test it was used specimens already manufactured by PhD candidate Stanislav Shchebetov. It was tested a series of nine specimens without hole, with 4,5mm (Seen in Figure 22) and with 5,9mm holes in the centre. It was a 25 x 250mm specimen made by resin infusing UD glass fibre with vinyl ester resin. They were tested in an Instron 100kN test machine without tabs. The measurement fibres were bonded on each side, 1mm from the hole, along the longitudinal direction as well as one in transverse direction on the rear side. For the specimens without holes it was suggested by Stanislav to bond two polyimide fibres parallel but with different lengths bonded to the specimen. It was used CN glue for the bonding.

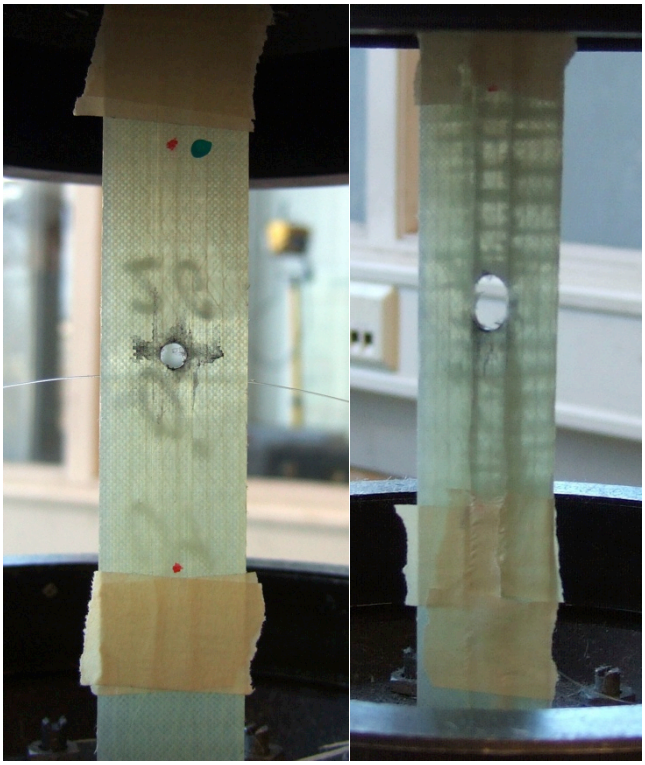

Figure 22: Glass fibre specimen with 4,5mm hole before and after test.

6.4.2 Results

The comparison of polyimide and acrylate was confirmed with several specimens, but only two curves are necessary to illustrate the evident solution of the experiment. In Figure 23 it is clearly visible that the acrylate coating is not suitable for strain measurements. The coating is too soft, which lead to bad shear transfer as well as hysteresis. Only the fibre bonded in the longitudinal direction is presented, and the end of the polyimide coated fibre is removed due to a scattered curve. The polyimide coated fibre shows a good ability to measure stress concentrations and is the coating material used in this thesis. The result is also confirmed by the research done by de Oliveira in [39].

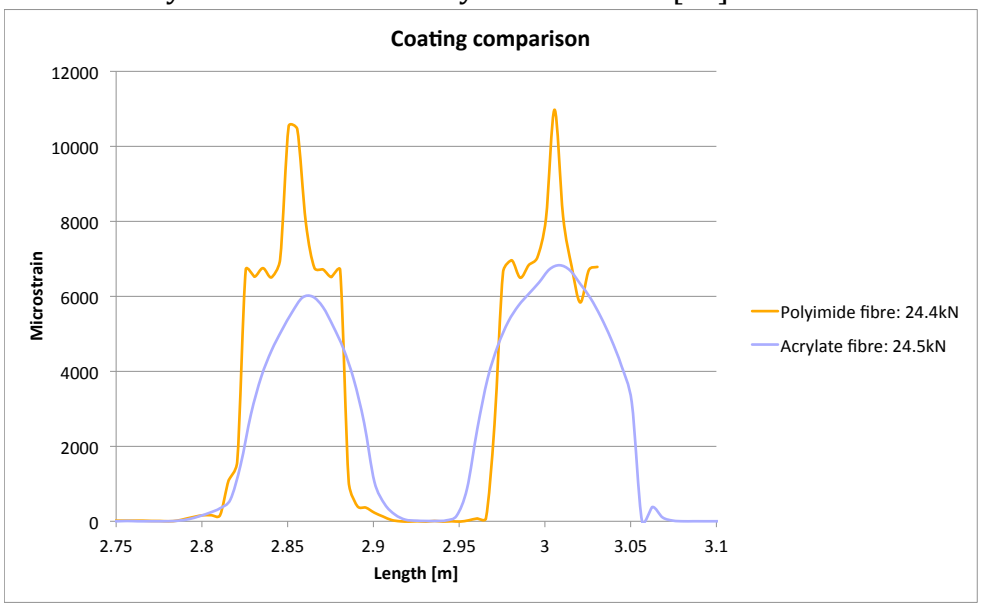

Figure 23: Comparison of measurements with acrylate and polyimide coated fibre.

The two polyimide coated fibres bonded in parallel gave very good results, and as expected. As seen in Figure 24, the strain measured is equal in both and the strain transition is short. A straight, even strain level is expected in a specimen tested like this, but was not achieved by using the acrylate coating.

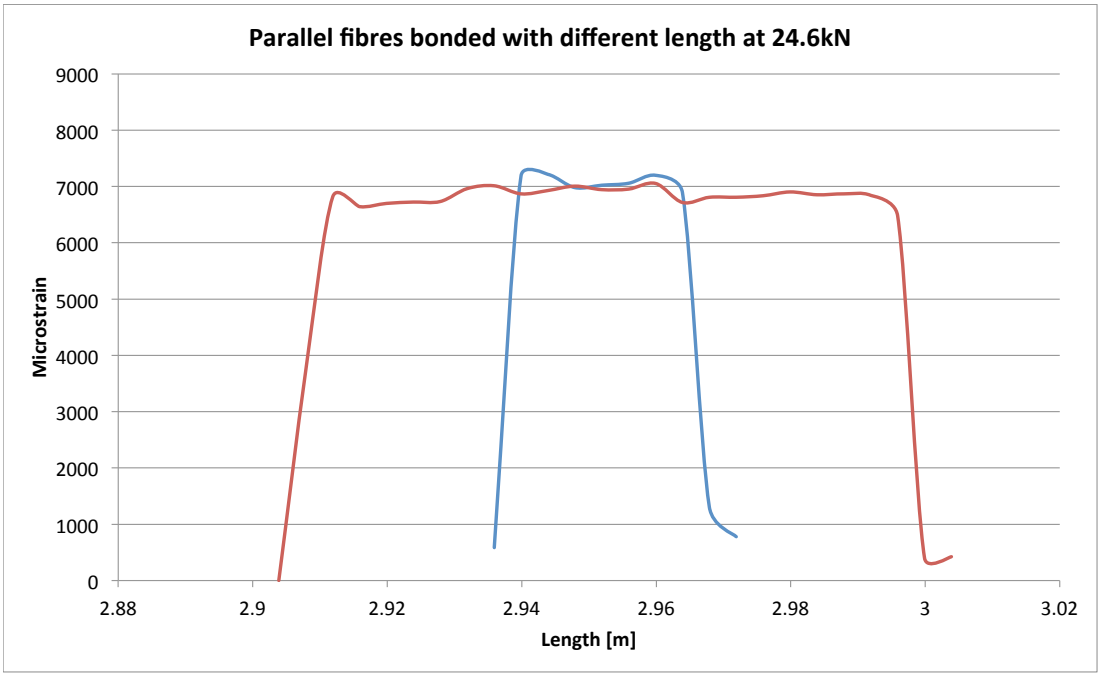

Figure 24: Polyimide fibre bonded parallel on specimen.

6.5 Single lap specimens - Co-Patch

As a part of Stud. Techn. Nina Thorvaldsen's project work some of her single lap specimens for the Co-Patch project was instrumented with fibre optics. The specimen production was done by N. Thorvaldsen, except the fibres.

6.5.1 Specimens

The specimens where manufactured as plates, seen in Figure 25, before they were water jet cut into smaller specimens. The composite patch was cured in a separate process and was bonded to the steel by wet layup of the glass fibre galvanic protection before bagging and curing everything under vacuum in room temperature.

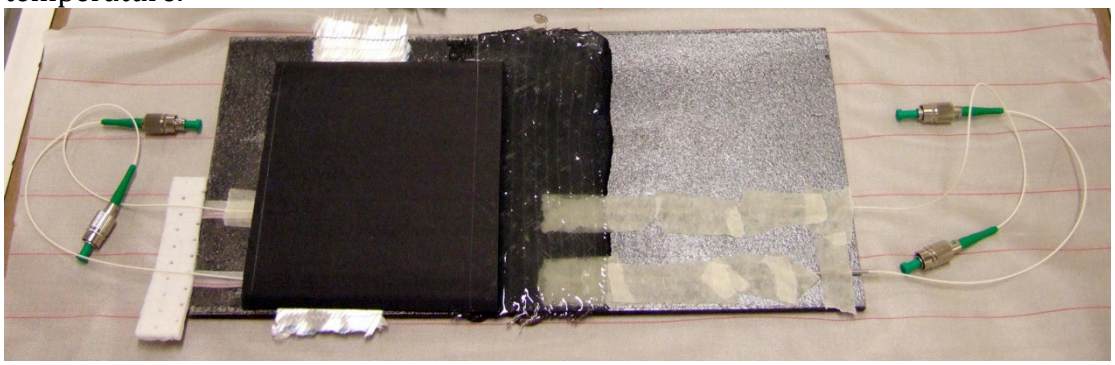

Figure 25: 12mm single lap specimens during manufacturing.

The series of tests were of specimens with different length and adhesive length, but the same width. Because of shortage of carbon most of them were made with

glass fibre. The only specimen with results worth mentioning here is a glass fibre specimen with 200mm overlap, seen in Figure 26.

Figure 26: 200mm single lap specimen with glass fibre patch.

Several challenges arise when embedding optical fibres. Ironically it is the fibre outside the embedded area, (here: the patch) which is the problem. The sharp edges of the steel plate and some mistakes during manufacturing lead to the high number of failed fibres in this series.

6.5.2 Results

The two specimens from Figure 25 with 12,5mm overlap failed during clamping in the test machine. The result from the 200mm overlap specimen is presented in Figure 27. As seen in the plot, there were problems with noise in the measurements at higher loads. Hence the complete plot is not presented. It is in the Figure 27 visible an effect at the end of the patch that will be further investigated in this thesis in chapter 9.

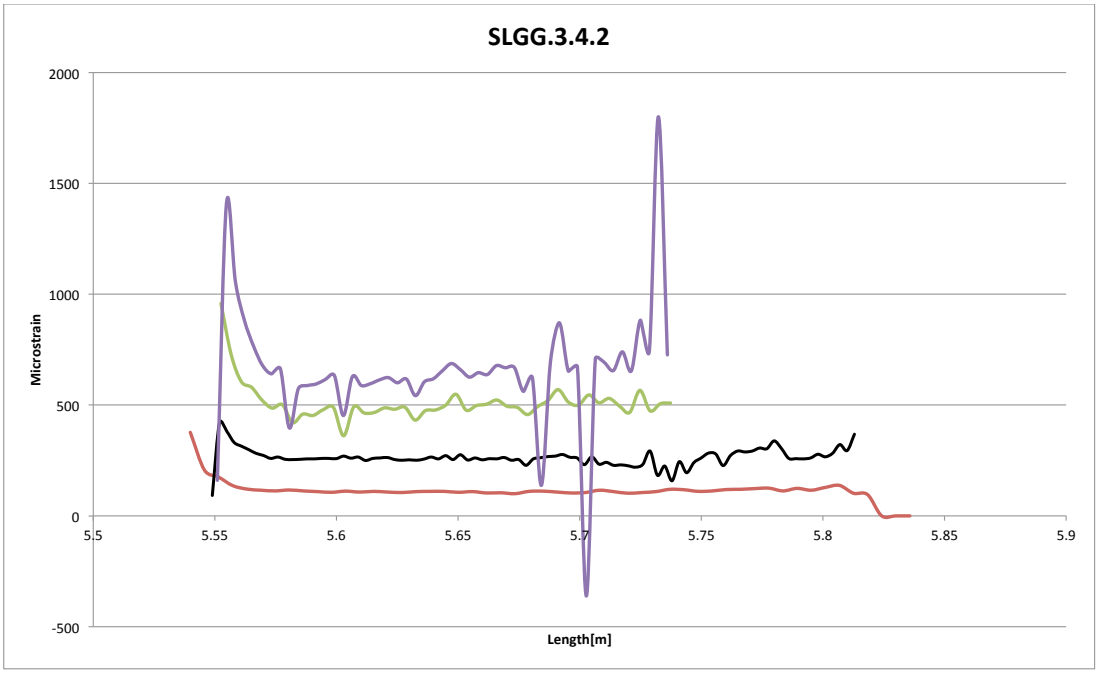

Figure 27: Fibre optical measurement results from 200mm overlap specimen

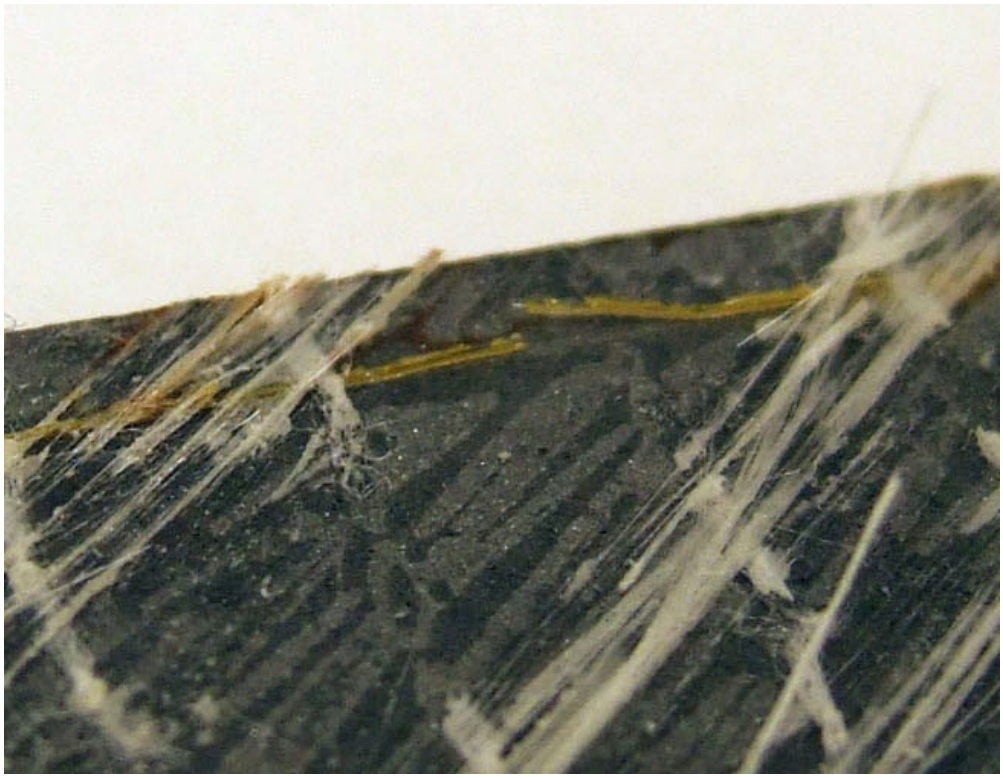

Figure 28: Close up of fibre in 200mm single lap specimen.

The surface of the failed specimen, which is presented in Figure 28, was interesting in several aspects. It failed partially in the galvanic protection (the adherend), and partially in the adhesive. Also visible is the fibre optic cable that have been broken and damaged by the crack growth/failure. This may be used to detect crack growth or damage by monitoring the fibre being shorter, but due to the lessons learned in the parameter testing this is not recommended. If the fibre is broken in a early state of the test or structure life, vital information is lost. Hence it is recommended to embed fibre in between layer one and two to increase the robustness.

6.6 Fibre proofing

Experience from tests using polyimide coated fibre lead to confidence in that coating material. A 155micron optical fibre from OFS was found interesting because of its temperature durability and a coating material apparently similar to the one supplied from Luna Technologies. A proof test was conducted with a sample received from OFS comparing the measurement results with electrical strain gauges.

6.6.1 Specimens

The specimens was identical to the specimens used in the coating test in chapter 6.4, but with 90° fibre direction and no hole. The fibre was bonded to the specimen in the centre along the longitudinal direction, and the strain gauge on the rear side.

6.6.2 Results

Due to the transverse fibre direction low strength, but high displacement and some distorted optical measurements were expected. The fibre gave good

results; despite a strain difference up to 23% it was an average of 9%. In Figure 29 the fibre optics and strain gauges are compared in a stress-strain curve. The stress is calculated with data from the load cell and a cross-sectional area of 86,1mm^2. The strain value from the fibre optic measurement is an average over a length of 40mm.

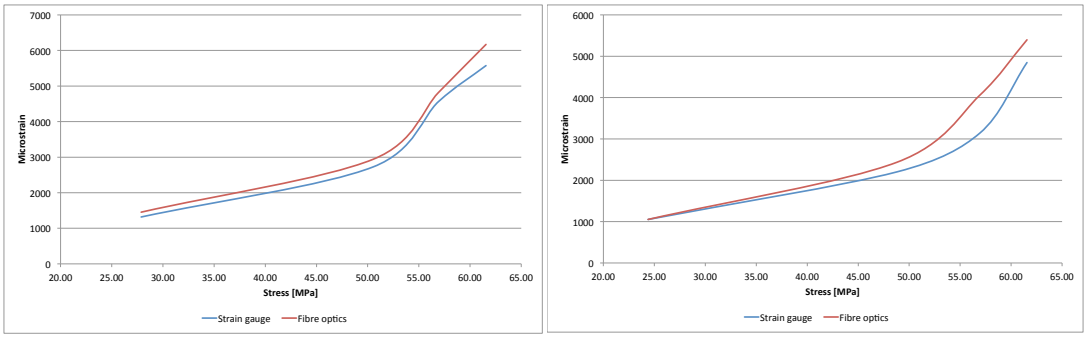

Figure 29: Fibre optical strain measurement compared to strain gauge.

6.7 Temperature measurements

In the course *Experimental Methods in Process Engineering* in autumn 2011, a small project was conducted by doing some experiments with the temperature measuring capability to the OBR 4600. It is interesting to understand how temperature affects the fibres, and it might be interesting in several other projects at the department. The work resulted in a poster presented on a poster session.

6.7.1 Experiment

The experiment was conducted using a constant temperature bath (Julabo MW-12) with a length of fibre optic cable taped on the surface of a glass fibre laminate countersunk in its water tank. The temperature bath is capable of maintaining a constant temperature between 40 and 80°C using water, and is using a circulating pump to keep a fairly homogenous temperature in the container. As a reference a type K Thermo couple was used. As it might be seen in Figure 30, the fibre was on the laminate facing away from the pump and with the thermo couple in front of it.

The measurement of temperature (as well as strain) is dependant of a correct calibration factor. Ten measurements were done at 40 and 60°C, and linearization then gave the factor -0,7249. It was then done a series of measurements with six measurements every 10°C between 40 and 80°C and the average from each was used in the results.

Figure 30: Temperature measurements in a temperature bath using fibre optical sensor.

6.7.2 Results

The temperature bath proved not to be the best tool for a good calibration if an accurate absolute temperature is desired. Ice water and boiling water was also discarded for the same reasons. A smaller scale test with another type of equipment is suggested. But besides these problems, the temperature measuring ability proved to be good. The results from the calibration are found in Table 1. Figure 31 presents the measurements done at 70°C. The fibre is a length of about 3m and the maximum amplitude is about 1,3°C, but the source of the temperature differences is not known. As seen in the Figure 31 the temperature measured is stable within the 50 seconds between first and last measurement.

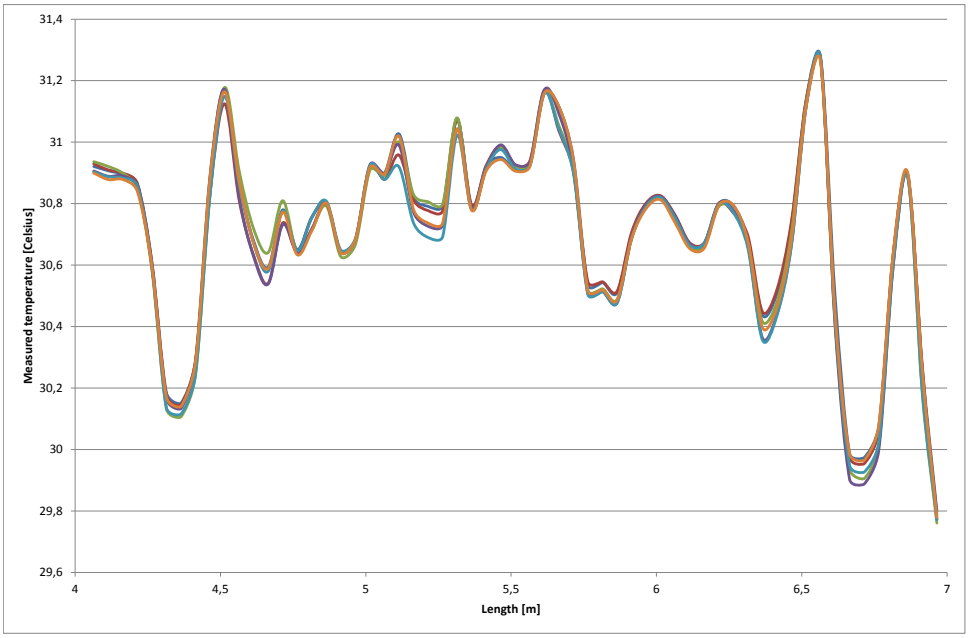

Figure 31: Temperature measurments at 70 °C

6.8 Entering and exiting of fibre in a laminate

During all the experiments performed with embedding of the fibre optical cable, there is always the entering/exiting of the fibre into the laminate/patch during that is critical. The challenges are different for the different manufacturing methods, but valid for all of them are that the measuring fibre has to be protected from the exit of the shrinking tube applied after splicing of the connecting fibre and the patch/laminate. The connecting cable should be protected by normal precautions such as protecting it from sharp edges, resin and against strain during removal of bag, sealing tape, etc.

The measuring fibre should be protected against any external force against the exit of the shrinking tube and sharp edges. Preferably all the measuring fibre should be inside the patch/laminate. Different protections and techniques have been tested where the latest is working well, but for a commercial structure further development should be done. As seen in Figure 32 an unprotected fibre close to a patch broke during manufacturing. In Figure 33 a piece of glass fibre mat was placed on top and a piece of tape below the fibre to protect it against the pressure from the vacuum, but it was not an unconditional success.

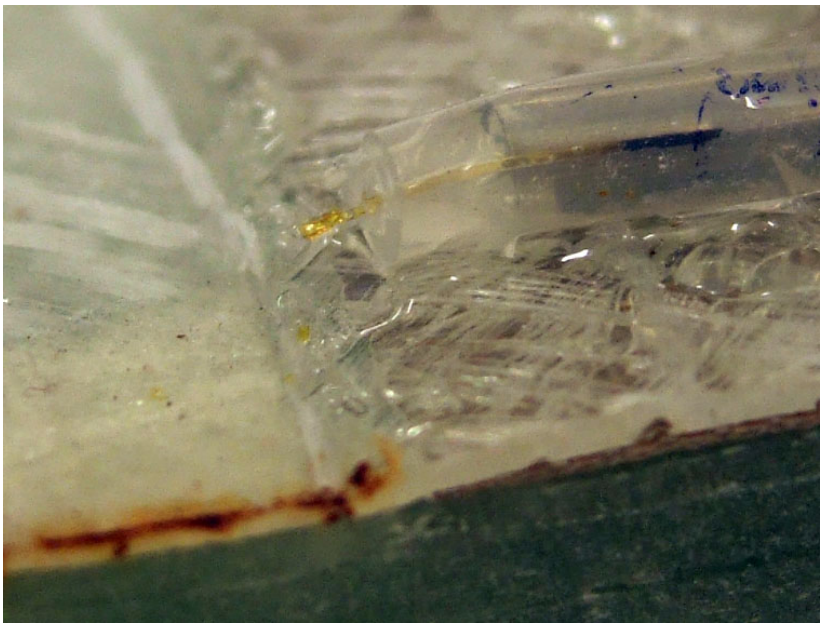

Figure 32: Unprotected measuring fibre broken during manufacturing.

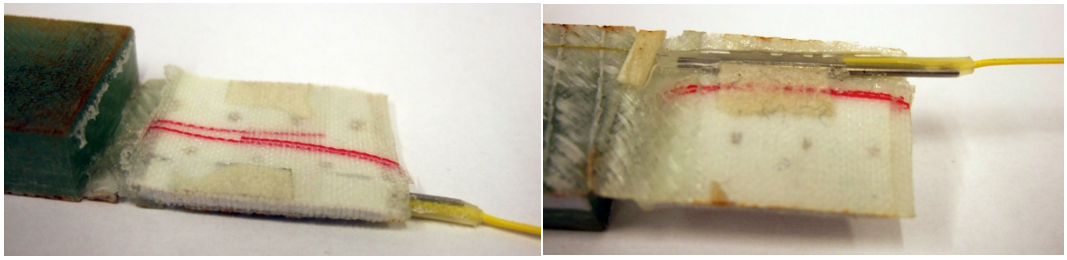

Figure 33: First attempt in protecting the measuring fibre during manufacturing.

The protective sleeve that has been used for all the specimens manufactured during this thesis was developed prior to the manufacturing of the P3 specimens

in Portugal. It was a need for a protection that would withstand handling of a potentially inexperienced operator, shipping of fibre and finished specimens, both hand layup and infusion as well as testing. The design was tested in a test-infusion prior to shipping to Portugal with success. In addition to the components illustrated in Figure 34, the connecting fibre is placed in a zip-lock bag with "resin brake" on each side. The "resin brake" is seen below the fibre in Figure 35 and is a thick mat intended to absorb resin near the outlet during infusion. Also seen in Figure 35 is that vacuum combined with the heat during curing of prepreg permanently deforms the fibre, but no negative effect has been observed on the signals.

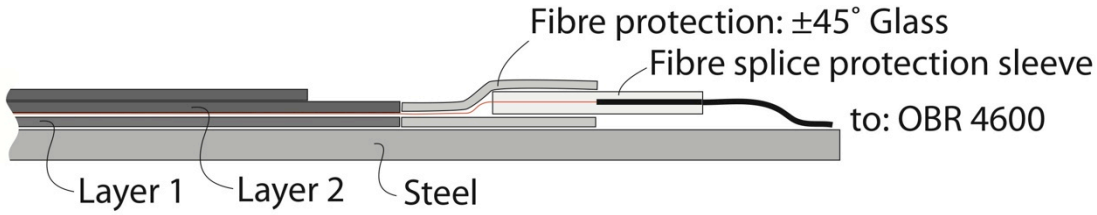

Figure 34: Optical fibre protection

The design of the protection is simply a 30x60mm 200g/m^2 glass fibre weave that is folded from the sides such that the fibre is protected with two layers on the top. Airtac 2 spray adhesive are spread onto the mat through a stencil, such that it will hold together, but no glue towards the centre. It is then possible to thread the sleeve onto the fibre, over the shrinking tube and secure it with a piece of tape seen in Figure 35. With this it is possible to adjust the position of the sleeve to accommodate the laminate/patch length slightly. In appendix 14.1 the technical paper describing how the fibre should be handled and embedded for the P3 specimens is attached. There was made a separate one in Norwegian for the IPE-100 beams. This has worked with three different manufacturers, which proves that with prefabricated fibres it is completely feasible to use these sensors in an industrial setting. Figures in chapter 8 show the protection in use.

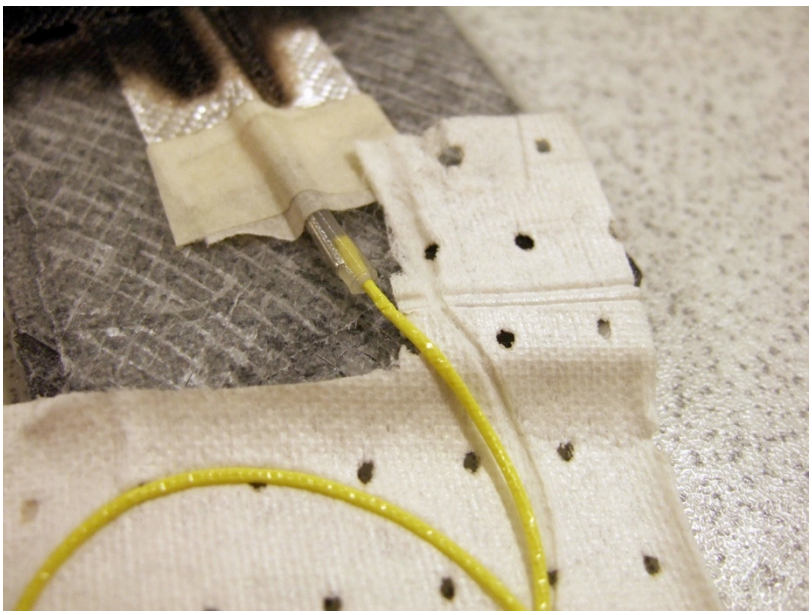

Figure 35: Detail picture of fibre exiting the relaxation test specimen.

Experience from the bending test of the IPE-100 beams showed that it would be best if the protective sleeve were attached to the patch and not to the beam. Delamination during the testing lead to fracture of the fibre at the interface before the patch failed.

Suggested protection that may be utilized in future work is the same protective tubing used by FBG sensor manufacturers called either “Buffer tube protection”, “Fibre furcation tubes” or “Fibre jacketing”. It is an approximately 100mm long, thin polyimide tube placed over the fibre where it exits the laminate/patch. This might combine the shrinking tube, protecting the fibre splice, and the protection when exiting the laminate. The only downside is to introduce a 1mm diameter tube at the edge of the patch/laminate that could cause stress concentrations.

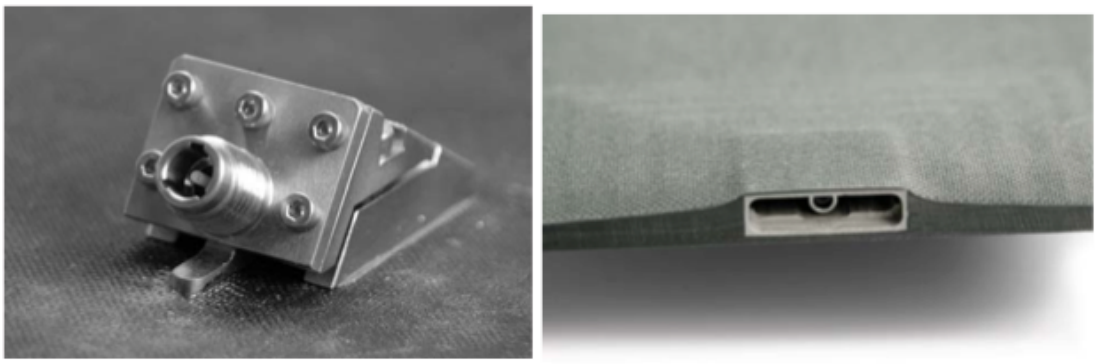

Figure 36: Left (a): The EMPIRE connector and right (b): embedded connector. Pictures from Deutsch “Fibre Optics” catalogue. Literature Code: FO-D08005-2008.

For the industrial application and larger structures where there may be unstrained areas of the composite that give more options. For those applications it would also be desirable to avoid the cable outside the patch/laminate. Deutsch, a large interconnect solution provider, have developed two types of connectors seen in Figure 36. The EMPIRE connector (a) is only partially embedded, which should affect the composite less than the embedded (b), but the embedded is less likely to be damaged by a hit. Sjögren have in [40] performed static tests of embedded edge connectors in CRFP laminates. Loading transverse of the embedded connector, of specimens where the connector was more than 50% of the width, reduced the strength up to 70% in tension, but by doubling the width of the specimen the reduction of strength was only 25%. In Figure 37, MT-ferrules with two different methods of embedding is seen in a 6,4mm thick laminate where (a) is recommended by Sjögren.

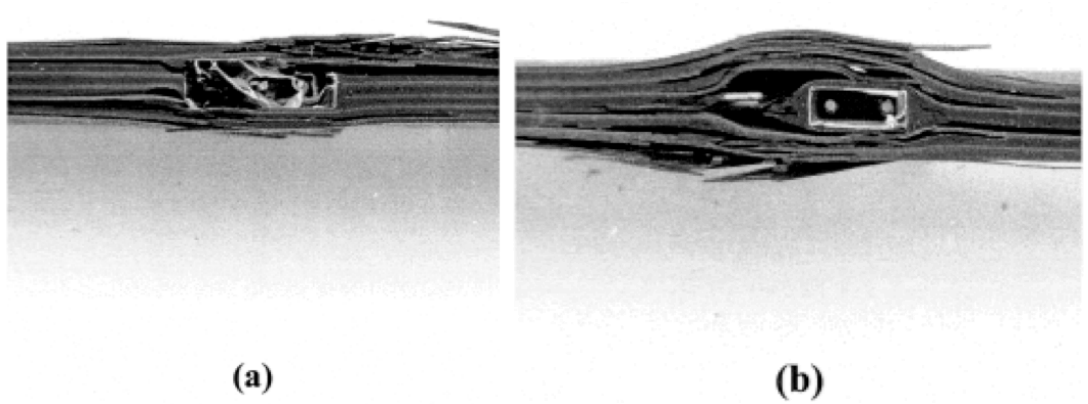

Figure 37: Pictures of tensile failure for specimens with embedded MT-ferrules. (a) with cutouts, and (b) no cutouts. From [40].

6.9 Filament winding with optical fibre

Because it was planned to embed fibre optical cable in one of Umoe Advanced Composites' (UAC) pressure vessel test tanks as a part of this thesis, work was done to investigate if this was feasible and to develop a strategy for the execution. The OBR 4600 is able to measure distributed strain in a 70m cable, and by winding one cable in hoop and one in helical the pressure vessel would have a grid of sensors ideal for health monitoring.

The test was conducted by winding glass fibre on a cylindrical mandrel with elliptical ends (L: 645mm, D: 194mm) using soap as resin. The fibre optical cable was introduced after the resin bath, but before eye of the carrier. That would ensure that the fibre was wound together with the glass fibre independent of the winding program. A length of fibre was placed in a small bag and attached close to the openings of the mandrel during a stop in the winding program. It was carefully placed over the dome during the first turn before the program could continue as normal only with a slight tension to the fibre optical cable applied manually. When the 70 meters is wound the end is simply embedded and no precautions is needed. After the test the OBR 4600 was connected to the fibre to confirm that it was not damaged. In Figure 38 the fibre optical cable may be seen at the tip of the arrows. The test was a success, but for implementation in a production process further work should be done to design a connector and including the fibre optical cable and bobbin in the winding program and machine.

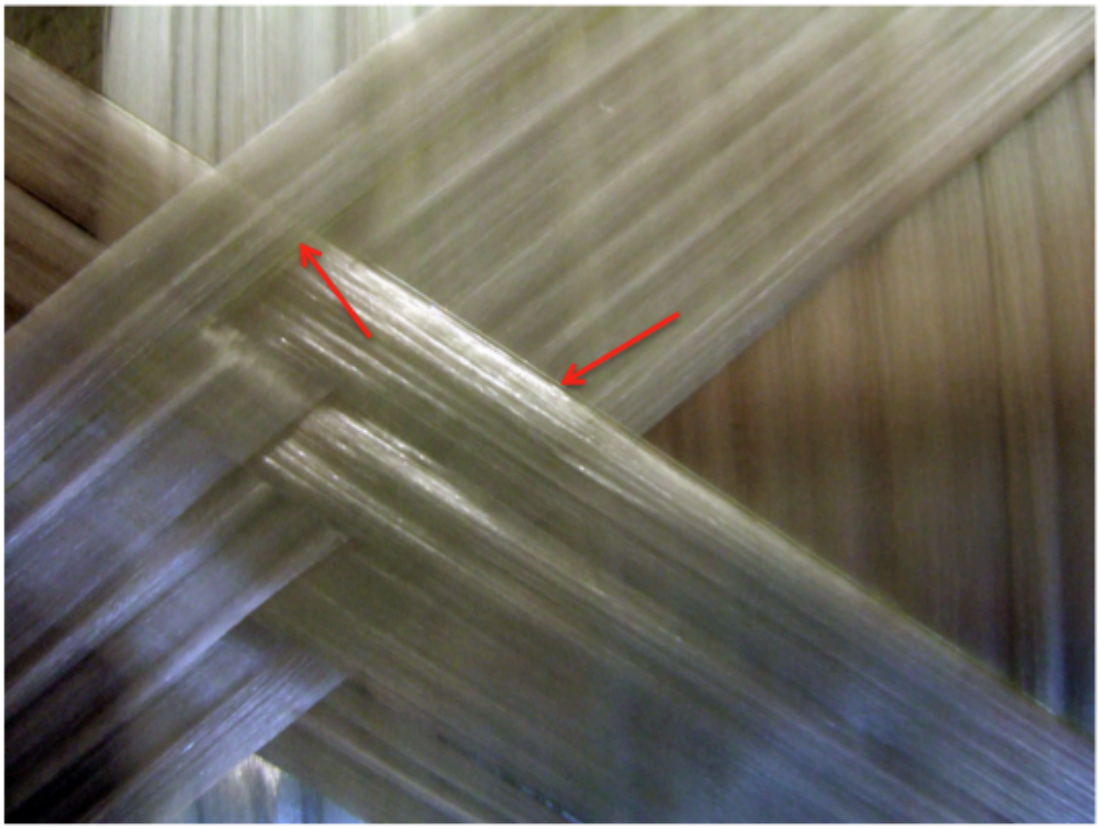

Figure 38: Close up of filament winding with fibre optical cable barely visible at the tip of the arrows.

7 Calibration

Calibration has two missions in this thesis: Calibration of accuracy against conventional strain measurement equipment and evaluation of the accuracy when measuring strain next to stress concentrations. The calibration against conventional equipment is necessary for publications and future research as the OBR 4600 is not necessary recognized as trustworthy strain measurement equipment. Its ability to measure large strain gradients from stress concentrations and local strain concentrations is important in the Co-Patch project as well as other health monitoring situations.

Less than intended work has been put into calibration in this thesis, but several of the experiments performed have been equipped with additional instruments. This is not considered calibration, as there are too many unknown factors, but it may give a good indication.

Below is an improvised experiment presented, using an extensometer calibration tool. In chapter 6.6.2, measurements with fibre bonded to the surface of a specimen were compared to strain gauges. In the conference paper to be published by Grave, Håheim and Echtermeyer fibre optical measurements were compared to strain gauges and FE-modelling, which are attached in appendix 13.2. In the P3, presented in chapter 9, the results from the OBR 4600 and FBG sensors are compared. FBG sensors have during the last decades become an acknowledged strain measurement technology.

7.1 Calibration of fibre in air

Experiments have been performed using an extensometer calibration tool in an attempt to compare measurements with simple, indisputable physics. With the fibre glued to the fixtures of the tool and a 0,001mm accuracy of the displacement the results should be according to the formula for strain (16).

$$\varepsilon = \frac{\Delta L}{L_0} \tag{16}$$

The L_0 was measured with an internal micrometre before increasing the displacement by increments of 0,05mm. New measuring fibre was used three times, and five tests were performed. (Test 1, Test 2 & 3 and Test 4 & 5)

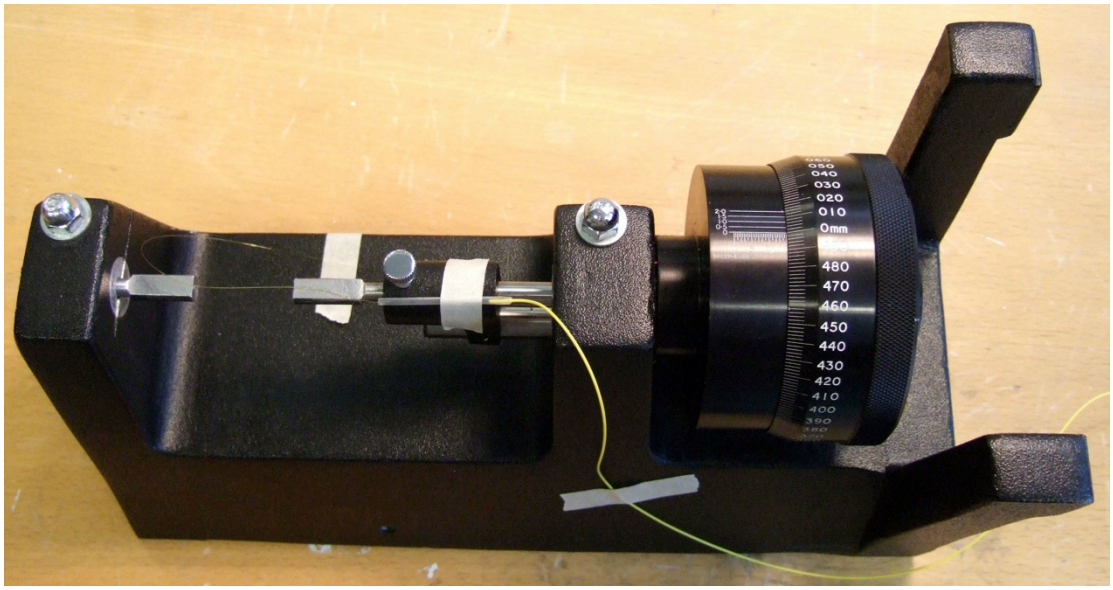

Figure 39: Experimental setup calibration in air

Below are three plots with data from the tests. Figure 40 shows the average strain measured between the two fixtures. As clearly visible, at 0,3mm displacement and about 6500 microstrain there is a cohesive failure preventing measurements of higher strain levels.

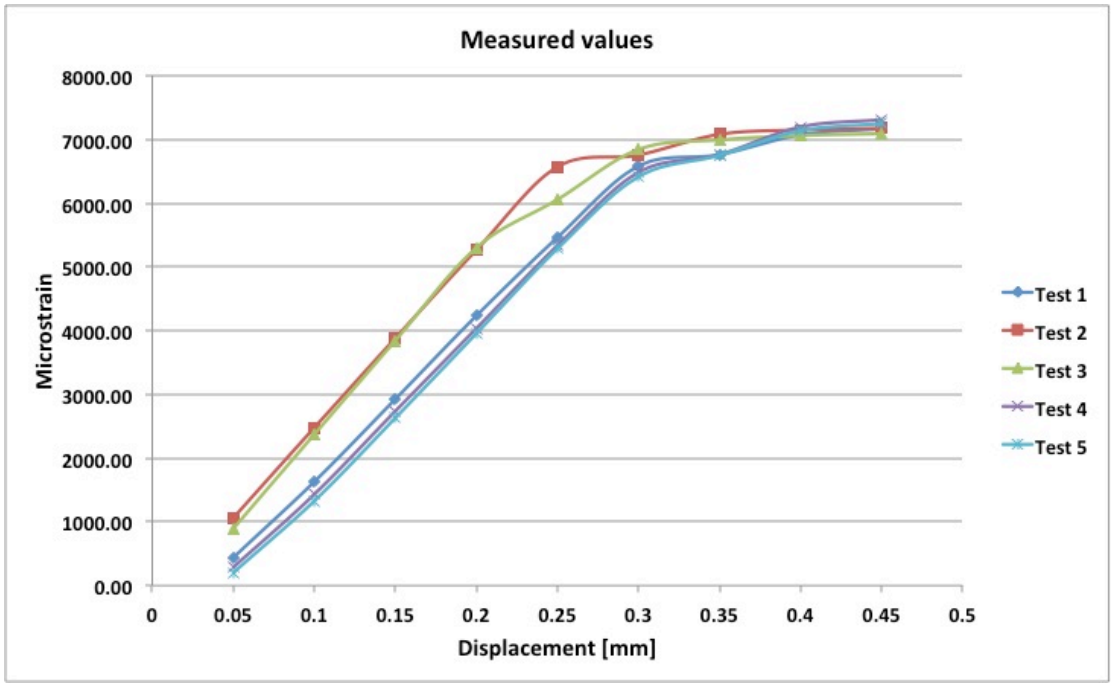

Figure 40: Total strain measured

Most likely because of thickness variations and other small variations in the fibre there is a small standard deviation in the measured values between the grips. It is unknown why two of the tests have a higher level of deviation. As visible in Figure 41 it is, except the two mentioned, almost constant standard deviation at different strain levels.

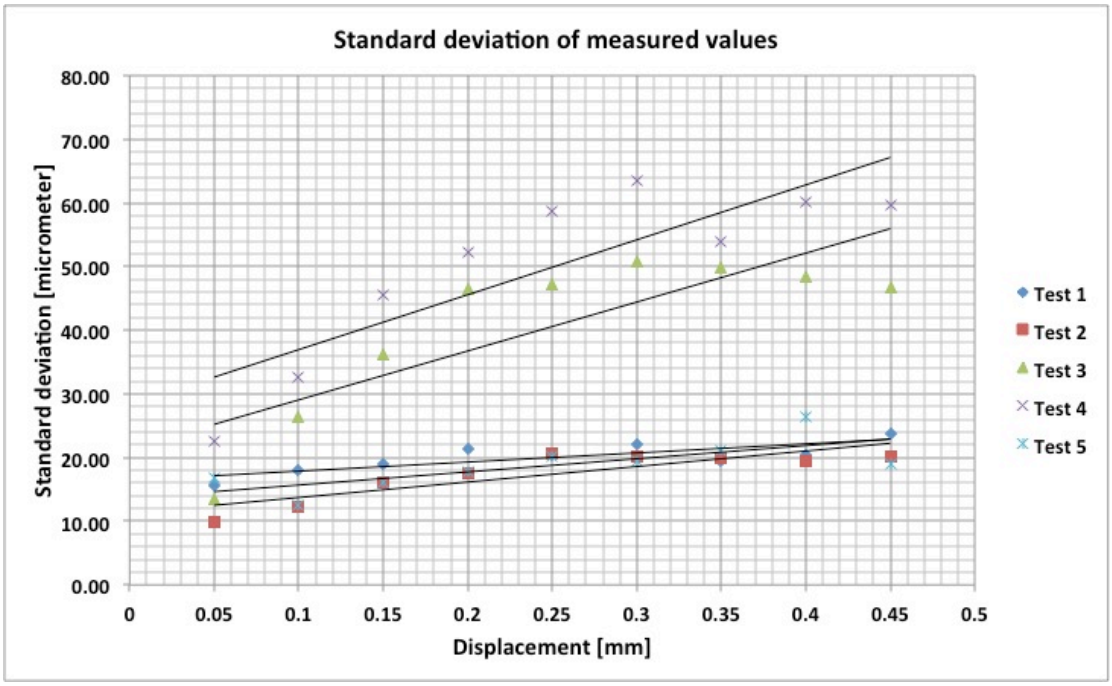

Figure 41: Standard deviation of incremental values

Because of slack in the fibre in the first increments and cohesive failure in the last, it is most interesting to compare the results for each increment. As seen below in Figure 42, there is fairly small deviation in the results for all the tests, at several of the increments. For all the increments the calculated value from the equation (16) is higher than the measured.

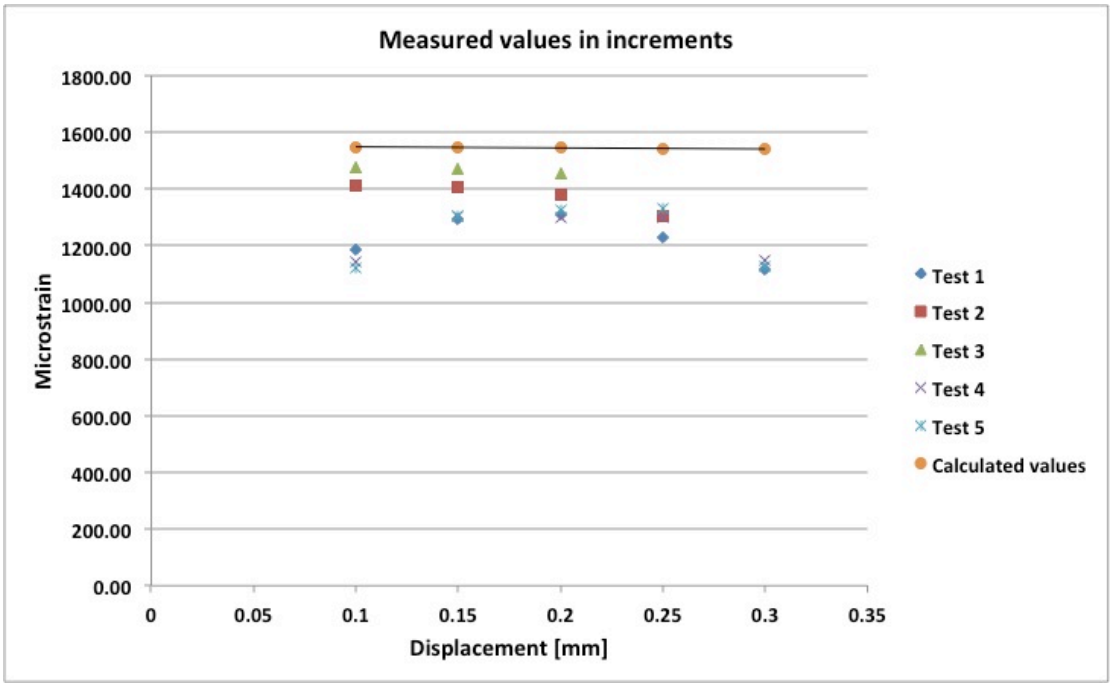

Figure 42: Measured values at the different increments

In addition to the measured data presented above, several interesting effects were measured. As mentioned the behaviour of the glue was visible at higher strains. One of the intentions of this test was to do measurements on a setup where we have good control over the length measured and a well defined fixture

area. This worked fairly well, but the transfer from loaded fibre to fixed fibre was not as sharp as expected. Even at low strain levels the shear transfer in the glue was clearly visible, and was confirmed with measured residual stress and relaxation after the fibre was unloaded. Below, in Figure 43, are the plots from one end of the fibre with the edge of the fixture indicated with vertical lines.

The sensor spacing, hence the distance between the data points are here 0,6mm. Because of curve fit in Excel the curves are not totally realistic. Even though the spacing between the data points are significantly larger than the increments in displacement, there is no sign of a change in where the curve brakes down when the length of the fibre increases.

At both end of the fibre the strain level does not drop instantly to zero due to the not sufficient shear transfer capabilities of the adhesive. Notice also the residual strain caused by slipping in the adhesive measured when unloaded.

The maximum shear strength for this setup is very consistent, and could be seen in the charts in the appendix 14.5.1.

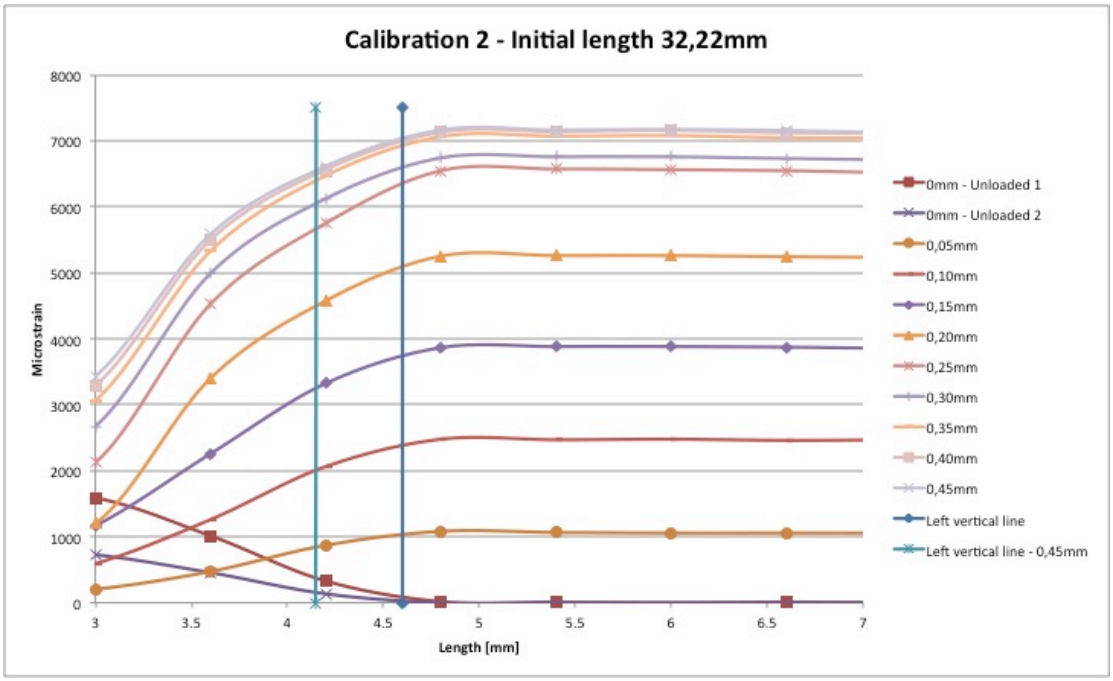

Figure 43: Measurements from one side in test 2.

8 Experimental work

The experimental work for this thesis consists of four topics in addition to the previous work and the calibration test. Everything concerning the test specimens, test setup and planning of the test are performed by the responsible in the Co-Patch project for the test. The candidate has been responsible for the fibre optical strain measurements planning, implementation and data analysis, hence the test setup are only briefly introduced.

During the test the OBR have been remotely controlled with a laptop and the software presented in appendix 14.5.2 are used to make the measurement a on-button operation. Results are stored in separate text files, where a MatLab script (14.5.2) have been developed to collect them into a single Excel spread sheet.

8.1 WP3 – Task 3.2 - P3

Task 3.2 – P3 is the mid-scale short-term test of patched plates with an initial crack. The specimens where manufactured at ENP (*Estaleiros Navais de Peniche SA*) in Portugal with both FBG and OBR fibre and tested at Aimen (*Asociación de Investigación Metalúrgica del Noroeste)* in Spain.

8.1.1 Specimens

Four specimens were tested with fibre optic strain measurements. The material and preparation details are listed in Table 4. The dimensions of the specimens are showed in Figure 44 and the placement of the FBG and the OBR fibre is illustrated in Figure 45.

Table 4: P3 specimen properties

Specimen number	Steel	Patch	Surface treatment
1 & 2	Marine grade A steel	Hand layup Carbon/Epoxy	Grit blasting
3 & 4			Needle gun

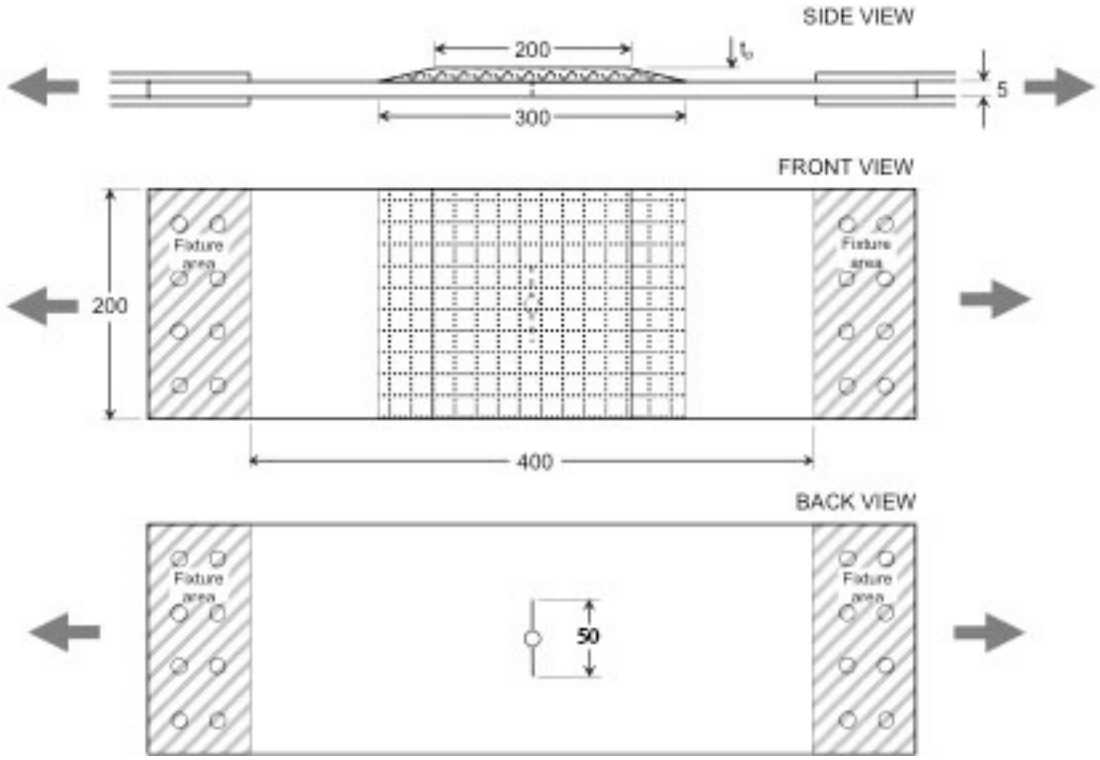

Figure 44: P3 specimen dimensions. By J.H. Grave

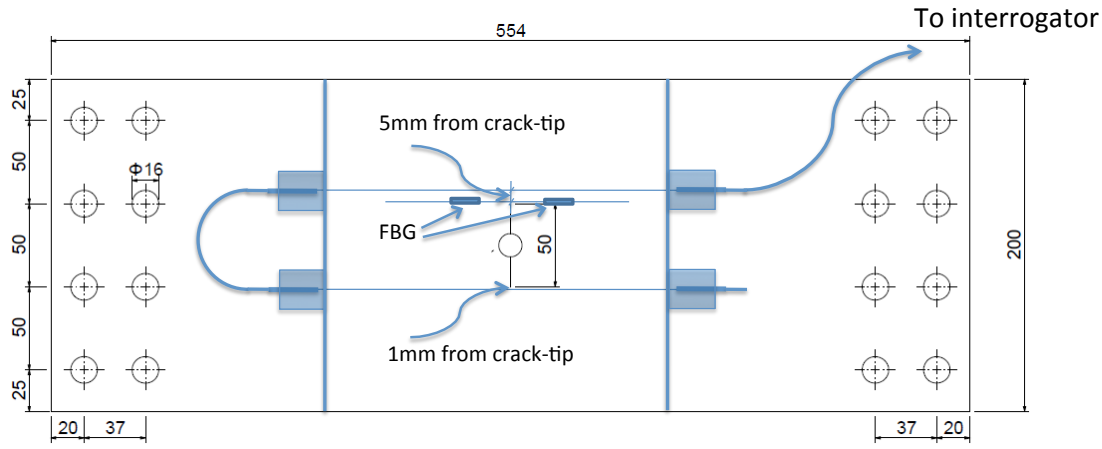

Figure 45: P3 specimen fibre sensor placement.

There are a couple of reasons why the fibre is placed like it was. AIMEN had decided to place their fibres, as indicated in Figure 45, on each side in longitudinal direction next to the crack on one side. They glue their fibre on the steel, as seen in Figure 64 in chapter 9.1.1. Our experience is that the fibre is likely to break during delamination, mentioned in chapter 6.5, and hence our fibre was placed between layer one and two of the patch. To be able to compare the results it was placed 1mm from the crack tip along the longitudinal direction opposite to the FBG. The fibre going on the "outside", 5mm from the crack tip, on the same side as the FBG was a backup if any problems occurred because of high strain level close to the crack, and to also be able to observe the strain gradient decreasing away from the crack.

The manufacturing of the specimens where performed by representatives from AIMEN. A couple of images from the manufacturing is seen below in Figure 46 and Figure 47.

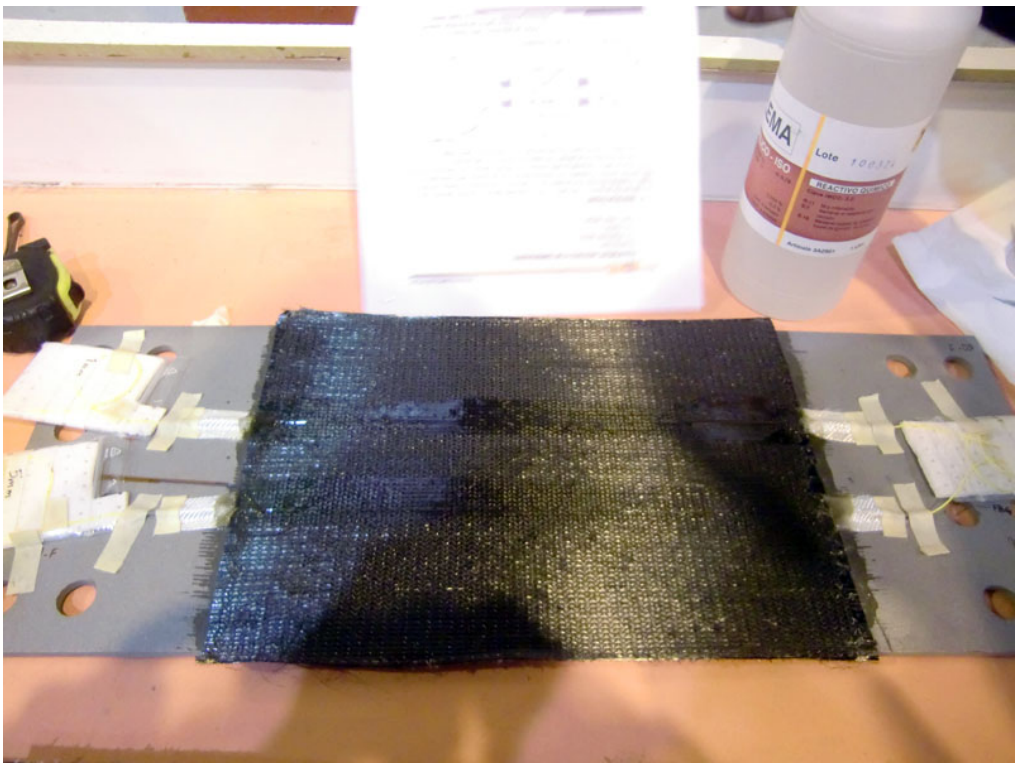

Figure 46: P3 specimens during layup. Photo by: AIMEN

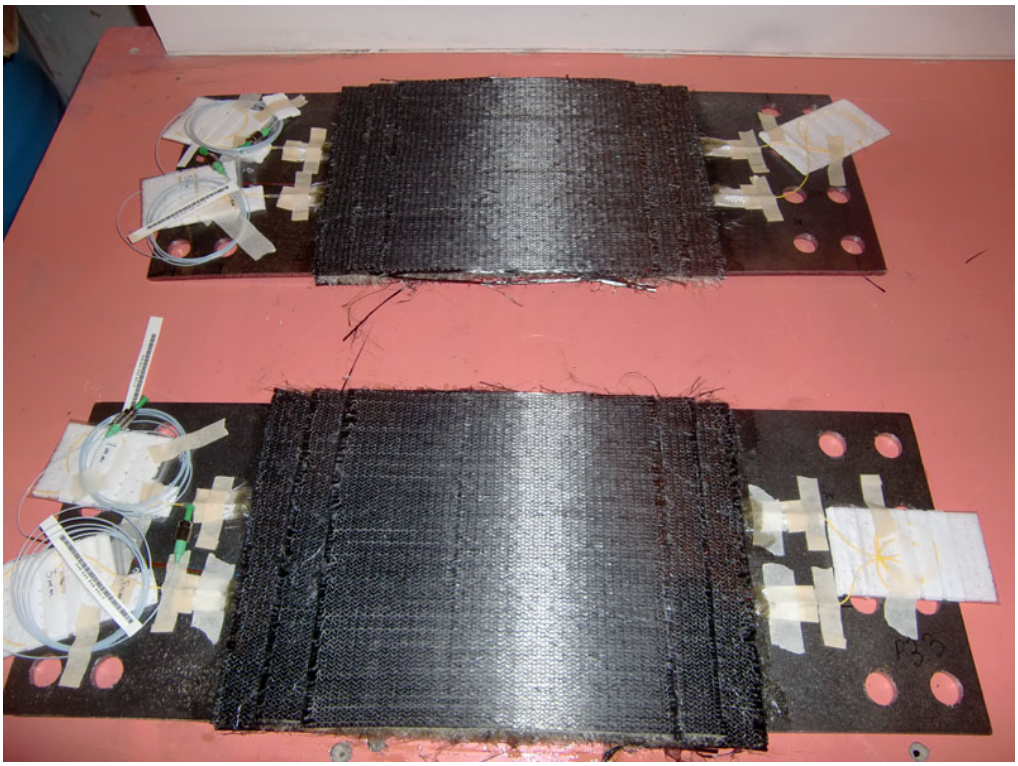

Figure 47: Finished P3 specimens. Photo by: AIMEN

In addition to the embedded fibres, it was bonded measuring fibre to the steel on the other side of the specimen. FBG on one side and OBR on the other side was glued 5mm from the crack tip along the longitudinal direction of the specimen. The OBR fibre was glued to the steel about 20mm outside the patched area in both ends, as well as an approximately 100mm length bonded to the steel transversely outside the patched area. This would be useful to monitor the behaviour of the steel during the test. The results from them are not presented here.

8.1.2 Testing

The four specimens to be investigated in this thesis were tested at Aimen in March/April 2012 in a fatigue test. The test was conducted in their test laboratory with one person controlling the test machine, two monitoring the FBG equipment, PhD candidate J.H. Grave organizing and communicating and the candidate the OBR equipment.

Figure 48: Test setup P3 fatigue test.

A fixture was used to bolt and clamp the specimen before placing it in the HOYTOM test machine. The machine used mechanical wedge grips and need the specimen to be loaded for them to work. Hence the reference for the measurements are not at 0kN load, but will be specified. The test machine and the OBR is seen in Figure 48

Before and after the test, each specimen was visually inspected and photographed as well as dimensions and surface roughness measured. For the needle gun treated specimen we were able to take the patch of after it failed to inspect the surface of the steel and patch. This was not possible for the grit blasted specimens, as they did not fail.

The load history for each of the specimens shows the improvisation done during the test because of shortage of time available. This can be seen in appendix 14.2. Despite that, all specimens are tested at a rate of 0,1 Hz and at the initially planned load ratio R = 0,1 (10-100kN) for the first 100 cycles. Measurements where done continuously with FBG at 1Hz and with the OBR at maximum and minimum load, before and after each series of load cycles.

8.2 WP3 – Task 3.2 - IPE 100 beams

Task 3.2 – IPE 100 beam test is the mid-scale short-term test of patched IPE 100 beams with an initial crack. The beams are manufactured with different methods and surface treatment by different people, but all tested at NTNU and manufactured according to the manufacturing note "Draft-NTNU-WP3-3.2-beam-v0". The responsible for the testing and manufacturing of the prepreg specimens at NTNU are PhD candidate J. H. Grave.

8.2.1 Specimens

In Table 5, made by J. H. Grave, the different specimens are listed. Four of the nine specimens tested are used for analysis in this thesis and are described in the result chapter.

Table 5: IPE-100 beam test scheme with progress report.

Material	Fabrication	Patch length 400 mm				Patch length 300 mm			
		Grit blasting		Needle gun		Grit blasting		Needle gun	
Fiber optic		Embedded	On top	Embedded	On top	Embedded	On top	Embedded	On top
Unpatched	NTNU (2)								
VI-C/E	NTNU (4)		AS2CON (2)		AS2CON (2)				
VI-C/V	NTNU (8)	UM (4)	-			UM (4)	-		
P-P	NTNU (10)	NTNU (4)	-	NTNU (2)	-	NTNU (4)	-		

	Not finished fabricated
	Ready for testing
	Testing is finished

Below in Figure 49 the dimensions of the specimen are presented as well as placement of the optical fibre. The fibre used in the patching by Umoe Mandal is placed as presented in the figure, but for the specimens made at NTNU there is only one fibre in the centre of the patch. The specimens made at AS2CON have no embedded fibre, and would need a fibre glued to the surface for monitoring.

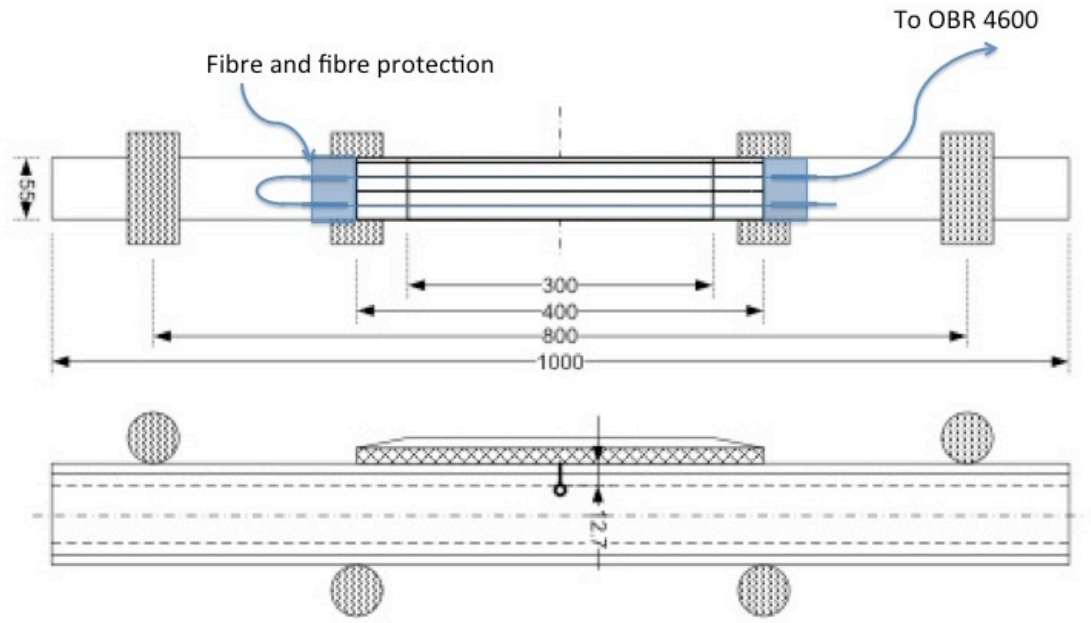

Figure 49: IPE-100 beams with fibre placement illustrated.

Before the test strain gauges was glued according to the manufacturing note at the locations illustrated in Figure 50. The length of the strain gauges is 5mm and is glued to the specimen using Cyanoacrylate glue.

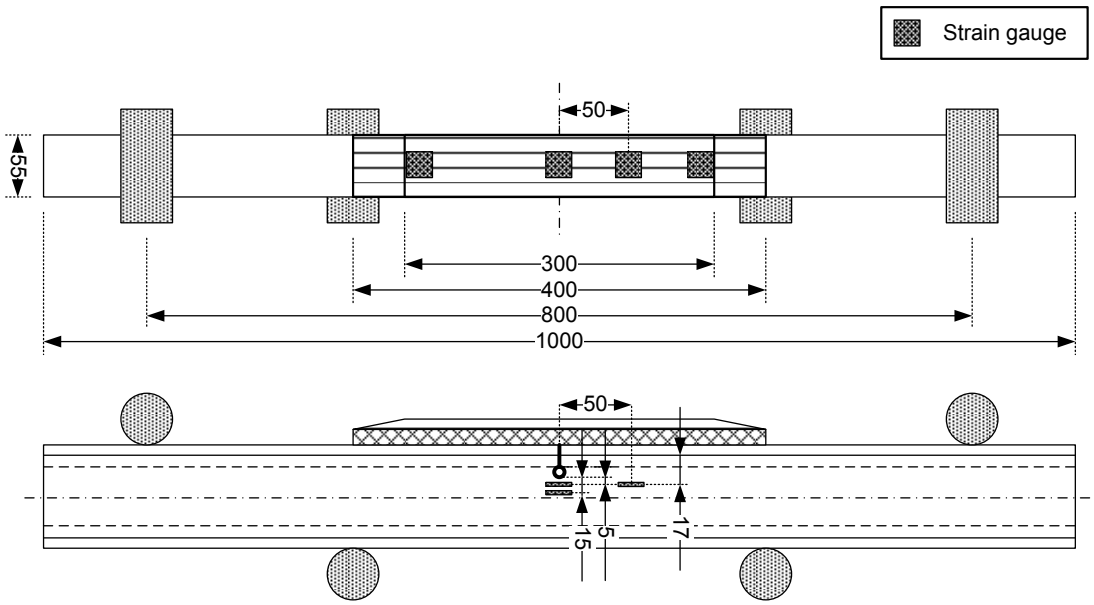

Figure 50: IPE-100 beams with strain gauge placement illustrated. By J.H. Grave

8.2.2 Testing

Testing of the IPE 100 beams were performed at NTNU on a 250kN test machine with a four point bending, test setup designed by J. H. Grave seen in Figure 51. It was loaded at a half of the support span. The beam is placed freely in the rig, but have supports on either side to prevent extensive movement during loading of at failure. It proved necessary to place aluminium plates between the rollers and the beam to increase the contact surface, due to deformation of the flange in initial tests.

Figure 51: Test setup IPE-100 beams

The loading of the beams was carried out at 0,3mm/min and logged at predetermined load/displacement steps with the OBR 4600. The strain gauges, LVDT, CMOD, load and displacement were monitored continuously¸ using HBM Catman Easy with 5Hz sampling rate. The LVDT is used to measure the deflection of the beam at the centre and the CMOD to monitor crack opening. Seen in Figure 52 is the CMOD mounted over the crack and the three strain gauges mounted on the web, where two monitor the strain field above the crack and one is a "far field" reference.

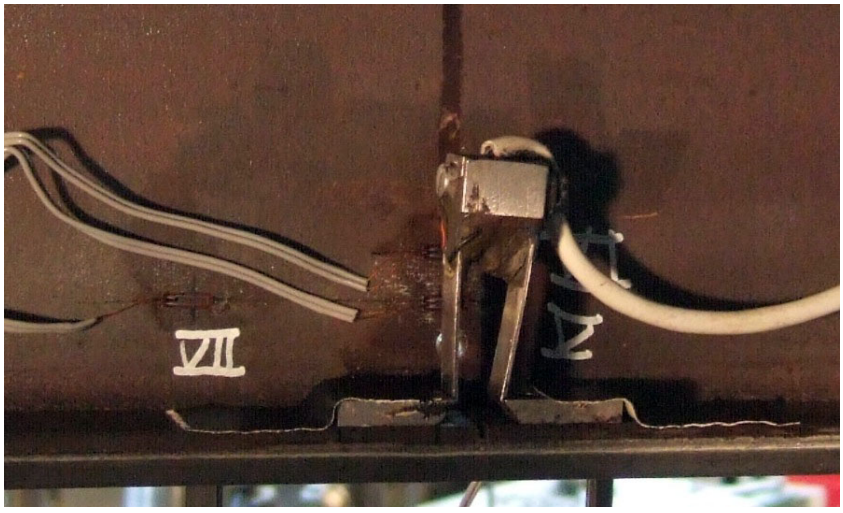

Figure 52: CMOD and strain gauges next to the crack.

From experience with a test beam used to verify the setup, there was decided to load and unload the beam three times within the elastic zone before testing to failure. This approach is the same as used in the steel characterisation in the Co-Patch project (UNIS-TR-WP3-1-v1) to decide the elasticity of the steel. Here it was to investigate if there was any permanent change of the strain field in the patch during the first load cycle as observed in the test beam. The result from one of these is presented in appendix 14.3.3.

8.3 WP3 - Relaxation test

Specimens made for the Co-Patch project with a carbon prepreg patch is cured in oven at 85 degrees for several hours. The steel and the carbon patch have very different thermal expansion behaviour. During the curing both is heated and the bond between them is created at that state. When the specimen is cooled to room temperature the steel will try to contract, but is prevented by the carbon patch that has slightly negative thermal expansion. Residual stresses are built up in the steel, and as a result of this, flat steel specimens tend to be bent.

As a part of the work to investigate the curvature of specimens made with prepreg patch, two specimens were manufactured by PhD Jon Harald Grave with embedded fibre optic cable. He would like to investigate if there would be a relaxation of the steel in room temperature over a longer period of time.

8.3.1 Specimens

The two specimens are made with the same steel, carbon and curing conditions as the other prepreg specimens. The dimensions are 350x50x5 mm steel and 250x50x5,7 mm UD carbon. The steel surface is grit blasted and the patch edges were not machined. The fibre optic cable is placed between the galvanic protection and the carbon patch. After curing a fibre optic pigtail was spliced to the fibre. A picture of the specimen is seen in Figure 53.

Figure 53: Relaxation test specimen.

8.3.2 Testing

The relaxation specimens were manufactured together with the IPE 100 beams on April 2nd 2012. Because of Easter holiday the first reference measurement with the OBR 4600 was done Monday 9th of April. After this measurements have been done regularly and the specimens kept in room temperature in between.

8.4 WP6 - Full scale test

During the last weeks of this thesis the monitoring of three composite patches on the WP6 full-scale test in the Co-Patch project was planned. Discussion of the monitoring setup will here be presented, but since the manufacturing and preparations of the test is not finished when this thesis is written, no results are presented. This test is interesting for this thesis due to its extra challenges of using the fibre optical strain measurements in a real life situation.

Figure 54: Overview picture of catamaran.

8.4.1 Test description

The full scale test summarizing many of the different small-, medium-, and large scale tests performed through the Co-Patch project. A catamaran boat is built by Francisco Cardama, S.A. shipyard in Vigo, Spain with numerous defects built into it. The different defects are spread out on the boat, and will be patched and monitored by the different partners. In Figure 54 an overview picture of the Catamaran is seen on the slipway at Cardama and in Table 6 the different defects and areas of responsibility for the different partners are outlined. NTNU is responsible for design of the two patches of the two crack 1, and monitoring of crack the two crack 1 in addition to one crack 2. In addition to the monitoring of the patches there will be bonded a “far field” fibre close to crack 2, which will work as a reference for normalisation and control for the other sensors as discussed in chapter 5.3.2.

Table 6: Monitoring plan, full scale test.

WP6 - Proposed locations for monitoring

	Portside			Starboard		
	Crack 1 (45 deg. diagonal, 100 mm long)	***Crack 2*** (40 mm long vertical)	***Crack 3*** (45 deg. diagonal, 60 mm long)	***Crack 1*** (45 deg. diagonal, 100 mm long)	***Crack 2*** (40 mm long vertical)	***Crack 3*** (45 deg. diagonal, 60 mm long)
Frame 3	Patched (Grit Blasting) Design: NTNU Applic.: UM Monitoring: CETENA (SG): Back side NTNU (OBR): Embedded	"Far field" 1 Monitoring: CETENA (SG)	Patched (Needle Gun) Design: AIMEN Monitoring: AIMEN (FBG) – Back side – Interface Steel – Patch – Top Patch	Patched (Needle Gun) Design: NTNU Applic.: UM Monitoring: CETENA (SG): Back side NTNU (OBR): Embedded		Unpatched Monitoring: AIMEN: (FBG)
Frame 6	"Far field" 2 Monitoring: CETENA (SG)	Patched (Grit Blasting) Design: NTUA Applic.: AS2CON Monitoring: CETENA (SGs): Back side NTNU (OBR): Embedded AIMEN (FBG): – Back side – Interface Steel –Patch – Top Patch	"Far field" 3 Monitoring: CETENA (SG)		Unpatched Monitoring: CETENA (SG) AIMEN: (FBG)	
Frame 9			Unpatched Monitoring: AIMEN: (FBG)			Patched (Grit Blasting) Design: AIMEN Applic.: ENP Monitoring: AIMEN (FBG) – Back side – Interface Steel – Patch – Top Patch
Frame 9	Upper part of BHD towards CL corroded Unpatched Monitoring: CETENA: SG rosette on corroded steel AIMEN: 1FBG – Corroded Steel			Upper part of BHD towards CL corroded Patched (Grit Blasting) Design: BV Applic.: AS2CON Monitoring: AIMEN: 1FBG – Interface Steel-Patch		

The test will be conducted as a fatigue test from July to October. The fatigue load will be applied by moving water from a ballast tank on the top centre of the catamaran and down into the pontoons and back, using pumps. This should bend the boat and apply load on the patches. This loading will degrade the patches, but different from the laboratory patches, it will be temperature changes, humidity, salt water and potentially other environmental affects as well. Measurements of the fatigue loading will be performed at a test session with all the partners in July, and although the FBG's and the strain gauges will monitor periodically, the OBR will only measure again at the end of the test.

8.4.2 Monitoring

The test and monitoring of this full scale test is the closest to industrial implementation and "real life" during this project, hence some extra concerns and interests were considered. Different environmental effects need attention, such as: Connectors are not waterproof, connecting cables does not withstand rough handling and potentially not rough weather and it will be big temperature changes during the day and year. All of this, except the temperature changes, are challenges that will have to be solved specially for each application. For this test we chose to use electrical tubing and connection boxes to protect the cables. The one used are rated for outdoor use, and by making a hole in the bottom and entering the cable through that before sealing/bonding the box to the structure, a sealed system was ensured. Such a box may be seen in Figure 56.

The temperature changes during this test will probably be an important factor for the degradation of the patch, due to thermal expansion/contraction of the steel during the day. As discussed in chapter 5.2.4, it is necessary to compensate

for temperature changes between measurements. For this test it suggested to only compensate for the temperature induced shift in the fibre optical cable, and not the thermal expansion of the steel. This will be achieved by having a short length of measuring fibre on the patch that is not bonded to the structure. Then, during the test, this part of the fibre will measure a "strain", which actually is the spectral shift caused by the temperature shift. This is then possible to add or subtract to the measurements inside the patch.

The strategy for the placement and alignment of the fibre optical cables are in this setting split in two. It is important to measure the strain in the patch along the load direction and to measure any opening of the crack. In addition there is a need to monitor the patch for any growing defects. For this purpose it is not important in which direction the fibre is placed, as long it is placed close to any potential defects. The fibre in the load direction will detect a defect by the decreased load transfer of the patch by comparing it to the far field sensor. The fibre e.g. close to the edge will detect at which corner the debonding happened by any nonlinear change in the strain field.

From the philosophy discussed above, the placement of the fibre for the patches will be presented below. Only rough sketches of the placement are presented since the accuracy is not interesting without the results. The direction of the fibre follow the ply directions, and is sewed into the ply, as described in chapter 6.2, in the two perpendicular first layers of the patch. The two layers were then sewn together along the edge with normal cotton thread to prevent movement during handling.

In addition to the fibres embedded in the patch, a measuring fibre is spliced to the end of the embedded fibre and bonded to the surface of the patch. This proved an efficient method to document through thickness effects in the IPE-100 beam tests. For this application it may also be a backup if the embedded fibre is damaged to ensure at least some monitoring. The fibre is placed over the embedded fibre next to the crack tip, and for crack 1 also one transverse to the crack. The Cyanoacrylate glue is used to bond the fibre to the surface.

A potentially big concern was discussed during the planning of the sensor network for this test. In the nature of the OBR 4600 system a weakness is that the comparison of two measurements obviously means that the exact same connecting cable have to be used. For this test it was necessary to have connecting cables from the patch on the catamaran to the equipment placed safely on the pier several meters away. A change in the length would represent measured strain, but in practice a change in length would be due to repairing of the cable and probably more than 10mm and out of range of any strain measurements. It would both be practically impossible to manufacture an exact similar cable, but also the fact that we measure the backscatter, the signal returning to the interrogator through the cable is influenced by the cable it travels through. Although the last statement is not investigated in this thesis. In conversation with Luna Technologies it was said that they might be able to use measurements from two different connecting cables by using a splice or

connector close to the patch as reference point due to the fairly distinct reflection from them.

Considering the concerns presented above, the following precautions were suggested for the sensor network and work prior to the testing:

- All patches are connected using a separate cable and not in series.
- All patches are reference scanned using all the four connecting cables for the test.
- All patches are reference measured connected both directions, in case one connector is damaged. Meaning that each patch have a connector in each end of the fibre.
- A separate connecting cable is used to do a reference measurement directly on each patch, which will be stored separate from the catamaran.

If by any chance one of the cables is damaged it will with all this redundancy at least be possible with a comparison between the initial state and the last. Without this, the damage development through the fall would have been lost if not Luna Technology could help.

Crack 1, Frame 3 – Port side:
The crack 1 is inside the pontoons of the catamaran and on the transverse stiffeners. The outside dimensions of the patch are 150 x 150 mm, the radius of the opening is 100mm and the length of the crack is 100mm and in a 45 degree angle. From the simulations done at NTNU it was discovered that this crack would not have developed in that angle. Hence it was chosen to design the patch according to the actual load directions and not perpendicular to the crack as normally done. The patch was made of a 18 ply, $[0, 90, 0, 0, 90, 0, 0, 90, 0]_2$ layup with carbon and vinyl ester. The distance between the parallel fibres are 35mm

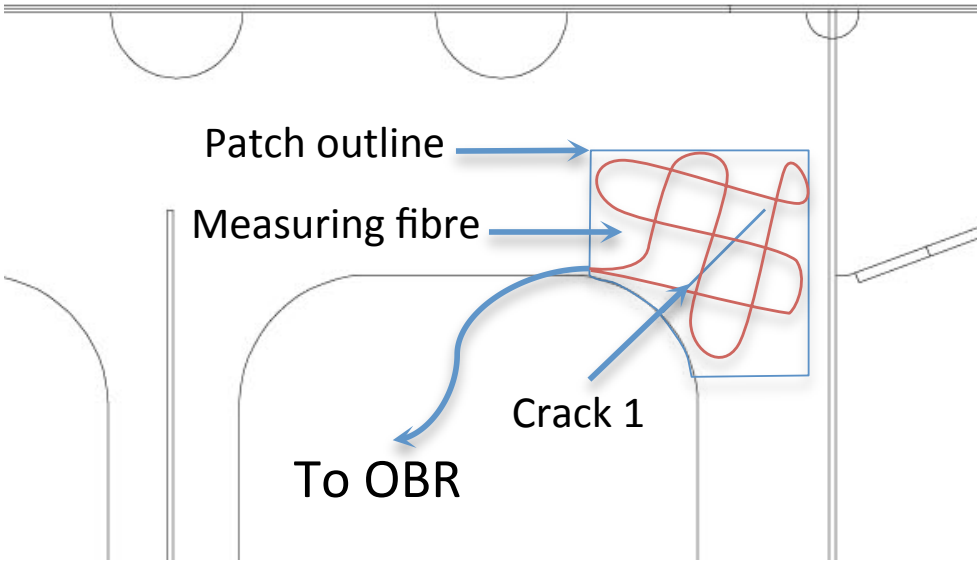

Figure 55: Sketch of fibre placement crack 1

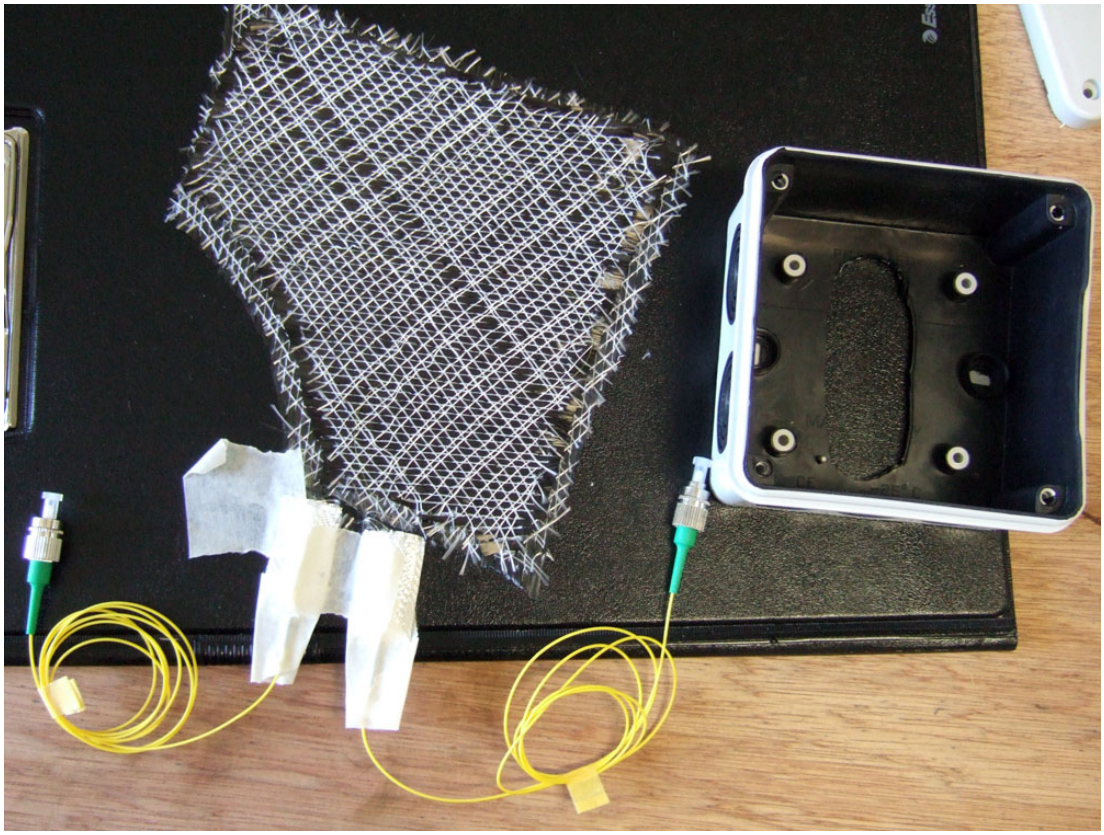

Figure 56: Patch of crack 1 with fibre sensors.

Crack 2, frame 6 – portside:

Crack 2 is on one of the main transverse beams of the catamaran. This crack will experience the most stress during the load cycles. The patch is designed by Aimen and was applied by Umoe Mandal. The external dimensions are 80 x 300mm. Because the loading is only in one direction, fibre was only placed in that direction. As seen in the sketch in Figure 57, it was chosen to place a fibre on each side of the crack tip as well as one placed on the top and bottom of the patch. The same considerations as for crack 1 were done to ensure complete monitoring of the patch.

Crack 2 is chosen to be monitored by all the three measurement systems. Strain gauges, FBG and the OBR will be installed and used during the fatigue testing. The FBG will be placed 5mm from the crack tip on the steel, so the comparison with the OBR will be the same as done on the P3 specimens. The strain gauges are placed on the steel on the other side, 5mm from the crack, and will probably give a different absolute value. The damage growth and nonlinear increase in strain at the crack tip will be observed similar to the OBR measurements.

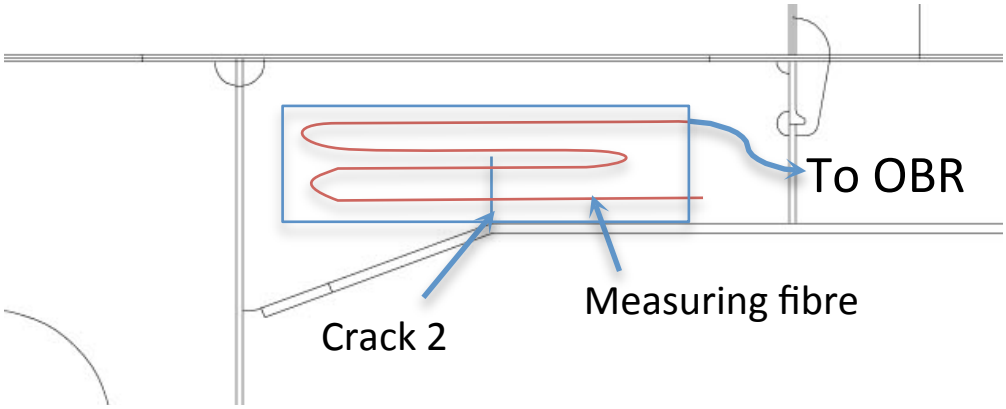

Figure 57: Sketch of fibre placement, crack 2.

Figure 58: Patch of crack 2 with fibre sensors.

9 Results

The results from OBR 4600 are acquired after a test by choosing a measurement as a reference and another measurement to compare for changes in strain. Then the sensing range which strain should be calculated from is chosen as well as gage length and sensor spacing as illustrated in Figure 59. These two parameters are two of the boundary conditions used by the algorithms to compare the reference and the measurement and calculate the strain. Chapter 6.3 describe this in more detail. For each setup it is advisable to control and confirm which parameters that give the best results. Stress concentrations often lead to scattered curves if the parameters are not correct. The choice of parameters is a trade-off between smooth, nice curves and potential detection of small changes in strain. Sensor spacing determines the spatial resolution, hence the number of data points along the sensing range and from the work in this thesis 0,1cm have proven to give good results with a decent resolution. The gage length has the highest influence on the signal-to-noise ratio, and seen in Figure 60 is an example from P3_4 with varying gage length. For most of the data presented in this thesis 0,6 or 0,8cm have been chosen.

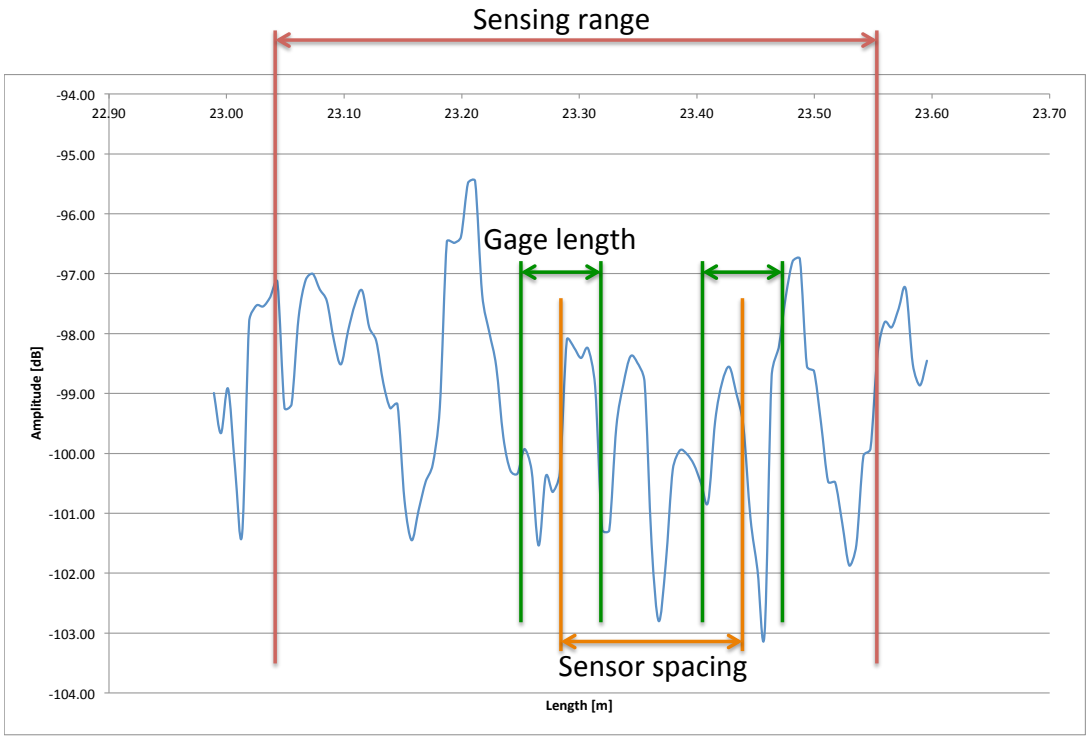

Figure 59: Sensor parameters to be chosen for strain calculations with the OBR 4600.

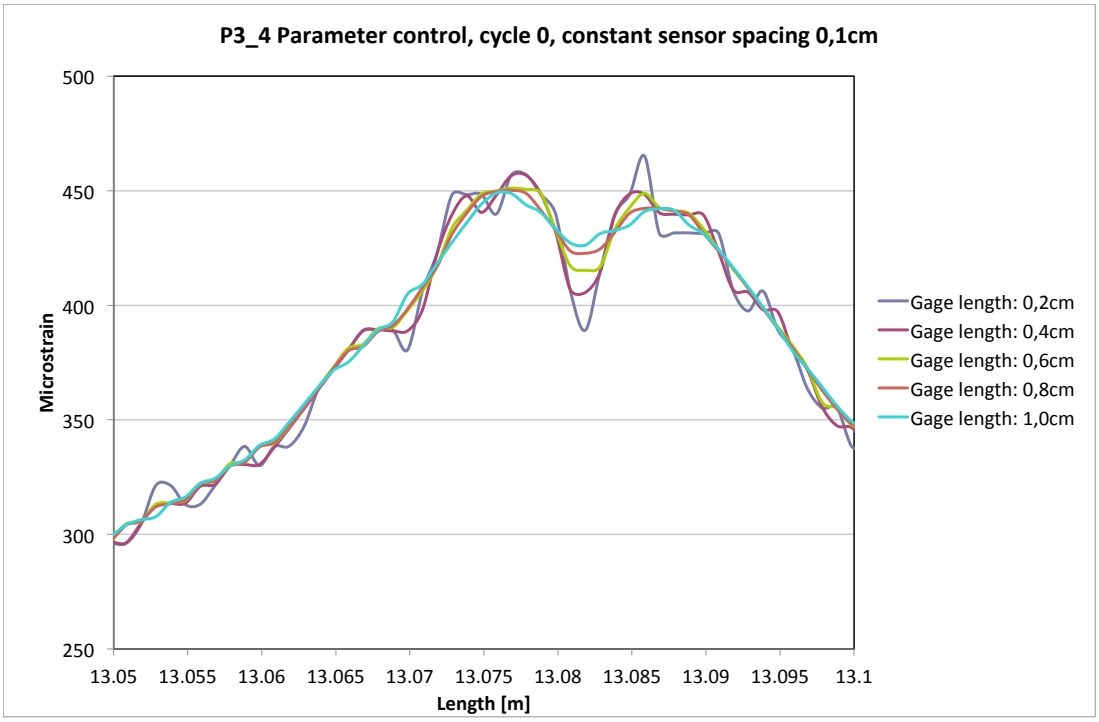

Figure 60: Illustration of influence of gage length on P3_4.

9.1 WP3 – P3

The fatigue test of the P3 specimens gave several interesting results. Below are the results presented for the P3_4 specimen, as well as a comparison between OBR and FBG at the end. The results are separated in measurements at the cycle maxima and minima and the load level is indicated in the chart legend. The results for the three other specimens are found in appendix 14.2 with only a short comment.

9.1.1 P3_4

The P3_4 specimen is a needle gun treated specimen, and at the fatigue test at Aimen this gave the most interesting measurement results. This is due to the early failure and hence it failed within the time available. In Figure 61 measurements of the embedded fibre optical fibre 1mm from the crack is presented. As expected a higher strain level is observed above the crack, but already from the first cycle a strain level higher than at the crack is measured at one end of the patch. The shape of the strain field at the crack is observed on all the specimens, and may be explained by standard fracture mechanics or the crack width that may cause a separate stress concentration on each side. The distance between the peaks are 10mm, which could be expected considering the fibre is placed between layer one and two, which means the stress concentration at the crack tip have been somewhat spread already at the fibre. The distance from the peak to the average strain level in the patch is 50mm, which means the crack is only causing an increase in the strain level in on third of the patch length.

The high strain level at the right side of Figure 61 increases from cycle 0 to cycle 1, before it drops at cycle 10. Then after 100 cycles the strain level at that area have dropped a lot. The strain level from the centre towards the side is unchanged, but drops instantly 100mm from the centre. Such a decrease in strain could only indicate a debonding, and now a part of the patch that is unstrained. 50mm from the edge of the patch is the end of the tapering, and might explain why the first debonding stopped here. The increased stiffness of the patch changes the conditions for the joint.

Two times 100 cycles are performed after the first debonding, where nice growth of the debonding is measured. The strain level at the crack is unchanged, but at 300 cycles the strain level on the other side of the crack also is decreased. Measuring every 100 cycles could have monitored further growth, but it is decided to do 700 more cycles. At 1000 cycles almost half the patch is debonded. The load is increased and further cycles are carried out until the other side of the patch also debonds. The initial length of the debonding is also here 50mm.

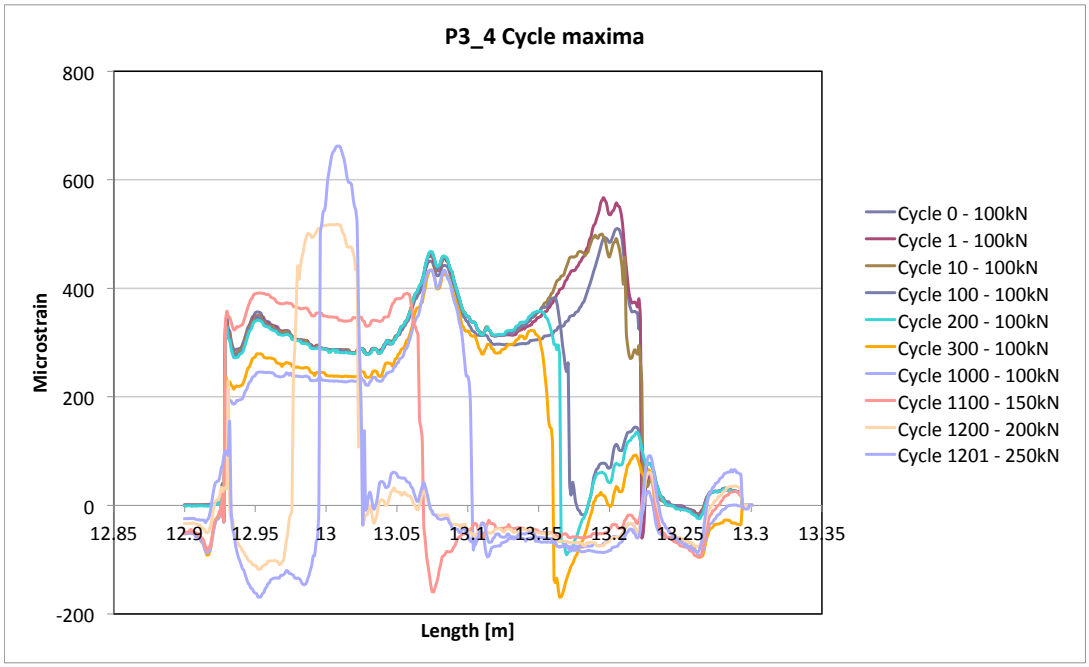

Figure 61: P3_4 cycle maxima

More or less the same history is observed on the measurements at cycle minima in Figure 62. Worth mentioning is the measured compression in the debonded area. This indicates that the specimen was slightly strained from the manufacturing. Although the reference measurement was done at 3kN load, the compressive strain is larger than expected. It could also be seen that the debonding at the left side has not yet occurred at 1200 cycles at the cycle minima, this because this was measured before the cycle maxima where the load was increased. Hence the debonding happened during static tension and not during fatigue.

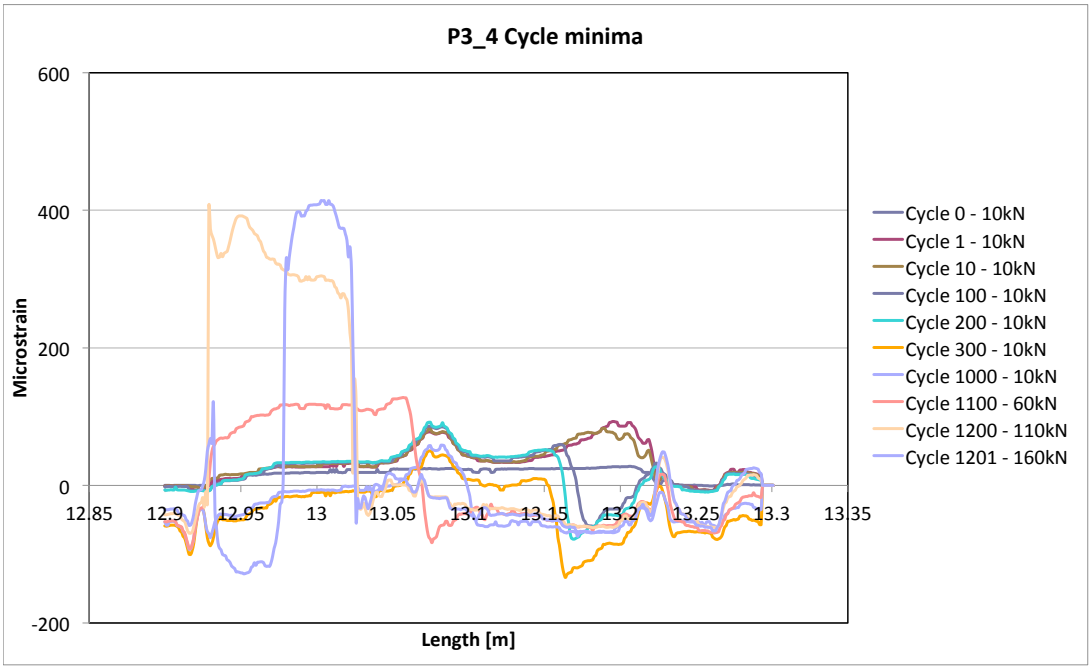

Figure 62: P3_4 Cycle minima

Below in Figure 63, normalization of the measurements at the crack at cycle maxima is presented. The introduction to this is presented in chapter 5.3.2. Here this is performed by normalizing against the average strain in the average strain area of the patch. The debonding at the end of the patch is not visible, but it illustrates the point that not until cycle 300 and 1000 there is a change in the strain distribution in the patch close to the crack. Debonding is observed in the same way as for the standard strain plots by dropping to zero. Only 50% higher strain at the crack is the lowest observed in the three specimens.

In appendix 14.2 the normalization plots for the other specimens are presented. It is obvious that there is a difference between the grit blasted and the needle gun prepared specimen, where the grit blasted have an large increase in strain level at the crack during the fatigue test. They generally show better adhesion on the whole patch, hence it is the crack that causes the damage development and not the edges.

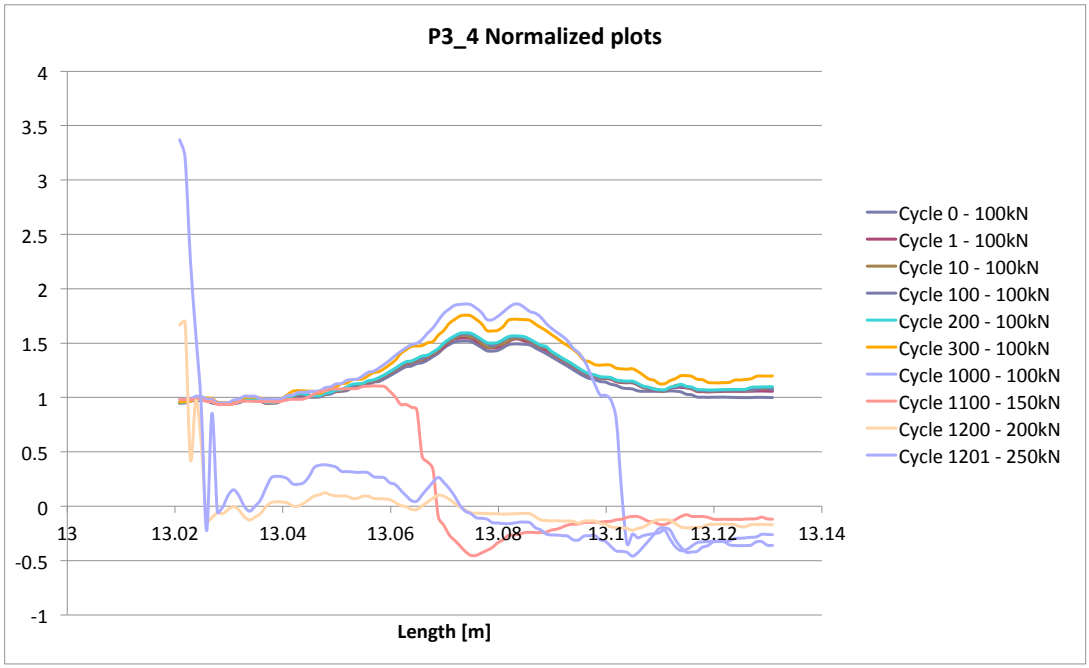

Figure 63: P3_4 Normalized plots

As described in chapter 8.1.1 there was also used FBG sensors embedded in the specimens. Even though the FBG was bonded to the steel below the patch and the OBR fibre was above on layer one there is good agreement between the measurements. In Figure 65 and Figure 66 there have been extracted the strain value from the OBR measurements at the same location as the FBG. They have been plotted for each of the measurement stops at the different cycles. As seen in both figures the FBG sensor indicates very high strain when the debonding has reached the sensor. The reason for the FBG is measuring such high strain is probably because it is bonded to the steel, and when the patch no longer arrest the straining of the steel higher strain level will be experienced. Figure 64 show how the crack opens after the patch failure and the plastic yielding at the crack tip is visible. As seen in Figure 61, this is not experienced by the OBR sensor, which is inside the patch, which was debonded. The numerical values of this comparison is shown in appendix 14.2.

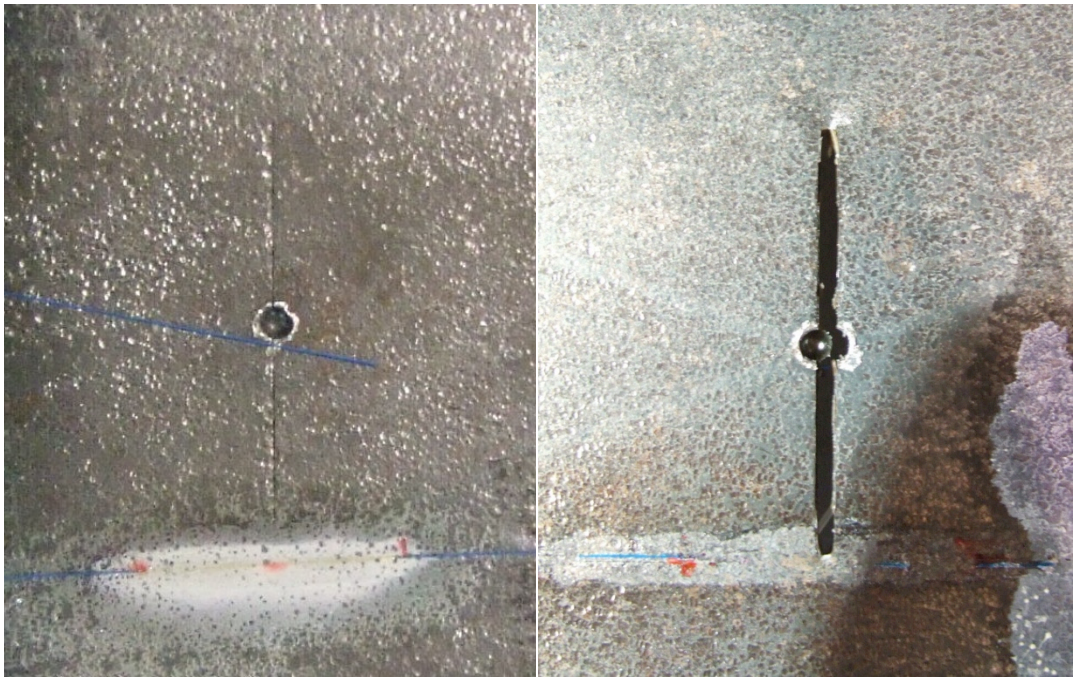

Figure 64: Crack in P3 before (left, steel side) and after (right, patch side) patch failure.

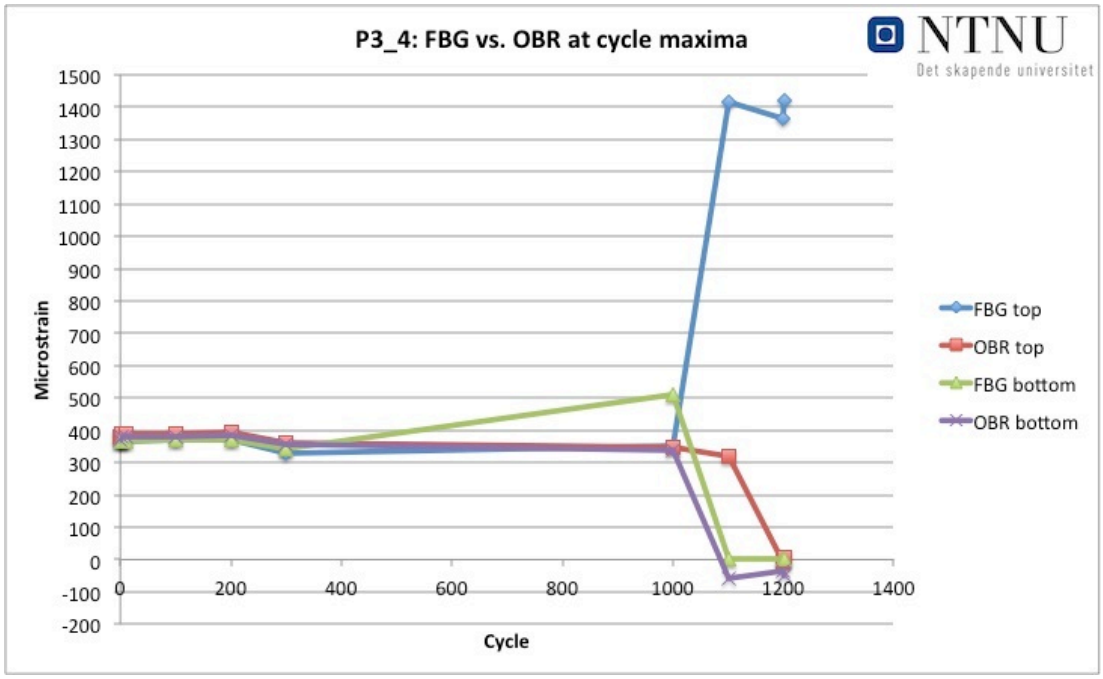

Figure 65: P3_4 - Comparison of FBG and OBR at cycle maxima.

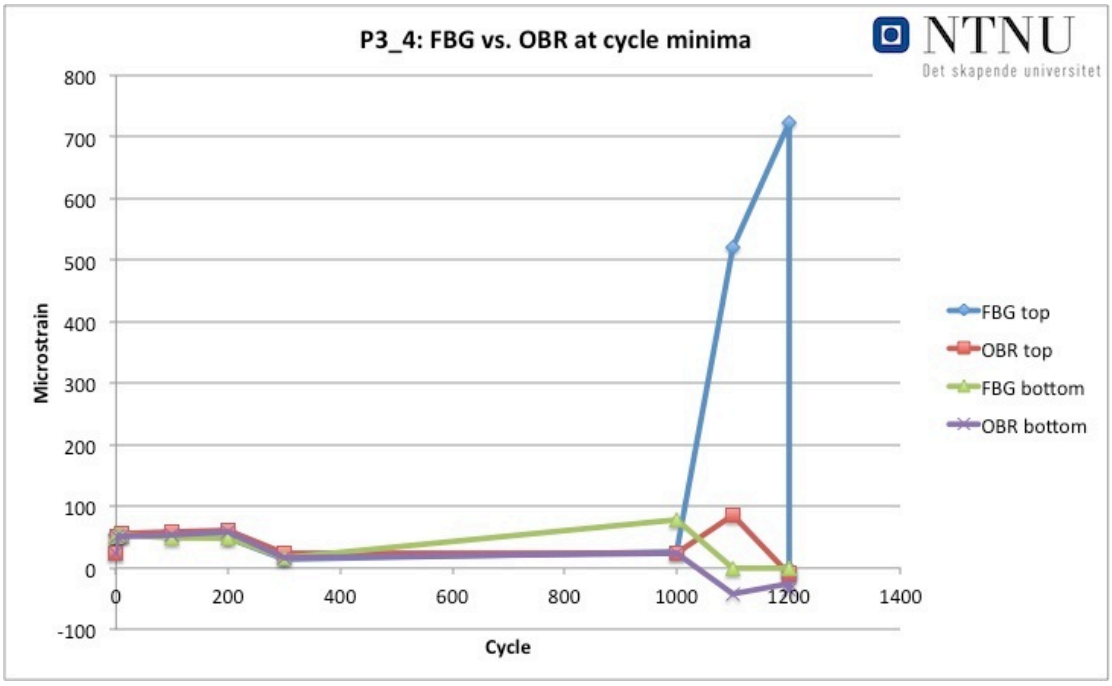

Figure 66: P3_4 - Comparison of FBG and OBR at cycle minima

9.2 WP3 – Task 3.2

Nine IPE-100 beams have been tested at NTNU. One will be discussed and the results from three other are in appendix 14.3. The two grit blasted specimens, GB #1 and GB #2 showed almost identical failure pattern.

9.2.1 GB #2

The strain measurements from the OBR 4600 are presented in Figure 68 and the normalized results in Figure 69. The normalization has been performed as described in the P3_4 results.

Seen on the strain measurements is the same effect as on the P3 specimens, where one end of the patch has a strain level as high as over the crack. Here there is in addition something probably from the manufacturing that is causing scatter in the results. Discussed in 5.2.1 micro bending of the fibre may cause noise like what is seen here.

A linearly increasing strain is observed in the patch during loading, except at the crack. This is most easily seen in the normalization plot how the strain at the crack decreases by loading, but is more and more spread out. It is easily visible at 117kN and then at 133kN the strain field splits into two. At 148kN the patch fails from the right side and the beam was bent similar to the specimen in Figure 67. Unfortunately there is no measurement between 133kN and the failure load, but a possible trend is visible in the plots, that the right side of the crack has a larger strain field. Together with the high strain at the right side of the patch, it was fairly evident that it would fail on that side.

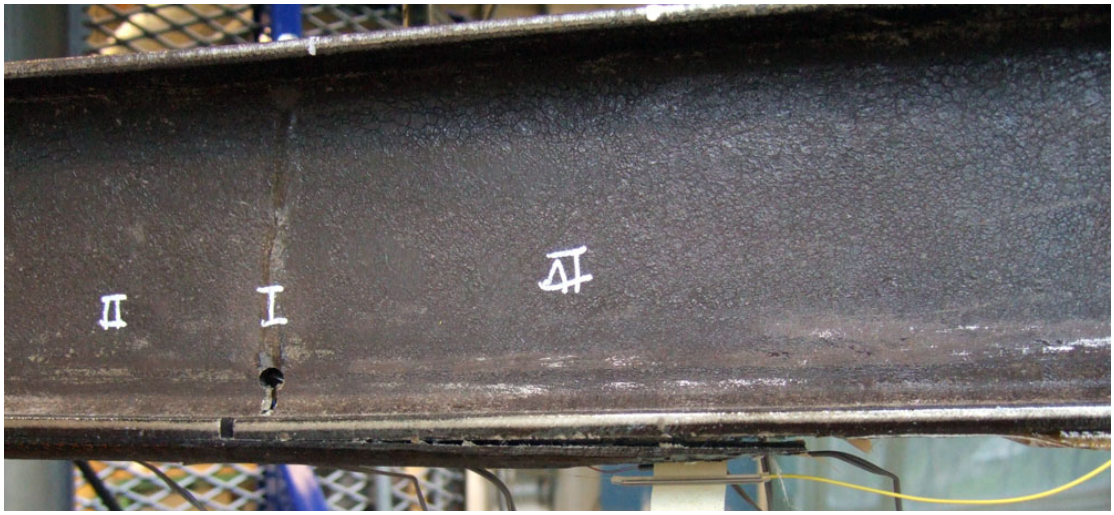

Figure 67: Specimen VI-C/V #4 after failure.

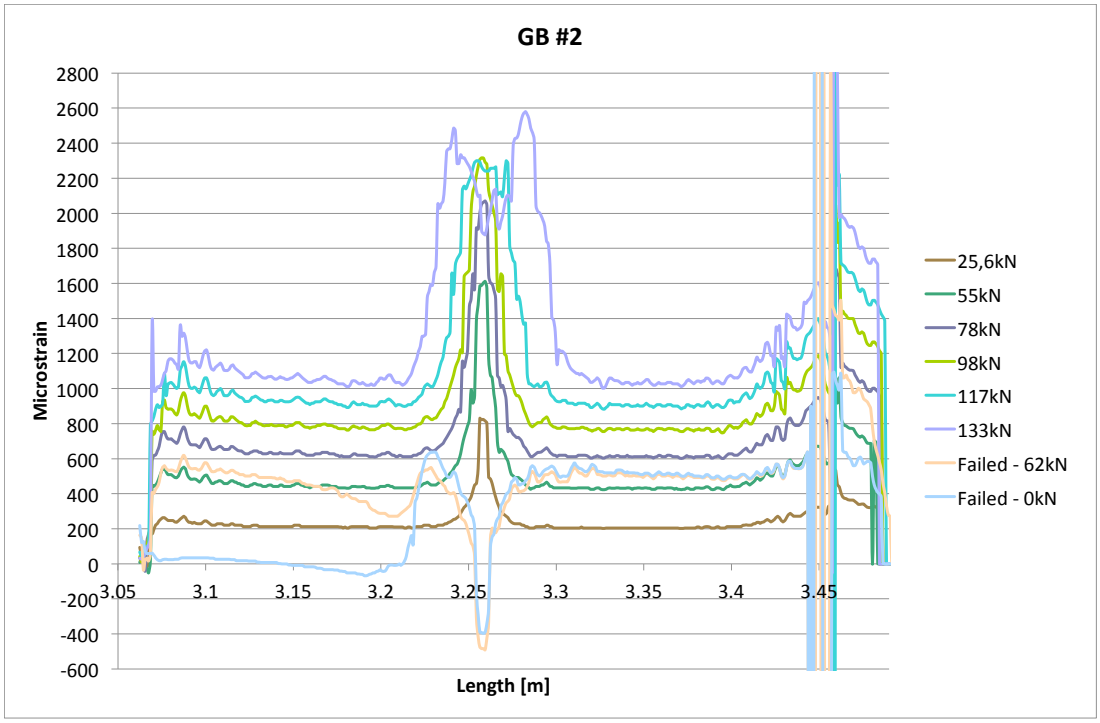

Figure 68: GB #2 Measurement results

The linear behaviour of the high strain level at the right side of the curves (67) makes it not likely that it is caused by a stress concentration. The same shape of the curve is observed on the GB #1 specimen, and there is nothing with the manufacturing that should cause such a large difference. And the fact that this is not observed on the two vacuum infused specimens VI-C/V 1 and 4 that is shown in appendix 14.3 indicates that this needs further investigation on the other specimens. Also interesting is the fact that GB #1 proves that it is not the source of the failure when the test fails on the opposite side.

The two strain curves plotted in Figure 68 from after the failure show the total opposite of those from P3. It is the right side of the specimen that failed, which shows an average strain level of about 500 microstrain independent of the loading. The reason for this is the residual stresses caused by the curing of the

prepreg. The reference measurement is done after the curing when there is compressive strain in the patch caused by the contracting steel. When the patch have debonded it is allowed to expand, and the value of the residual strain is easily seen in the figure. Worth noticing is that this residual strain is equally large to the strain caused by the load when approximately 60kN is applied in the four point bending. Why such large residual stresses do not significantly affect the failure load of the specimens tested here is outside the scope of this thesis, but it demonstrates the importance of knowledge about boundary conditions for the measurements in a SHM system.

The behaviour measured at the crack has a couple characteristics similar to the theory presented in chapter 5.1.2. The 4mm uniform strain level over the crack may be interpreted to be that the 1,6mm crack is so wide that the patch is freely loaded between the two flanges. Due to the 1mm spatial resolution and the glass fibre below the fibre, a small error is expected. The effect of the strain field that is distributed away from the crack is described in the theory as the yielding of the adhesive due to the stress concentration. The adhesive is plastically deforming which distributes the load in the patch, which is good for joint strength, but not when arresting cracks. The reason why no such effect is observed on both sides of the patch is due to the tapering. The patch may be considered as two joints which are presented in the theory where one end have a stress concentration, and the other have a tapering to prevent stress concentration and peel stresses.

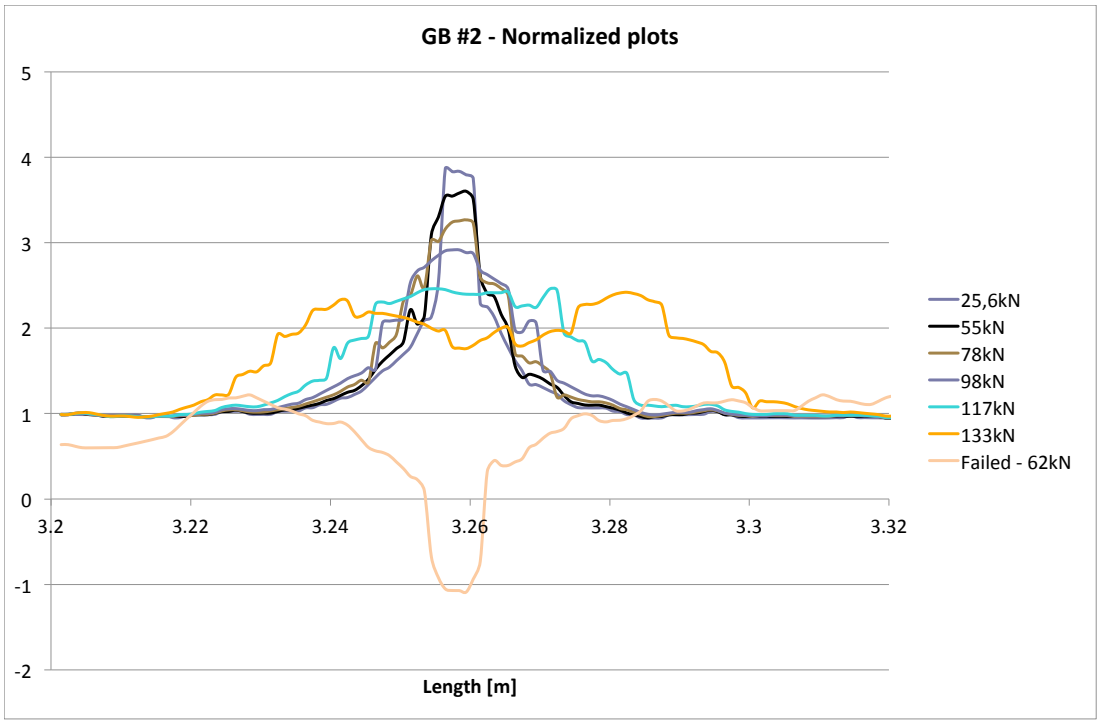

Figure 69: GB #2 Normalized plots

9.3 Relaxation test results

The relaxation test is a good example of the OBR 4600 used for a SHM application. As long as the fibre is intact, it can be connected to the OBR any time and be scanned. It is fast and simple to set up for a measurement, and results could either be extracted at once or later. For this test the temperature is constant and no temperature compensation were done.

The results are fairly surprising, because except some small changes the first days nothing happened, as observed in Figure 70. The experiment may be continued, but it is evident that no major changes are measured and hence the deformation caused by the thermal expansion during curing is stable when kept in room temperature. Considering a linear expansion coefficient of steel of e.g. $12 \cdot 10^{-6} /^{\circ} C$ it will according to $\varepsilon_{thermal} = \alpha_L \cdot \Delta T$ result in a strain caused by heating from 20 to 85°C of 780 microstrain. It is dependant of the chemical properties and the curing process of the resin, but a residual strain in the specimen of several hundred microstrain would be expected.

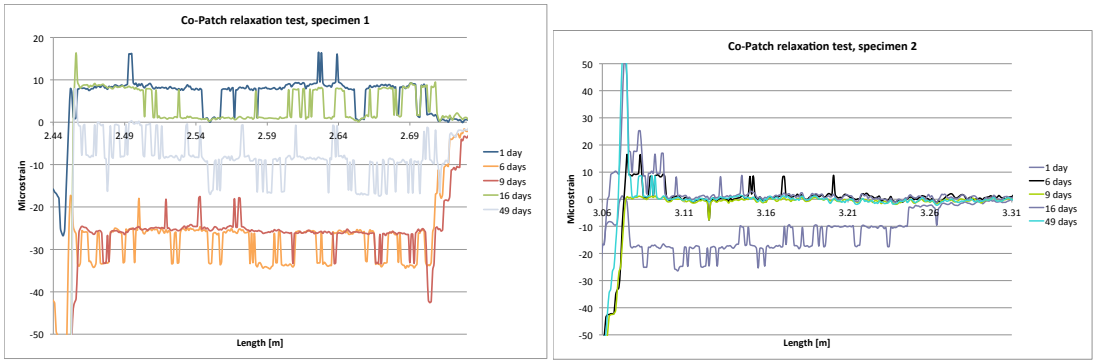

Figure 70: Strain measured in relaxation tests

10 Discussion

Health monitoring of composites using optical fibres have in this thesis been presented, developed, discussed and tested. The OBR 4600 have been used in many experiments to measure strain in composites, and have in several occasions been compared to other measurement systems to establish knowledge about the accuracy of the system. The tests for the Co-Patch projects were all on specimens with stress concentrations caused by cracks in the steel that is patched, where the system performance at stress concentrations is easily observed.

The comparison of measurements with other sensors in the experiments performed in this thesis has given good results. They are not valid as calibration of the OBR measurements due to the complexity of the specimens and distance between the sensors. They give a good indication of calibration results that could be expected. The calibration experiment on the extensometer calibration tool gave interesting results, but high accuracy was not obtained. The deviation in the measurements and the lower accuracy could be explained by the setup and the fixture. Between 6 and 22% lower measured strain than calculated could be explained by yielding of the adhesive, due to the increasing difference with increasing displacement. A mechanical grip could have worked better, but the fibre would need protection against crushing that would deform similar to the adhesive. The best confirmation of results was seen in the work done for the paper to the ECCM15 conference attached in appendix 13.2. Measurements with fibre on the surface of the patch of a IPE100 beam agreed very good with strain gauges, and measurements from the embedded as well as from the surface corresponds very well with the FE analysis of J.H. Grave.

From the SHM theory of this thesis, a list over components necessary for a SHM system, by Kessler and Spearing [25], are presented and during the thesis several of the topics are investigated and discussed on general basis:

- **Architecture:** For a structure using the fibre optical system presented in this thesis, a sensor network will be designed by placing a fibre optical cable suitable for measuring on the locations, layers and direction that is desired. The network must locally consist of one fibre, but on a larger structure or on a structure consisting of several parts it will need separate cables. The conditions for placement of the fibre are discussed in 6.2. As discussed in preparations to the full scale test in chapter 8.4, the architecture of the sensors may have several purposes, namely strain and temperature sensing as well as damage detection. Both functions have successfully been demonstrated in the experiments in this thesis.

  The advantage of the OBR 4600 system is the possibility to have a sensor in a structure without knowing where damage or the highest strain levels will be. A moving strain field is possible to measure along the length of the fibre, which is not possible with FBG or electrical strain gauges. It is

recommended to place it close to critical areas, but caution should be shown to prevent that the fibre is ruptured or damaged by damage development. In the Co-Patch patch repairs this meant placing the sensor in the layer above the critical layer.

Transfer of signal from the embedded sensor to the measurement system has in this thesis been accomplished with a simple, but effective protection of a cable exiting the side of the laminate. In chapter 6.8 potential solutions to avoid the cable is presented.

Strain and temperature influence must be isolated by having a temperature compensating sensor on the structure during strain measurements, and vice versa. This was discussed in chapter 5.2.4.

- **Damage characterization:** In the experimental work in this thesis with patch repairs, the damages expected were yielding of adhesive and delamination. Delamination and damage growth was easily monitored using the optical fibres during fatigue testing in the P3, and to some extent on the IPE 100 beams. Yielding was believed to be detected in the investigation of the normalized plots of the IPE 100 beams and the grit blasted P3 specimens. The importance of characterization of expected damage was demonstrated by the difference in measurements of delamination for the heat cured prepreg specimens versus the vinyl ester specimens of Task 3.2. The OBR 4600 is only able to do static measurements; hence potentially dynamic changes and properties of the specimens are not recorded.
- **Sensors:** The sensors that may be used for the OBR 4600 system is standard single mode fibre optical fibres. Different diameter cables are available, from 80-250 micron, where a 155 micron was used in this thesis. The diameter and possible bending radius will affect the quality and possibilities during manufacturing, but most important is the coating material that govern the shear transfer from the host material to the fibre; hence the measurement quality. Polyimide is recommended by Luna Technologies and confirmed in literature to give good results.

  The sensing possibilities with the OBR 4600 are strain and temperature, but with further software development and analysis, optical fibres have proven many sensing applications as discussed in 5.2. Micro bending, curvature, vibrations, etc. are examples of such sensors.
- **Computation:** The OBR 4600 consists of the interrogator and a laptop that works as a system controller as well as computational software. The software algorithms analyse the measured Rayleigh backscatter to produce the strain or temperature data. Additional software for analysis of measurement results could either be implemented on the same laptop, or externally. Any nonlinear events detected from normalization of the results such as presented in 5.3.2 and demonstrated in chapter 9 could trigger an alarm and would predict failure, severity and location directly.
- **Communication:** Communication between sensor and interrogator have do be done with fibre optical cables. The maximum length is normally 70m cable, but the software features a “spot scan”, that enables up to 2km connecting cable before a sensing length of 2m. A set of sensors may be

connected in series, but for increased security it is recommended to connect them in parallel and use a fibre optical switch, or manually scan the different sensors. With todays price level the OBR 4600 will probably not be installed on a structure, but brought to it for inspection. It is in either way possible to remotely control the interrogator through the instrument laptop using TCP/IP network connection. Hence it is possible to control it and receive data from the other side of the world through internet if necessary.

- **Power:** The fibre optical sensors are passive and do not need any power. The interrogator and instrument laptop does need standard power outlet with 220 or 110V.
- **Algorithms:** Algorithms to analyse the results have not been developed in this thesis. For such algorithms it is proposed to use the knowledge about measurement scatter from the parameter influence in 6.3 and the normalization in 5.3.2. Important for the algorithms for this system would be to reduce the amount of data presented to the user. Tests would have to be done with the structure to analyse what results are obtained from different damage scenarios such as those seen in this thesis.
- **Interventions:** No work has been done in this thesis to investigate intervention mechanisms.

The weaknesses and challenges of this system are in many ways similar to other fibre optical strain measurement systems. As presented above, there are several areas that need further development, such as entering of the fibre into the composite, software, communication and of course that the system is not today able to be used on vehicles. The power need, the intolerance for vibrations and price makes it most suitable for measuring at service stops and stationary structures, which is against SHM philosophy. The system are today not able to monitor continuously, due to the high need for computer performance. As seen in the specifications of the OBR 4600 in appendix 13.3, they claim it is able to have a sample rate of 3hz, but then possible measured strain is limited. Decreasing the wavelength range of the OBR recuses the amount of data, and thereby the scan time. The wavelength range is as seen in chapter 5.2 connected to the strain level possible to measure. The advantages of FBG systems are the small interrogators, possibility for high sample rate and several channels.

The introduction of fragile fibre optical fibre in a composite manufacturing environment is a challenge. Embedment of fibres is labour intensive, and with the method used in this thesis, the cable exiting the laminate is vulnerable. Even though the OBR a lot easier to design a sensor network, it still need planning and design. The placement of the fibre needs to be accurate if a location is to be located. In the specimens tested in this thesis the crack have been an effective reference for such. A successful embedment is when there is no sharp bends or fractures that causes signal loss and no results. Micro bending, or reflections from the end of the fibre may influence a section of the fibre and results are difficult to extract. A concern is that the fibre will brake from damage of the composite, which then will cut the connection with the rest of the “sensors”. Caution should be exercised when considering fibre placement and connection point to prevent this, which have been discussed in the experimental work of this thesis.

11 Conclusions

In this thesis the candidate have shown with extensive experimental work that the OBR 4600 system is suitable for health monitoring of composites. Through the work there have been gained a lot of experience in using fibre optical strain sensors in composites for both strain measurements and damage detection. During this thesis it has, from the experiments, been obtained credible results with the developed techniques and the results have been discussed.

The results and experiences obtained are confirmed by literature on similar fibre optical sensors. In addition the measurement results have been easy to interpret and to explain with composite or adhesion theory, which is a big advantage for a SHM system. Further development and implementation of the OBR 4600 in a SHM system would be feasible. From the experiments it is seen that there are still some practical issues to address, and in the theory it is seen that many of the challenges for the OBR 4600 system is similar already implemented SHM systems such as damage characterization, computation and algorithms.

The measurement performance has through this thesis been tested in different tests. It has generally given slightly lower and non-consistent strain values in bonded applications, but very good agreement with FBG in the P3 specimens and FE-analysis in the paper. This indicates that a different gage factor should be considered for the different applications. Further analysis should be considered to improve the performance on bonded applications.

The methods that have been developed through the thesis have constantly been used in the experiments. The practical use of the fibre optical sensors, but also analyses, software and theory has been implemented. Finally the experience was used in the full scale test in the Co-Patch project. It proved to be a difficult application due to the lack of information and control over parameters. No algorithms or computational software was developed for the test, but an advantage with the OBR, is that all the measurements and data are available for post processing at a later stage. The test will give valuable information and results for further development of the system.

In further work attention should be on implementation and communication with other systems, software development to reduce post processing time and robustness and predictability of the system. This will be necessary to be able to reach the level 4 of SHM that predicts remaining service life, where several types of sensors would be necessary to determine e.g. fatigue cycles from use.

Although the OBR 4600 are not normally mentioned when listing sensor technologies for SHM, this work have demonstrated that with some further development it should be a natural competitor to the FBG in the future.

12 References

1. Kreuzer, M., *Strain Measurement with Fiber Bragg Grating Sensors.* p. 27.
2. NTUA, T.a. *Co-Patch flyer*. [cited 2012; Information flyer for the Co-Patch project].
3. da Silva, L.F.M., Öchsner, Andreas, Adams, Robert D., *Handbook of Adhesion Technology*. Vol. Volume 1. 2011: Springer.
4. A. Ghatak, K.T., *Optical Waveguides and Fibers*, in *Fundamentals of Photonics*, C. Roychoudhuri, Editor 2000, Spie: Spie Press Book. p. 249-292.
5. Knowles, S.F., et al., *Multiple microbending optical-fibre sensors for measurement of fuel quantity in aircraft fuel tanks.* Sensors and Actuators A: Physical, 1998. **68**(1–3): p. 320-323.
6. de Oliveira, R., et al., *Optic fibre sensor for real-time damage detection in smart composite.* Computers & Structures, 2004. **82**(17–19): p. 1315-1321.
7. Zhou, Z., J. Li, and J. Ou, *Interface transferring mechanism and error modification of embedded FBG strain sensors.* Frontiers of Electrical and Electronic Engineering in China, 2007. **2**(1): p. 92-98.
8. Duck, G. and M. LeBlanc, *Arbitrary strain transfer from a host to an embedded fiber-optic sensor.* Smart Materials and Structures, 2000. **9**(4): p. 492.
9. Galiotis, C. and A. Paipetis, *Definition and measurement of the shear-lag parameter, β, as an index of the stress transfer efficiency in polymer composites.* Journal of Materials Science, 1998. **33**(5): p. 1137-1143.
10. Cox, H.L., *The elasticity and strength of paper and other fibrous materials.* British Journal of Applied Physics, 1952. **3**(3): p. 72.
11. Okabe, Y., N. Tanaka, and N. Takeda, *Effect of fiber coating on crack detection in carbon fiber reinforced plastic composites using fiber Bragg grating sensors.* Smart Materials and Structures, 2002. **11**(6): p. 892.
12. Martin, J.M.M. and A.G. Gordo. *SHM Using Fiber Sensors in Aerospace Applications*. 2006. Optical Society of America.
13. Levin, K., *Durability of Embedded Fibre Optic Sensors in Composites.* 2001.
14. Etches, J.A., *Interfacial and durability aspects of extrinsic faby-perot interferometric sensors in carbon fibre composites*, in *Engineering systems department*2004, Cranfield university: dspace.lib.cranfield.ac.uk. p. 207.
15. Balac, I.e.a., *Stress Field Analysis around Optical Fiber Embedded in Composite Laminae under Transverse Loading.* FME Transactions (2006), 2006. **34**(1): p. 4.
16. Grattan, K.T.V. and T. Sun, *Fiber optic sensor technology: an overview.* Sensors and Actuators A: Physical, 2000. **82**(1–3): p. 40-61.
17. Voisin, V., et al., *Self-Referenced Photon Counting OTDR Technique for Quasi-Distributed Fiber Bragg Gratings Sensors.* Sensors Journal, IEEE, 2012. **12**(1): p. 118-123.
18. Güemes, A., A. Fernández-López, and B. Soller, *Optical Fiber Distributed Sensing - Physical Principles and Applications.* Structural Health Monitoring, 2010. **9**(3): p. 233-245.

19. Kreger, S.T., et al. *High Resolution Distributed Strain or Temperature Measurements in Single- and Multi-Mode Fiber Using Swept-Wavelength Interferometry*. 2006. Optical Society of America.
20. Soller, B.J., M. Wolfe, and M.E. Froggatt. *Polarization Resolved Measurement of Rayleigh Backscatter in Fiber-Optic Components*. 2005. Optical Society of America.
21. Soller, B., et al., *High resolution optical frequency domain reflectometry for characterization of components and assemblies.* Opt. Express, 2005. **13**(2): p. 666-674.
22. Hall, S.R.a.C., T. J., *The Total Data Integrity Initiative—Structural Health Monitoring, The Next Generation.* Proceedings of the USAF ASIP Conference, 1999(2nd).
23. J. M. Menendez, A.F.a.A.G., *SHM with Embedded Fibre Bragg Gratings and Piezoelectric Devices.* Structural Health Monitoring: Proceedings of the Third European Workshop, 2006: p. 7.
24. Rytter, A., *Vibration based inspection of civil engineering structures.* Ph.D. dissertation, 1993.
25. Kessler, S.S., S.M. Spearing, and C. Soutis, *Damage detection in composite materials using Lamb wave methods.* Smart Materials and Structures, 2002. **11**(2): p. 269.
26. Rainieri, C., Fabbrocino, Giocanni, Song, Yi, Shanov, Vesselin, *CNT composites for SHM: A Literature review*, in *NDT in Canada 2011*2011: Montreal, Qubec, Canada. p. 10.
27. Worden, K., et al., *The fundamental axioms of structural health monitoring.* Proceedings of the Royal Society A: Mathematical, Physical and Engineering Science, 2007. **463**(2082): p. 1639-1664.
28. Ciang, C.C., J.-R. Lee, and H.-J. Bang, *Structural health monitoring for a wind turbine system: a review of damage detection methods.* Measurement Science and Technology, 2008. **19**(12): p. 122001.
29. Kirikera, G.R., O. Balogun, and S. Krishnaswamy, *Adaptive Fiber Bragg Grating Sensor Network for Structural Health Monitoring: Applications to Impact Monitoring.* Structural Health Monitoring, 2011. **10**(1): p. 5-16.
30. KOJIMA, S., KOMATSUZAKI SHINJI (Hitachi Cable, Ltd.) KUROSAWA YOSHINORI (Hitachi Cable, Ltd.) HONGO AKIHITO (Hitachi Cable, Ltd.), *Embedding type strain sensors using small-diameter fiber Bragg grating to composite laminate structures.* Hitachi Cable Rev (Web), 2004. **23**: p. 11-15.
31. N Takeda, Y.O., T Mizutani, *Damage detection in composites using optical fibre sensors.* Proceedings of the Institution of Mechanical Engineers, Part G: Journal of Aerospace Engineering, 2007. **221**(4/2007): p. 12.
32. Takeda, N., et al., *Development of smart composite structures with small-diameter fiber Bragg grating sensors for damage detection: Quantitative evaluation of delamination length in CFRP laminates using Lamb wave sensing.* Composites Science and Technology, 2005. **65**(15-16): p. 2575-2587.
33. Baker, A. *Structural Health Monitoring of a Bonded Composite Patch Repair on a Fatigue-Cracked F-111C Wing*. 2006. 52.
34. Tsamasphyros, G.J., N.K. Fournarakis, K. Kalkanis, A.C. Christopoulos, G.N. Kanderakis., *Structural Health Monitoring Of Composite Patch Repairs*

Using Embedded Fiber Bragg Grating Sensors and Neural Network Techniques, in *4th International Conference on NDT*2007, HSNDTint: Greece. p. 10.

35. Tsamasphyros, G.J., et al. *Detection of patch debonding in composite repaired cracked metallic specimens, using optical fibers and sensors*. 2003. SPIE.
36. Farrar, C.R. and N.A.J. Lieven, *Damage prognosis: the future of structural health monitoring.* Philosophical Transactions of the Royal Society A: Mathematical, Physical and Engineering Sciences, 2007. **365**(1851): p. 623-632.
37. Mueller, I.e.a. *An Integrated Health Management and Prognostic Technology for Composite Airframe Structures*. 2009. 15.
38. Luyckx, G., et al., *Strain Measurements of Composite Laminates with Embedded Fibre Bragg Gratings: Criticism and Opportunities for Research.* Sensors, 2010. **11**(1): p. 384-408.
39. de Oliveira, R.d., Schukar, M., Krebber, K., Michaud, V., *Distributed strain measurement in CFRP structures by embedded optical fibres: Influence of the coating*, in ***16th International Conference on Composite Structures***2011: Porto.
40. Sjögren, B.A., *Static strength of CFRP laminates with embedded fiber-optic edge connectors.* Composites Part A: Applied Science and Manufacturing, 2001. **32**(2): p. 189-196.

13 Appendix A

Presented here are supplementary data and measurements from experiments.

13.1 Parameter influence

In chapter 6.3 the influence of changing the parameters during processing of the measurement data from the OBR 4600 was discussed. The rest of the different variations are presented below.

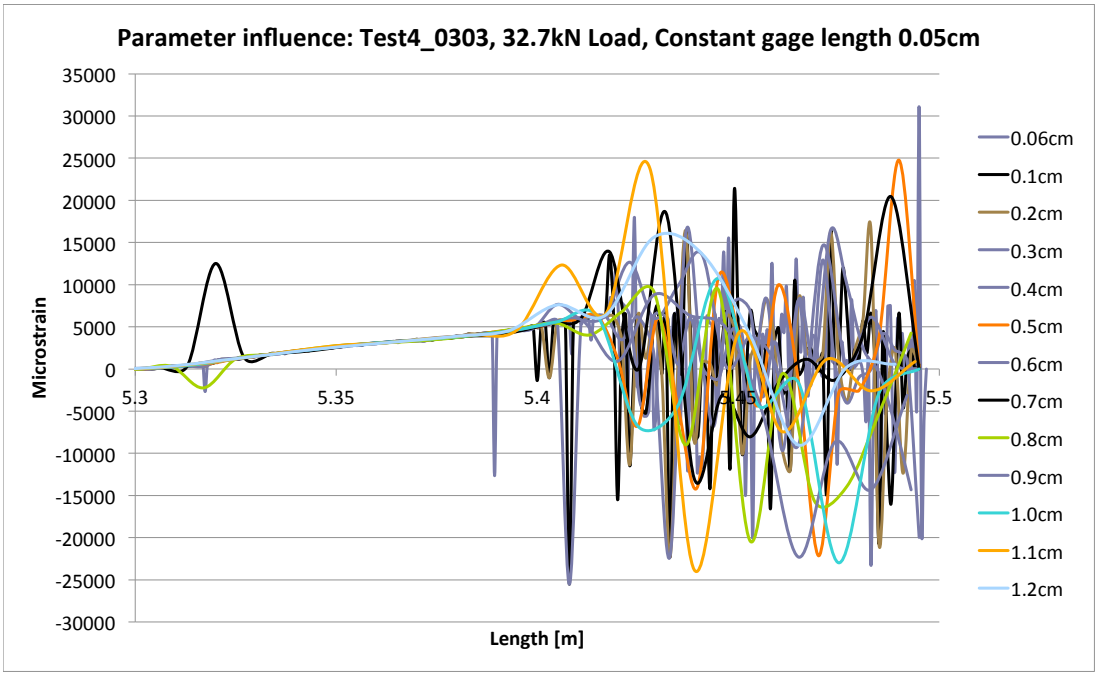

Figure 71: Parameter influence, 0,05cm gage length

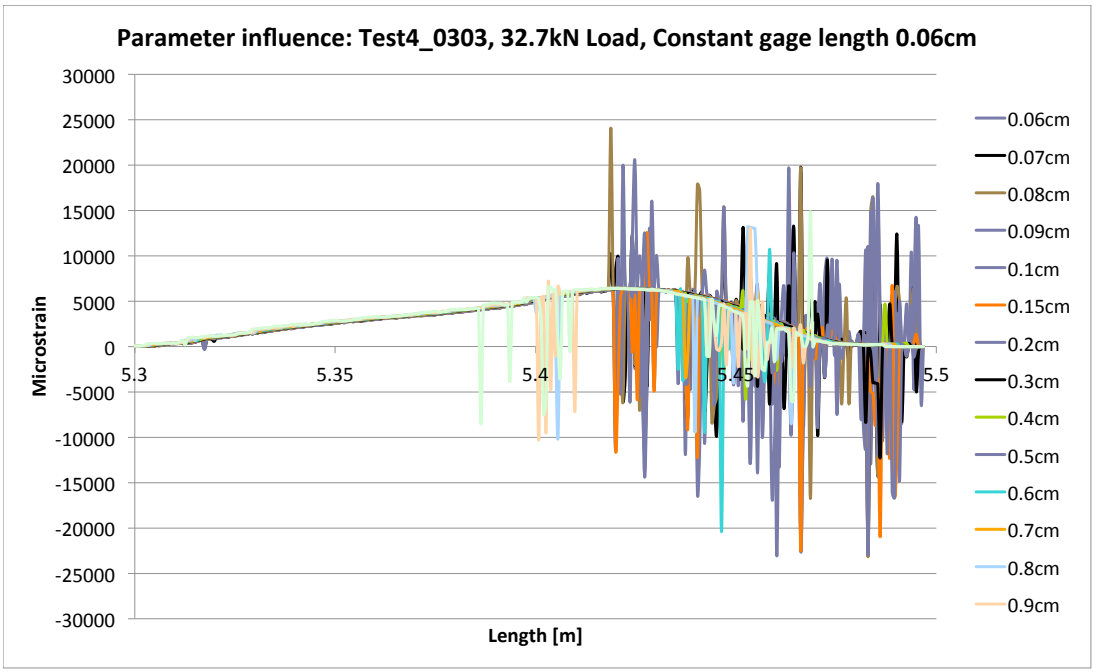

Figure 72: Parameter influence, 0,06cm gage length

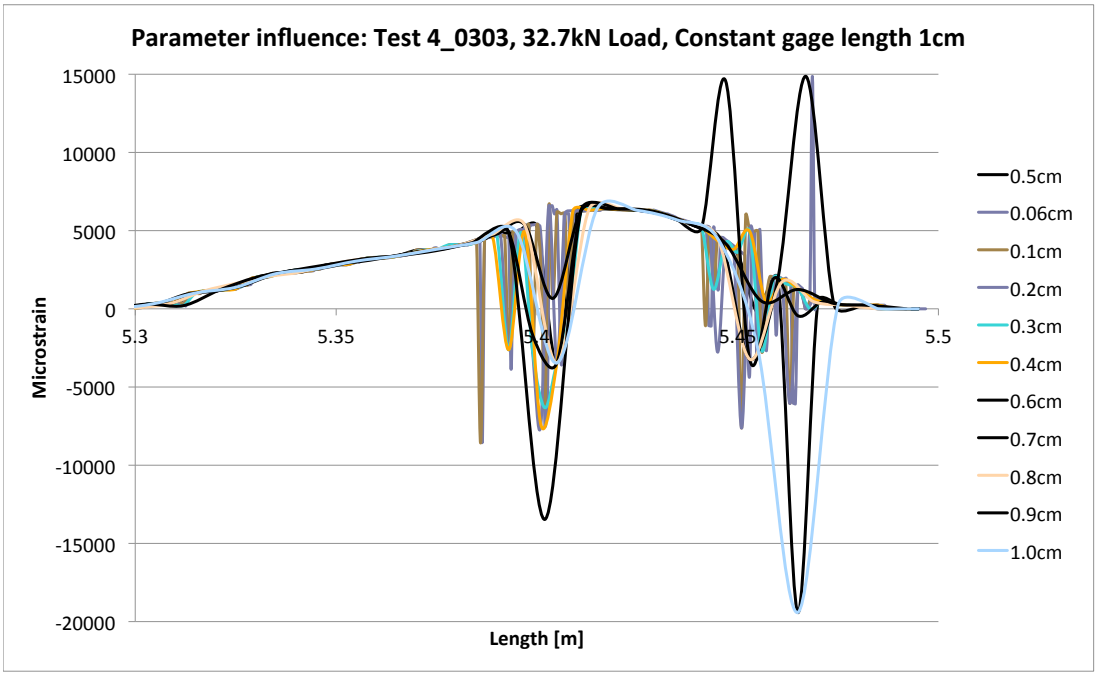

Figure 73: Parameter influence, 1cm gage length

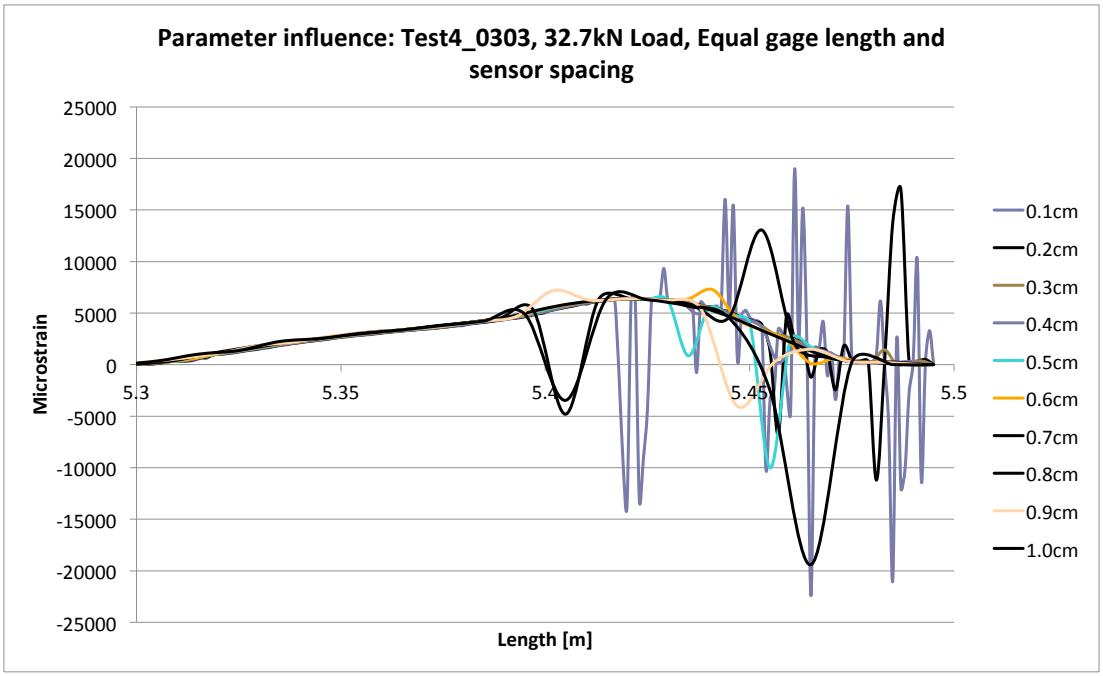

Figure 74: Parameter influence, equal gage length and sensor spacing

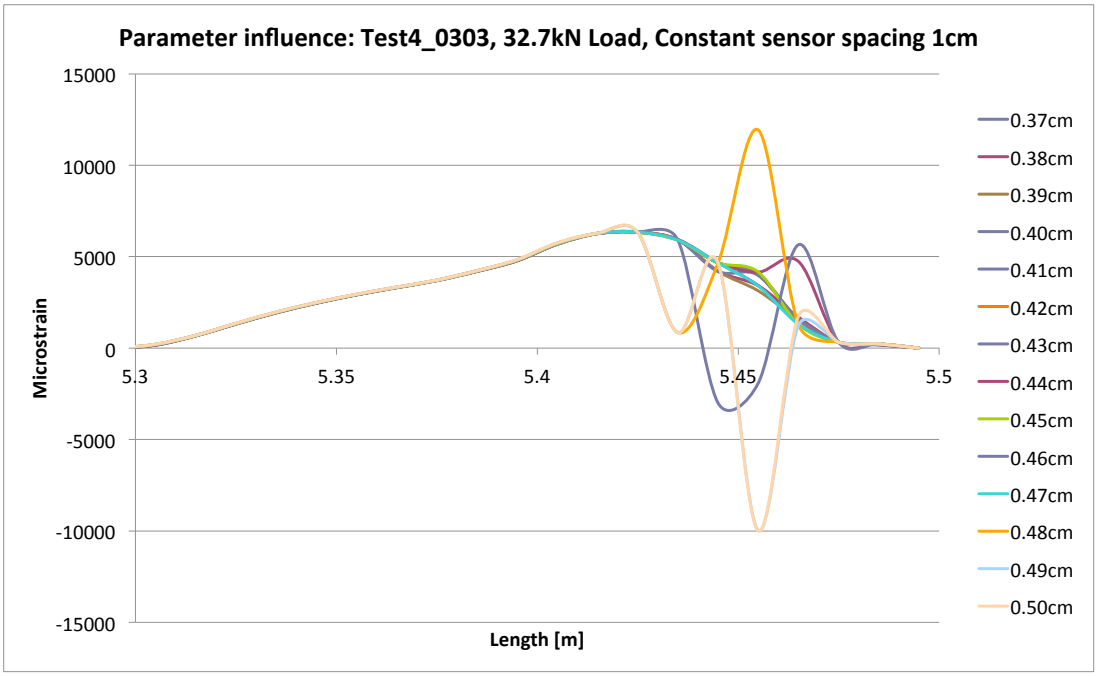

Figure 75: Parameter influence, 1cm sensor spacing

13.2 Conference paper

Conference paper to be published and presented at ECCM15. The fibre optical measurements and text is written by the author of this thesis. Some of the content is also used this thesis.

ECCM15 - 15TH EUROPEAN CONFERENCE ON COMPOSITE MATERIALS, Venice, Italy, 24-28 June 2012

EVALUATION OF THE STRAIN FIELD IN A COMPOSITE – METAL ADHESIVE JOINT WITH AN OPTICAL BACKSCATTER REFLECTOMETER

J. H. L. Grave[1], M. L. Håheim[1], A. T. Echtermeyer[1*]

[1] *Department of Engineering Design and Material, Faculty of Engineering Science and Technology, Norwegian University of Science and Technology, Richard Birkelands vei 2B, N-7491 Trondheim, Norway*
**andreas.echtermeyer@ntnu.no*

Keywords: Composite, Adhesive, Joint, OBR

Abstract

Knowing the strains and stresses in an adhesive joint is critical for the understanding and proper modeling of adhesive joints. To find a good method for measuring this has been a part of the work done by FP7 Co-Patch research program. Since the adhesive is sandwiched between the adherents the strains in the joint areas are difficult to measure. Movements of the entire joint can be measured with displacement transducers or crack opening can be measured with clip gauges. But these methods only allow an indirect evaluation of the conditions in the adhesive joint.

1 Introduction

Most large steel engineering structures will develop some cracks during their lifetime. Usually these cracks are repaired by welding, but in some cases the hot work associated with welding makes the welding repair unattractive. Examples are Floating Production and Storage Offshore units (FPSO) or tank ships, where hot work could cause fire and explosions [1,2]. Welding can only be done if production is shut down and all oil and gas is removed. Similarly electrical cables or other coatings on cruise ships may suffer from the hot work. Infrastructures like bridges are also often difficult to weld.

A method to avoid welding is patching with composite laminates. In this case the crack or corroded area is bridged by a patch made of a composite laminate. Stresses are transferred around the defect by the laminate, preventing the crack in the metal from growing further. The patch repair can be done without any hot work. A schematic of a patch repair is shown in the upper part of Figure 1. The crack in the metal is bridged by the composite patch. An adhesive layer lies between the composite patch and the metal. If the patch is made of carbon fiber composite the adhesive layer is usually called a galvanic corrosion protection layer. It is filled with a glass mat, ensuring that there is no electrical contact between the carbon fibers and steel that could lead to galvanic corrosion.

The main technical challenge is designing and producing a strong and durable adhesive joint between the steel and composite. The joint studied here was a carbon fibre laminate patched over a cracked metal I-beam. This type of test has been used successfully before to characterize joints [1,2] and it has been adopted recently in DNV´s recommended practise for composite patch repairs [3].

ECCM15 - 15TH EUROPEAN CONFERENCE ON COMPOSITE MATERIALS, Venice, Italy, 24-28 June 2012

Getting a better understanding on how adhesive joints work and eventually fail will be essential for wider use of this technology, especially long term use in critical application. A good method is needed to measure strains in the adhesive joint system during an experiment. These measurements can be compared to stress analysis done by the finite element method allowing improvement of modeling techniques leading to better designs. The strain measurement system investigated here is an optical fiber coupled to an Optical Backscatter Reflectometer (OBR). The optical fibre was glued onto the top surface of the patch, and embedded inside the patch between the galvanic protection layer and the carbon fibre laminate. Strains could be measured continuously along the entire length of the optical fiber.

2 Strains in an adhesive joint

It is well known that adhesive joints work by transferring shear through the adhesive layer from one substrate to the other. The shear stress has typically a stress concentration at the edges of the adhesive joint and lower shear stresses in the middle [4,5]. The shear stress distribution is often referred to as the "bathtub curve". In the case of a patch repair stress concentrations are also present at the mouth of the crack in the metal, as shown in Figure 1. The system can be seen as two adhesive joints in series with two "bathtub" curves.

It is not possible to measure shear stresses directly. But the shear stresses cause axial stresses and strains in the adhesive interface and the composite patch laminate. These axial strains can be measured by the optical fiber, as shown on the bottom of Figure 1. Any change in the shear stress distribution due to damage development will result in changes of the axial strain. It is also important to note that the axial strains will change through the thickness of the laminate. Adhesive joint models analyze typically the stresses right at the interface. Going away from the interface towards the surface of the patch the strain concentrations will be reduced due to redistributing stresses by interlaminar shear.

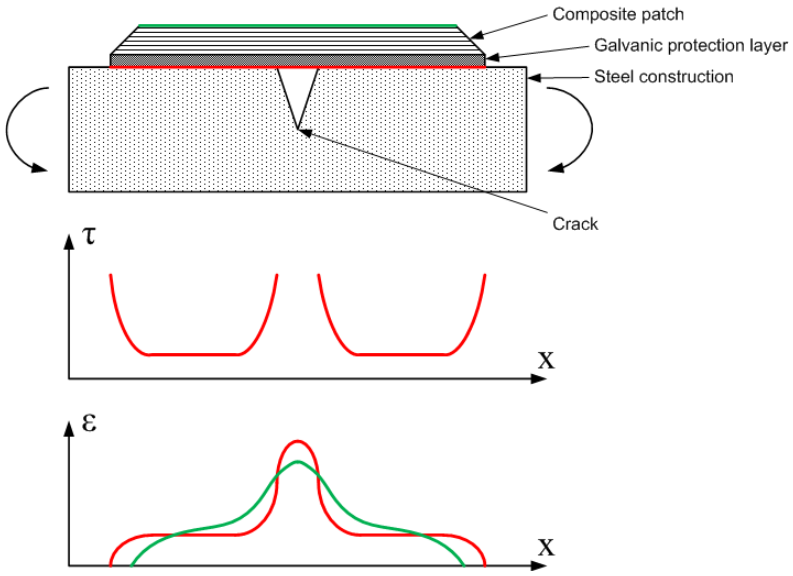

Figure 1. Shear and strain stress distribution between the galvanic layer and composite patch.

3 Optical Backscatter Reflectometer

Fibre bragg grating (FBG) and especially electrical strain gauges are well known and acknowledged methods to measure strains locally on a structure or specimen. It is difficult to decide where to place the strain measuring points. The strain concentrations shall be evaluated and compared to smooth far field strains. However, it is not known in advance where the strain concentrations will be if damage develops and moves them. The system used here allows continuous strain measurement along the optical fibre making the placement much easier.

The system is called Optical Backscatter Reflectometry (OBR) and consists of a tunable laser source and an Optical Frequency Domain Reflectometer (OFDR), used to measure the Rayleigh backscatter, in an interferometry setup [6]. Interferometry enables the system to measure the amplitude and the phase of the Rayleigh backscatter and with the help of Fourier transform [7] they are able to get information about changes in the backscatter profile and the position along the length of the fibre [8]. The use of multiple wavelengths in swept wavelength interferometry (SWI) enables the system to achieve high spatial resolution of the measurements.

The Rayleigh backscatter profile of fibre optic cables is a result of a heterogeneous reflective index, randomly distributed along the length of the fibre. This is a result of the manufacturing of the fibre and is unaltered until any external stimulus (like strain) causes a temporal and spectral shift locally in the backscatter pattern [6]. These shifts are used to calculate the changes in strain along the length of the cable when compared to the unstrained reference state.

4 Experimental method

Four point bend testing was used to measure the strains in the patch. An IPE100 beam was tested with a composite patch repairing a pre-made crack in the top flange. The loading span was ½ of the support span. The width of the support span was 800 mm and the load span was 400 mm (see Figure 2). The shear web will achieve low shear stress and constant moment between the load span.

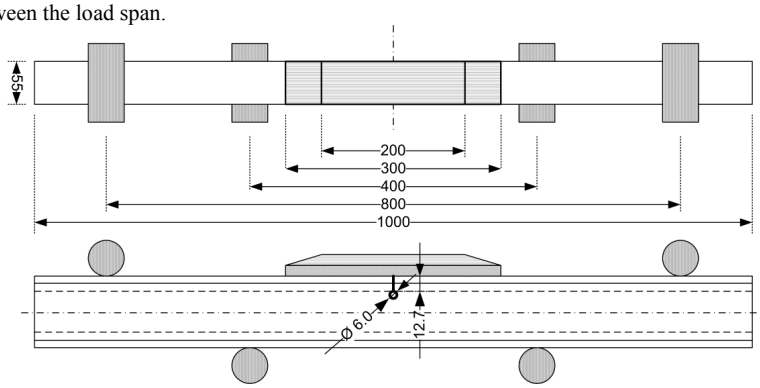

Figure 2. Experimental setup for a 300mm patched IPE100 beam with four point bending and 1/2 loaded.

The thickness of the carbon laminate was calculated to achieve the same stiffness as the cracked flange. The laminate was tapered at both ends to reduce peel stresses. The stresses will be highest near the opening of the crack in the metal beam. The fiber direction of the laminate was unidirectional, with the fibers running along the long axis of the beam.

The fiber optic cable was embedded between the carbon laminate and the galvanic protection layer, and it was attached to the surface of the patch. In addition, four electrical strain gauges were attached to the surface of the patch to compare the strain at these positions with the strain measured by the fiber optic cable.

Figure 3. Experimental setup at NTNU Fatigue lab of the patched IPE100 beam.

5 Materials

5.1 I-Beam

The beam used for the experiment is a 1m long PE100 beam with steel grade S355J2 [9]. A 20 mm long crack was machined in the middle of the top flange, i.e. 500 mm from the side. The crack passes through the top flange, and barely into the shear web, where it is terminated by a 6 mm diameter hole. A broach was used to reduce micro cracks around the hole.
The bonding area of the patch was cleaned according to ISO procedure [10], and grit blasted with a surface quality of SA 2½. The surface roughness was 136µm.

5.2 Patch

The grit blasted area was coated with a chopped strand matt (CSM) right after the surface treatment. This coating works as a galvanic protection layer, and the fiber optic cable for the OBR is applied at the middle of the flange over the whole patch length (300 mm). The patch was applied with a vacuum assisted infusion process.

6 Finite element analysis

A numerical model of the patch repaired I-Beam was done in Abaqus 6.11-1. Linear Hexahedron C2D8R elements were used over the whole model, and the maximum element aspect ratio was below 9. Standard material properties were used for the I-Beam with plasticity characteristic from the I-Beam material certificate. The CSM was modeled with engineering constants without plasticity, and the carbon laminate with ply property engineering constants measured by the Co-Patch project according to the standards [11-14].
Constraints between the three parts, I-Beam, CSM and patch are made with tie constraints. The parts are sharing the nodes, and parts are sectioned at the same places. Number of elements in patch are 13 440, galvanic protection layer 4560 and I-Beam 75 136, this gives a total of 93 136.
Symmetry plane for the I-Beam is over the area yz-plane in the shear web and neighboring surfaces in same plane. Also under crack ligament in the shear web to the bottom flange,

patch and galvanic protection surfaces in z-direction have the symmetry over the yx-plane. The load span is fixed by the nodes in y-direction, and support span contribute with displacement in negative y-direction. A stress distribution in the length direction is shown in Figure 4.

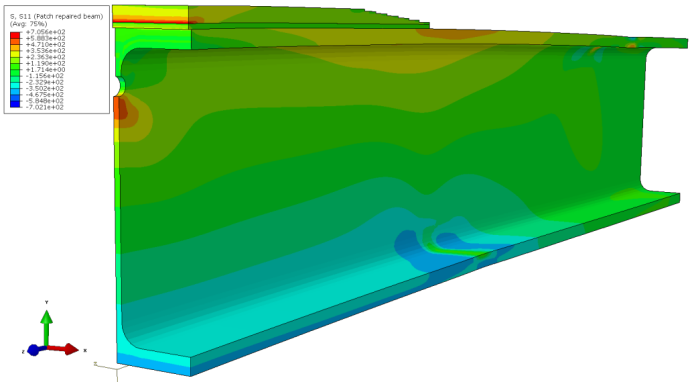

Figure 4. Numerical model for the patch repaired I-Beam. S11is stresses in z-direction.

7 Results

Testing of the I-Beam was done with 0.3 mm/min in displacement control. With this displacement speed, it was possible to do measurements with the OBR without holding the test. Measurements were done with the OBR every 10kN. Presented here is the comparison of measurements at two load levels: one within the linear elastic area, and one closer to failure and plastic behavior. Measurements done with strain gauges are presented live during the loading of the test, but results from the OBR are ready after some post processing.

7.1 Reading at 71 kN

The strain measurements from the optical fibre on the surface of the patch coincide well with both the FE-analysis and the electrical strain gauge readings. The strain gauge value at the crack is slightly higher than both the FE-analysis and the optical fibre. A reason for this is the 5mm gauge length of the strain gauge, which reads the average value over the length, compared to the 1mm “gauge length” achieved with the OBR. The top surface of the patch was displaced by 5 - 10 mm, hence the measurement with the optical fibre has an offset compared to the symmetrical FE-analysis. The positions of the strain gauge values are according to the placement on the patch surface measured from the center of the crack.
The embedded optical fiber corresponds well with the FE-analysis, except directly over the metal crack.
High strain gradients are a measurement challenge for the OBR. Too big changes will cause the cross-correlating algorithms for the spectral shift to fail. The result of this is sometimes an unrealistic value, seen as noise, but also entails uncertainty in the accuracy of the absolute value of the measurements at high stress concentrations. Improvements are achieved by post processing, but for the purpose of this comparison it is more interesting to evaluate the strain gradient leading up to the crack.

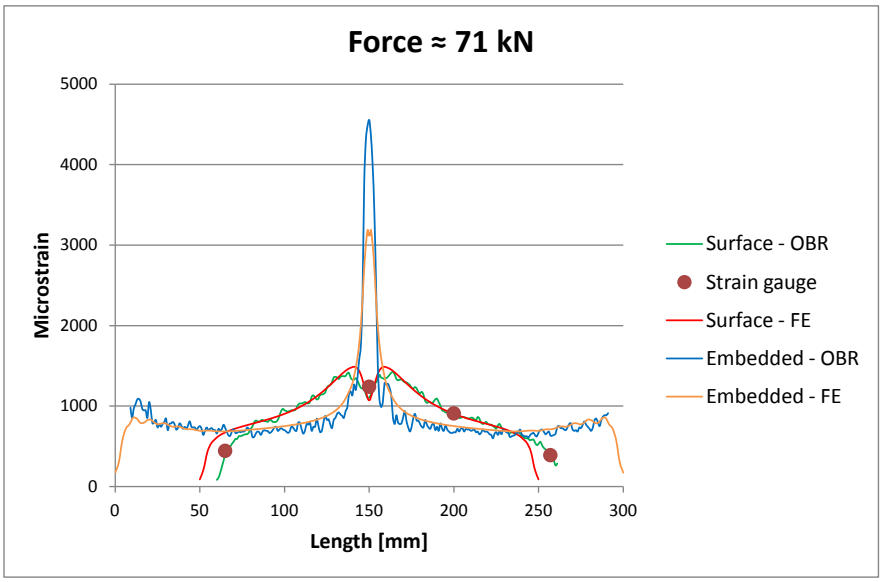

Figure 5. Strain in the patch at 71 kN.

7.2 Reading at 138 kN

The strain measurements of the optical fibre on the surface of the patch agree also here well with the strain gauge readings. However the FE-analysis deviates from the measured strain on the surface. The FE-analysis did not take into the account the possible degradation or cracking of the patch at the metal crack which is expected to happen at this high load. The spatial misalignment between the FE-analysis and the measurement by the fiber optic cable and the electrical strain gauges is probably due to a displacement of the patch, where the patch center is to the right of the crack.

The strain field of the embedded optical fibre is wider than the FE-analysis. This is due the effects of damage appearing at the crack tip, which has not been a part of the FE-analysis.

Future work will look into nonlinear FE analysis using progressive failure analysis to simulate damage growth. This should help to explain how the strain field changes with damage development. However, it is already clear now, that the optical strain field measurement can be used to monitor damage development.

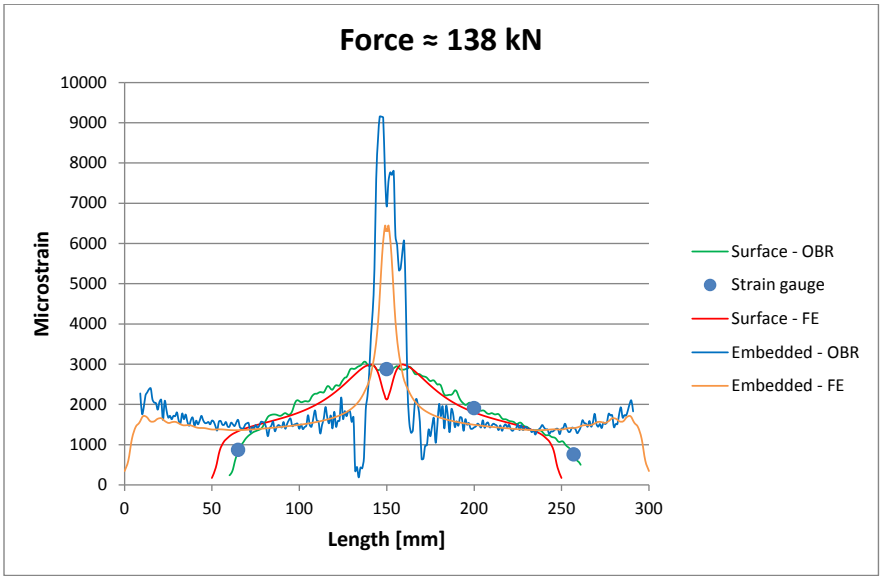

Figure 6. Strain in the patch at 138 kN.

8 Conclusion

The four point bend test has successfully been used to evaluate the repair of a cracked steel beam with a composite patch. The strain on the surface of the patch could be measured continuously with the optical back scatter method. The optical strain measurements agreed with local strain data obtained from classical electrical strain gauges. Strain could also be measured along the length of the sample with an embedded fiber inside the repair laminate at the interface between the load bearing patch and the galvanic protection layer. The strain measurements show that strains differ inside and outside the patch indicating that a 3-D analysis of the stress state in the patch is important.

The strains at low loading obtained from the simulations agreed well with the measured strains both inside the joint and on the surface. At high loads the shape of the experimentally measured strain field changed. The changes are understood to be caused by damage developing in the composite. This damage was not modeled by the linear finite element analysis. Progressive nonlinear failure analysis will most likely be able to relate damage development and observed changes in strain.

It is encouraging that the strain measurements pick up changes in the strain field. This method should have a good potential to be used as an early warning of damage developing inside the patch that could eventually lead to failure.

9 Acknowledgements

The research leading to these results has received funding from the European Community's Seventh Framework Program (FP7/2007-2013) under grant agreement n° 233969 (www.co-patch.com).

The authors gratefully acknowledge the contribution of project partner Umoe Mandal (T. Salvesen).

References

[1] Echtermeyer A. T., et al., *Repair of FPSO with Bondend Composite Patches* in proceeding of *Fourth International Conference On Composite Materials For Offshore Operations*, Houston, Texas, (2005).
[2] McGeorge, D., et al., Repair of floating offshore units using bonded fibre composite materials. *Composites Part A: Applied Science and Manufacturing*, 40, pp. 1364-1380 (2009).
[3] DNV-RP-C301. *Design, Fabrication, Operation and Qualification of Bonded Repair of Steel Structures*, (2012).
[4] Hart-Smith L. J., *Analysis and Design of Advanced Composite Bonded Joints*, NASA CR-2218, (1974).
[5] Kinloch A. J., Review: The science of adhesion. Part 2 Mechanics and mechanisms of failure. *Journal of Materials Science*, 17, pp. 617-651 (1982).
[6] Kreger S. T., et al., *High Resolution Distributed Strain or Temperature Measurements in Single- and Multi-mode Fiber Using Swept-Wavelength Interferometry* in proceeding of *Optical Fiber Sensors (OFS)*, Cancun, Mexico, (2006).
[7] Soller B. J., Wolfe M., Froggatt M. E., *Polarization resolved measurement of Rayleigh backscatter in fiber-optic components* in proceeding of *National Fiber Optic Engineers Conference (NFOEC)*, Anaheim, California, (2005).
[8] Soller B. J., et al., High resolution optical frequency domain reflectometry for characterization of components and assemblies in proceeding. *Optic Express*, 13, pp. 666-674 (2005).
[9] NS-EN 10025-2. *Hot rolled products of structural steels Part 2: Technical delivery conditions for non-alloy structural steels* (2005).
[10] ISO 4288. *Geometrical Product Specifications (GPS) -- Surface texture: Profile method -- Rules and procedures for the assessment of surface texture* (2006).
[11] ASTM D 3039M. *Standard Test Method for Tensile Properties of Polymer Matrix Composite Materials* (2007).
[12] ISO 14126. *Fibre-reinforced plastic composites -- Determination of compressive properties in the in-plane direction* (1999).
[13] ASTM D 3518M. *Standard Test Method for In-Plane Shear Response of Polymer Matrix Composite Materials by Tensile Test of a x00B1;45 x00B0; Laminate*, (2007).
[14] ASTM D 3171. *Standard Test Methods for Constituent Content of Composite Materials*, (2006).

13.3 OBR 4600 Datasheet

Breakthrough Functionality in Fiber Optic Testing

LUNA TECHNOLOGIES
A Division of Luna Innovations Incorporated

OPTICAL BACKSCATTER REFLECTOMETER™
(Model OBR 4600)

KEY FEATURES AND PRODUCT HIGHLIGHTS

- **Easily locate, identify and troubleshoot macro-bends, splices, connectors and breaks**
- **Locate Insertion Loss points at every point in the network or assembly – eliminate cut-back**
- **Look inside components to evaluate each interface for RL and IL**
- **Measure 30 m with 10 μm resolution in less than 7 seconds**
- **Continuously measure a 1 m segment at up to 3 Hz**
- **Test and troubleshoot short-run networks (<2 km)**
- **Automate pass/fail verification of fiber assemblies**
- **Monitor distributed temperature and strain profiles along network or inside a component or module**

The **OBR 4600** is the latest model of Luna Technologies' award winning Optical Backscatter Reflectometer™ product line. Designed for component and short-run network testing and troubleshooting, the OBR 4600 enables ultra-high resolution reflectometry with backscatter-level sensitivity. With spatial resolution as fine as 10 microns, zero dead-zone, options for integrated temperature and strain sensing and extended device length mode, the OBR 4600 offers the ultimate in fiber diagnostics.

MEASUREMENT PERFORMANCE HIGHLIGHTS

- -130 dB sensitivity
- 70 dB dynamic range
- 2 kilometer length range with no dead-zone
- Micrometer resolution up to 70 meters
- < 0.05 dB insertion loss resolution

The OBR 4600 offers unbeatable testing and troubleshooting capabilities now at unprecedented measurement speeds.

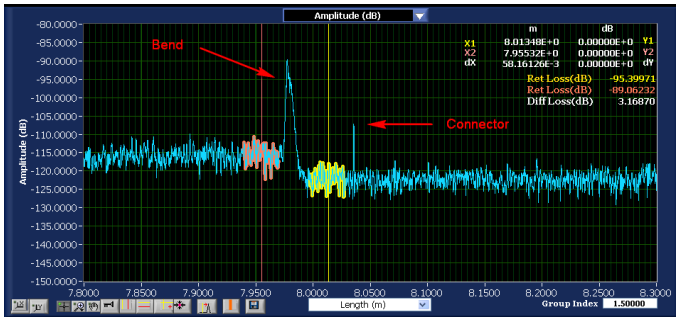

www.lunatechnologies.com
3157 State Street | Blacksburg, VA 24060
+1.540.961.5190 | Fax: 1.540.961.5191
solutions@lunatechnologies.com
Support phone: +1.866.586.2682

OBR 4600

PARAMETER	SPECIFICATION	UNITS
Maximum Device Length:		
Standard Mode	30 or 70	meters
Long Range Mode[10]	2000	meters
Spatial Resolution (two-point)[1]:		
	10 µm over 30 meters	
	20 µm over 70 meters	
	1 mm over 2 km	
Dead Zone:		
	Equals 2-pt spatial resolution	
Wavelength Range[2]:		
	1265-1335 or 1525-1610	nm
Wavelength:		
Resolution (max)	0.02	pm
Accuracy[3]	±1.5	pm
Integrated Return Loss Characteristics:		
Dynamic range[4]	70	dB
Total range	0 to -125	dB
Sensitivity	-130	dB
Resolution	±0.05	dB
Accuracy	±0.10	dB
Integrated Insertion Loss Characteristics:		
Dynamic range[5]	18	dB
Resolution	±0.05	dB
Accuracy	±0.10	dB
Group Delay:		
Accuracy	1.0	ps
Distributed Sensing[6,10,11]:		
Spatial Resolution	±1.0	cm
Temperature Resolution	±0.1	C
Temperature Accuracy[7]	±0.2	C
Strain Accuracy[7]	±1.0	µstrain

Measurement Timing[8]	Standard	Fast[9]	Spot Scan[9]	
5 nm scan time	3	1.6	0.3	s
Time vs. wavelength range	2.1 s+0.14 s/nm	1.3 s+0.06 s/nm	0.15 s+0.02 s /nm	-
Long Range (2 km) Scan Time		20		s

Specifications are for single-mode operation.
For multimode operation, specifications are nominal.
1 Over entire length range.
2 Ranges are nominal.
3 Accuracy maintained by an internal NIST-traceable HCN gas cell.
4 For the 2000 m option, return loss dynamic range is 60 dB.
5 The insertion loss dynamic range is the one-way loss that can be suffered before the scatter level of standard SMF (~ -100 dB/mm) is lower than the noise floor (~ -118 dB/mm).
6 Distributed sensing uses Rayleigh spectral shift method and is relative to reference scan.
7 Temperature and strain accuracies are calculated from spectral shift of Rayleigh scatter using 1 GHz = 0.8 C. [Othonos and K. Kalli, Fiber Bragg Gratings (Artech House, Boston, 1999)]. Spatial resolutions listed are ideal to get the Temperature and Strain Accuracies listed; they are not minimums or maximums.
8 Combined scan and analysis time in high-resolution mode. Times are for 30 m scan mode.
9 Times are with laser tuning speed set at 100 nm/s.
10 Extended range mode and distributed sensing are upgrade options.
11 Maximum sensing length is 70m.

LTOBR4600 REV.001
Date of Revision 09/03/2010

CLASS 1 LASER PRODUCT

LUNA TECHNOLOGIES™
A Division of Luna Innovations Incorporated

Measurement Timing Information

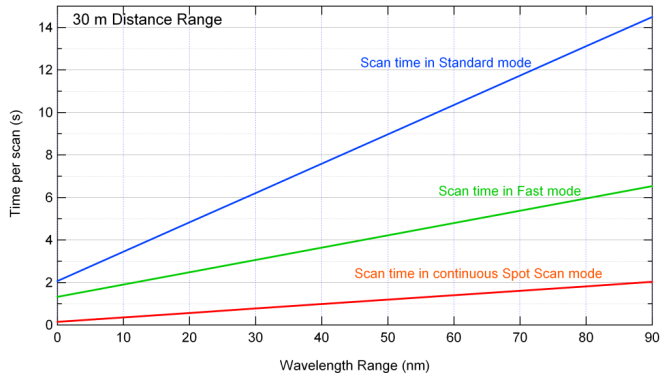

Time per scan vs. scan wavelength range for 30 m scans in standard operating, fast scanning and continuous spot scanning modes.

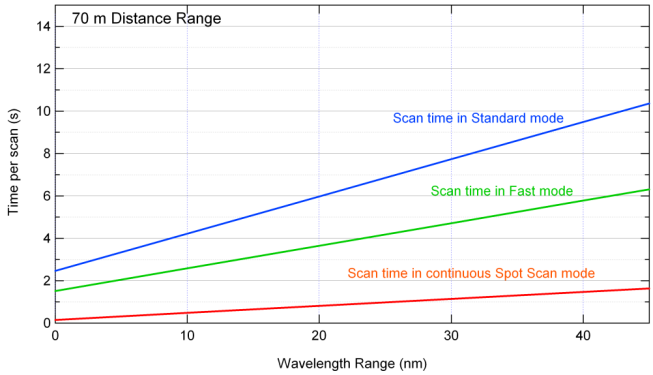

Time per scan vs. scan wavelength range for 70 m scans in standard operating, fast scanning and continuous spot scanning modes.

Wavelength Range (nm)	Spot Scan Rate (Hz) 30 m mode	Spot Scan Rate (Hz) 70 m mode
5	3.7	2.9
10	2.7	2.0
20	1.8	1.2
40	0.9	0.6
80	0.5	-

Scan repetition rates at various scan wavelength ranges for continuous spot scanning in 30 m and 70 m modes of operation. Rates are for laser tuning speed set to 100 nm/s.

LUNA TECHNOLOGIES™
A Division of Luna Innovations Incorporated